Introduction to electron paramagnetic resonance spectroscopy

Gunnar Jeschke, HCI F227, gjeschke@ethz.ch

Lecture : most important concepts treated by example

Script : in-depth discussion, including complications (www.ssnmr.ethz.ch/education/PCIV.html)

Exercises : hands-on experience, deeper understanding, will be part of examination material

---

Examination : pass by knowing concepts and having "exercise level"
get good grade by in-depth understanding

Examination content: will be specified in the last lecture (December 20th)

EPR lectures 19.11., 22.11. (Maxim Yulikov), 29.11., 6.12., 13.12., 17.12., 20.12.

Outline

- Introduction to EPR, Spin Hamiltonian, general and for the S =1/2, I = 1/2 system (19.11.)
  Lecture notes 2.1, 2.2
- g shift and hyperfine interactions (22.11., Maxim Yulikov)
  Lecture notes 3,4
- electron-electron interactions & forbidden transitions (29.11.)
  Lecture notes 5,6
- CW EPR spectroscopy, ENDOR (6.12.)
  Lecture notes 7, 8.1
- Distance distribution measurements (13.12.)
  Lecture notes 9
- ESEEM and HYSCORE (17.12.)
  Lecture notes 8.2
- Spin labels, slow tumbling nitroxide spectra, spin trapping (20.12.)
  Lecture notes 10

Exercise 8

Exercise 9

Exercise 10

EPR- the little big sister of NMR

The little sister

chemical bonding is electron pairing, spins compensate

EPR signals ⇔ Chemical reactivity

- transition metal catalysis (e.g. with Christophe Copéret)
- metalloproteins (e.g. with Don Hilvert, Rudi Glockshuber)
- radical reactions (e.g. with Antonio Togni, Erick Carreira)
- electron transfer reactions (e.g. photosynthesis)

Defect-based function of solid-state materials (with D-PHYS)

- color centres
- semiconductors
- conducting polymers

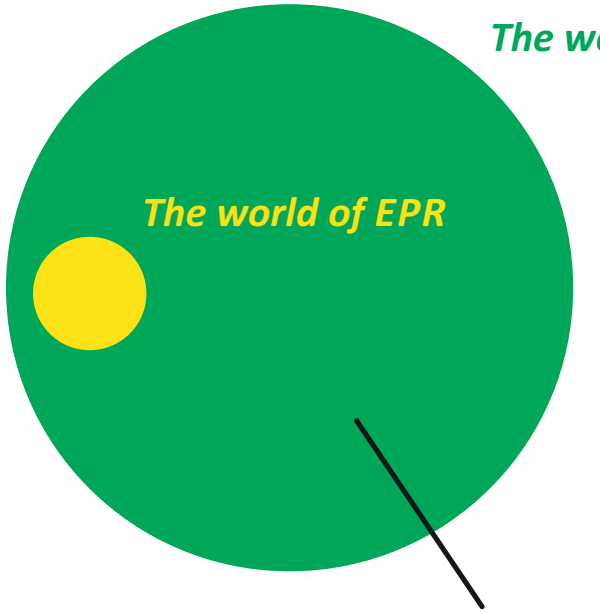

accessible by spin labeling

Integrative structural biology

with
Frédéric Allain
Roland Riek

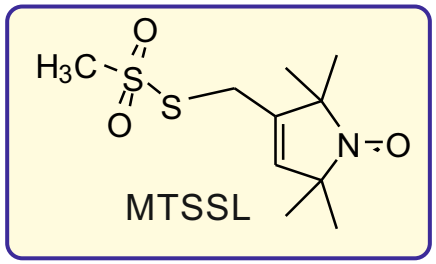

EPR- the little big sister of NMR

The big sister

angular momentum

$$\mu = -g\frac{e\hbar}{2m_e}S$$

larger charge/mass ratio than NMR ⇒ magnetic moment at least 680 times larger

- higher frequencies, shorter time scales: 10 ps… 1 ms
- higher sensitivity: ~10^{11} spins (2 µl at 100 nmol/l)
- longer distances: 0.5… 8 nm

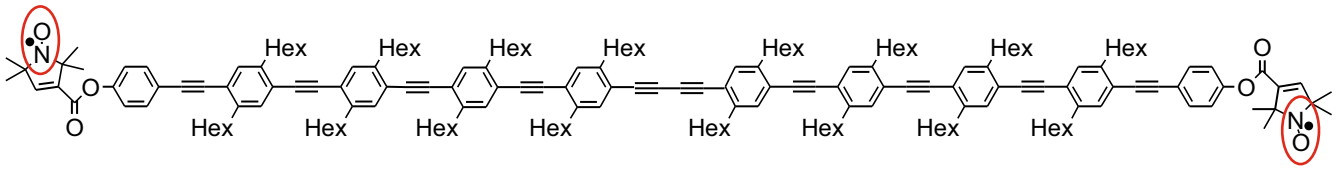

with Adelheid Godt
Bielefeld University

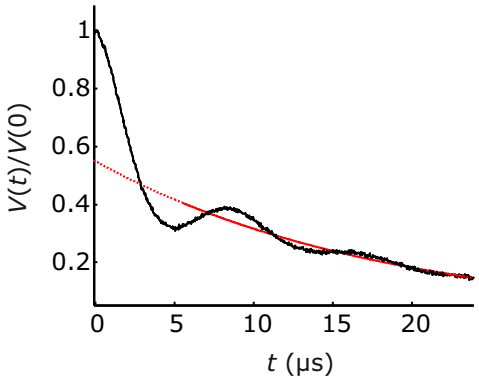

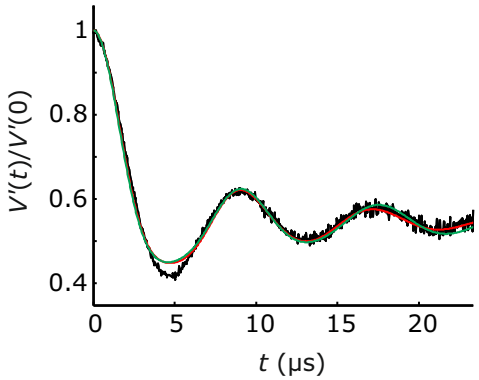

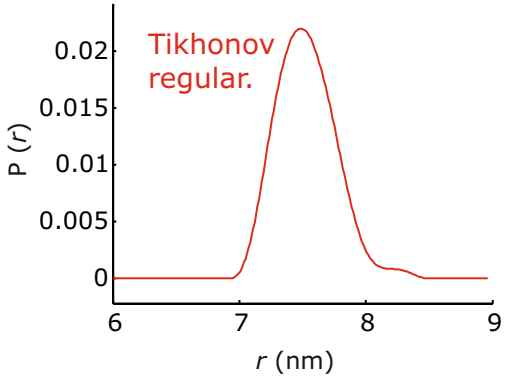

The unpaired electron is a magnetic point dipole

A rotating homogeneous sphere with charge *q*

has a magnetic dipole moment μ

$$\vec{\mu} = \frac{q}{2m}\vec{J}$$

$\vec{J}$: angular momentum

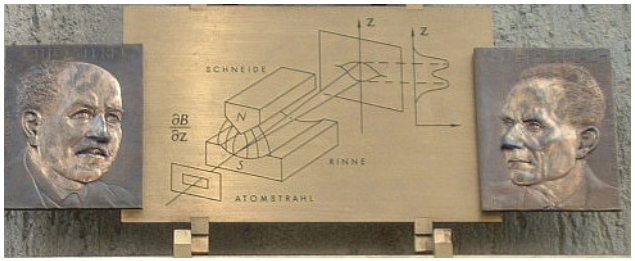

Stern-Gerlach experiment 1922

The electron has intrinsic angular momentum - Spin

$$\mu = -g\frac{e}{2m}\hbar S \qquad (\mu_B)$$

S = ½ : spin quantum number

g : quantum-mechanical correction

$\gamma_e = -g\,\mu_B/\hbar$

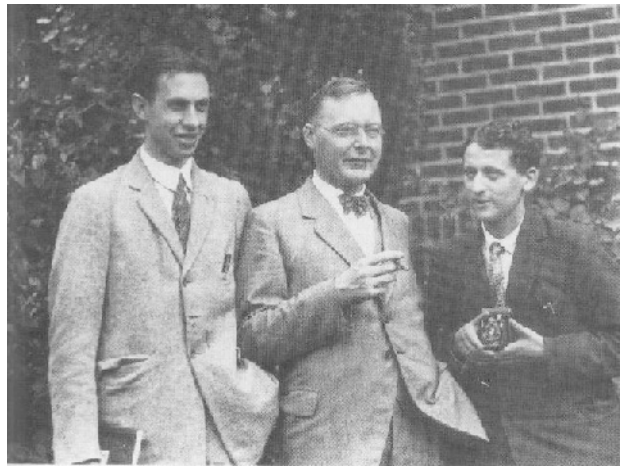

Uhlenbeck *Goudsmit*

1925

Quantum electrodynamics (Schwinger):

quantitative prediction of g_e for an unbound electron

g_e = 2.002319304

Electron spin in a magnetic field

- by convention: magnetic field B_0 along z

Two states with different energy, corresponding to different magnetic quantum numbers m_s

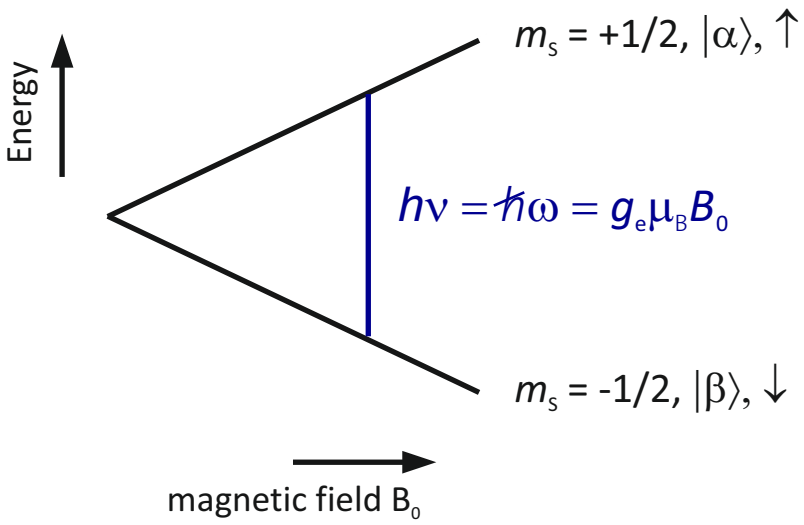

- typical fields: 0.1…1.5 T (high-field EPR 3.5…12 T)
- typical frequencies: 1…35 GHz (high-frequency 94…300 GHz)

- energy difference often smaller than thermal energy ⇒ small population difference 2ε

this high-temperature approximation can be violated in EPR (unlike NMR), e.g. ν = 94 GHz, T = 4.2 K

Relevant interactions in EPR spectroscopy

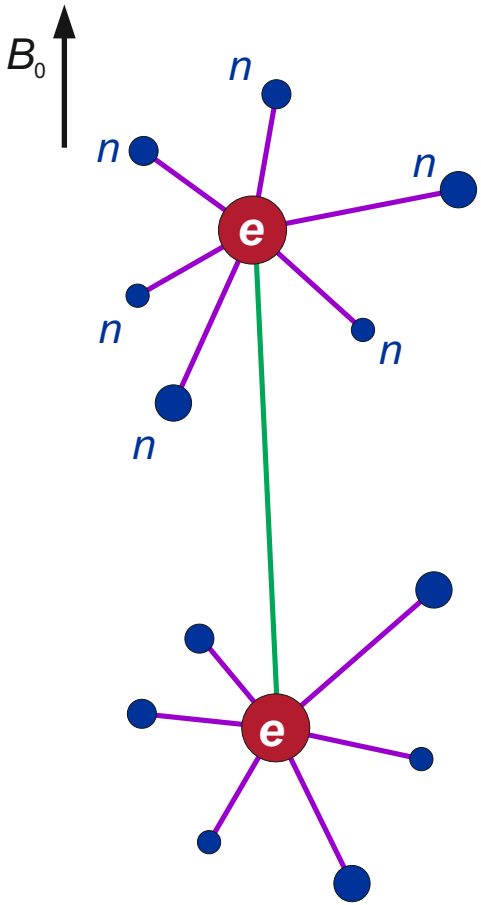

Type	Name	Hamiltonian	
electron spin/static magnetic field	electron Zeeman	$\hat{H}_{EZ} = \vec{B}_0 \vec{\vec{g}} \vec{S}$	
electron spin/nuclear spin	hyperfine	$\hat{H}_{HF} = \vec{S} \vec{\vec{A}} \vec{I}$	
nuclear spin/static magnetic field	nuclear Zeeman	$\hat{H}_{NZ} = \omega_I \hat{I}_z$	
nuclear spin/electric field gradient	nuclear quadrupole	$\hat{H}_{NQ} = \vec{I} \vec{\vec{P}} \vec{I}$	($I > 1/2$)
electron spin/electron spin (strong)	zero-field	$\hat{H}_{ZFS} = \vec{S} \vec{\vec{D}} \vec{S}$	($S > 1/2$)
electron spin/electron spin (weak)	exchange	$\hat{H}_{EX} = J \vec{S}_1 \vec{S}_2$	
	dipole-dipole	$\hat{H}_{DD} = \vec{S}_1 \vec{D} \vec{S}_2$	

Typical magnitude of interactions

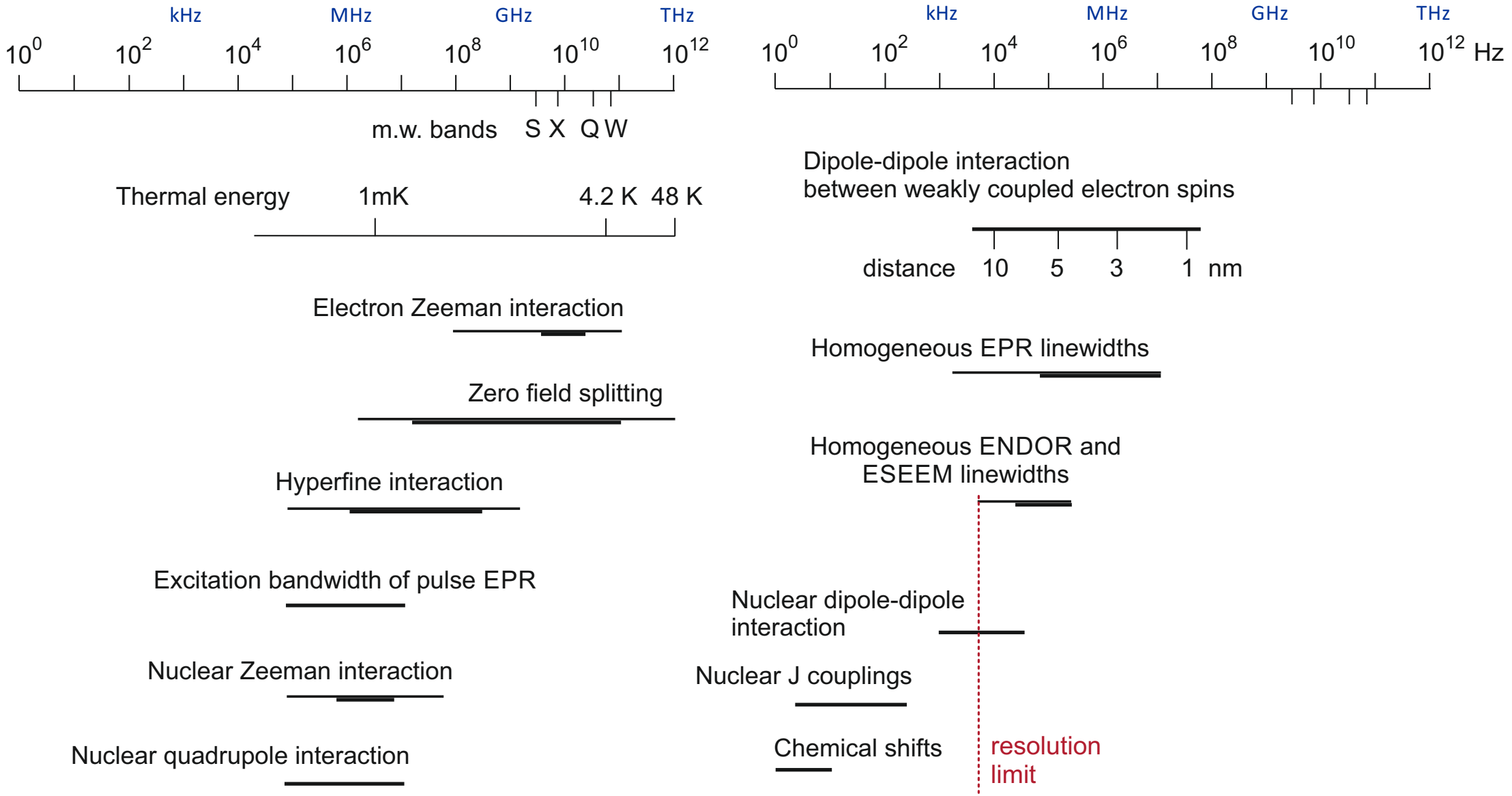

Electron Zeeman interaction

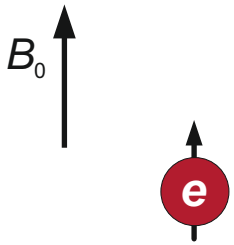

Free electron

$g_e = 2.002319304$

Bound electron (example)

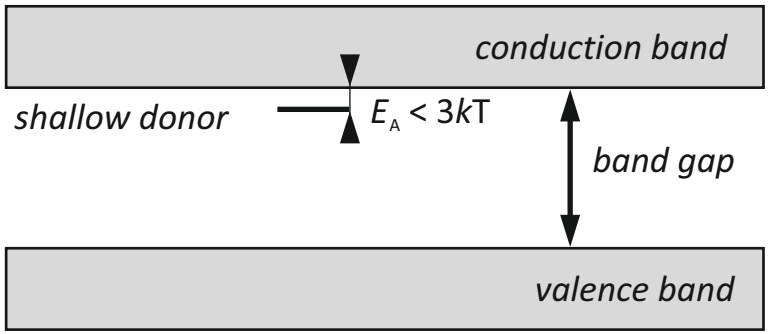

EPR spectrum of nanosized ZnO

ZnO reference

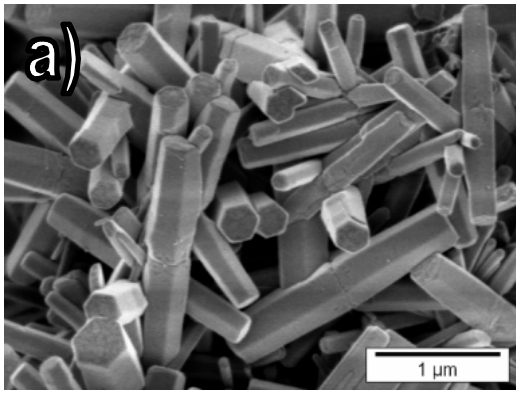

ZnO prep. with 1 g/L Latex

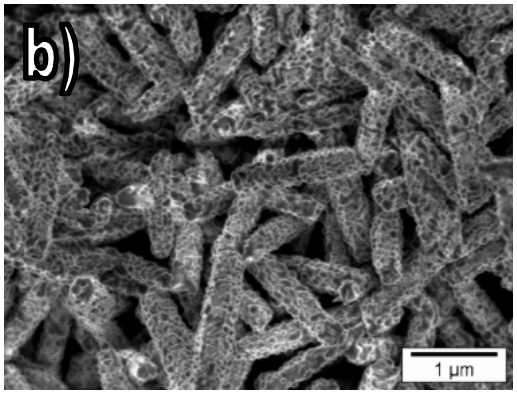

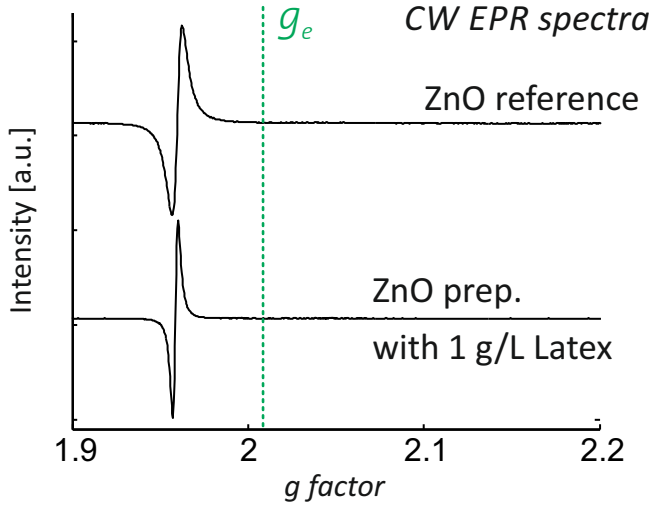

The Zeeman interaction revisited

$$\hat{\mathcal{H}}_{EZ} = \mu_B/\hbar \; \vec{B}_0^{\,T} \; \boldsymbol{g} \; \hat{\vec{S}}$$

magnetic field vector — *g* tensor — electron spin vector operator

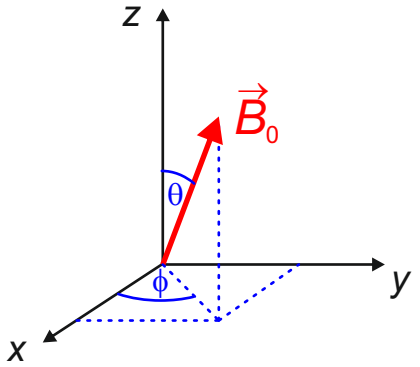

$B_x = \sin\theta \cos\phi \; B_0$

$B_y = \sin\theta \sin\phi \; B_0$

$B_z = \cos\theta \; B_0$

Explicit notation in the principal axes frame of the *g* tensor

$$\begin{pmatrix} g_x & 0 & 0 \\ 0 & g_y & 0 \\ 0 & 0 & g_z \end{pmatrix} \begin{pmatrix} \hat{S}_x \\ \hat{S}_y \\ \hat{S}_z \end{pmatrix}$$

$$(B_x \; B_y \; B_z) \quad (g_x B_x \;\; g_y B_y \;\; g_z B_z) \quad *$$

$$* \quad \hat{\mathcal{H}}_{EZ} = (\mu_B/\hbar)\,(g_x B_x \hat{S}_x + g_y B_y \hat{S}_y + g_z B_z \hat{S}_z) = g_{eff}\,\mu_B B_0/\hbar \; \hat{S}_{z'}$$

$$g_{eff} = \sqrt{\sin^2\theta \cos^2\phi \; g_x^{\,2} + \sin^2\theta \sin^2\phi \; g_y^{\,2} + \cos^2\theta \; g_z^{\,2}}$$

The tensor ellipsoid

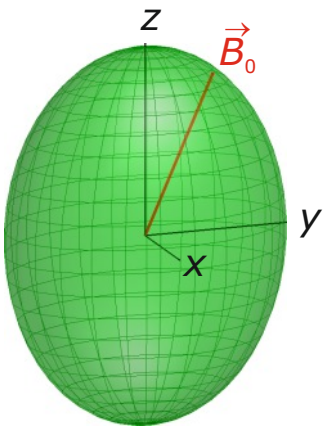

Powder lineshape for an anisotropic *g* tensor with axial symmetry

Equatorial orientations are more probable than polar (axial) orientations

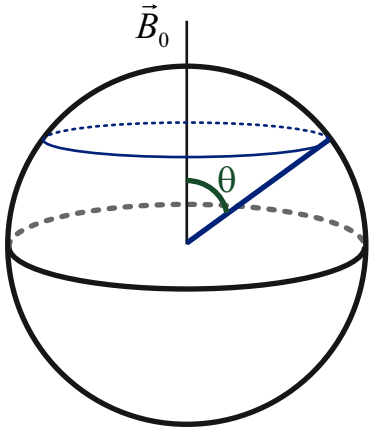

circumference:
$2\pi \sin\theta\, r$

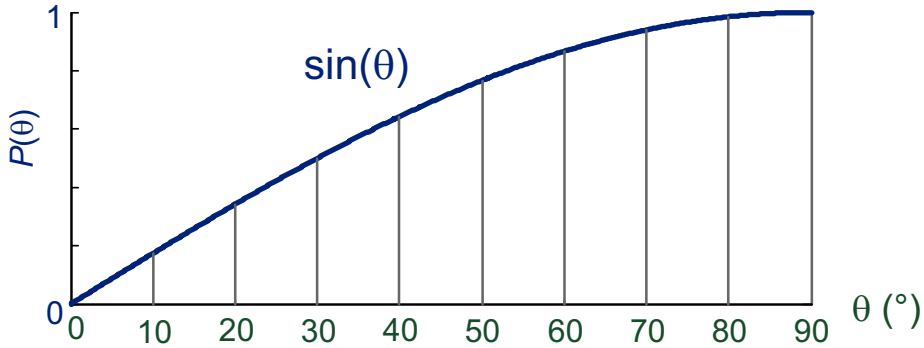

Intensity is higher at equatorial orientations corresponding to $g_\perp$

$$g_{eff} = \sqrt{\sin^2\theta\, g_\perp^{\,2} + \cos^2\theta\, g_{||}^{\,2}}$$

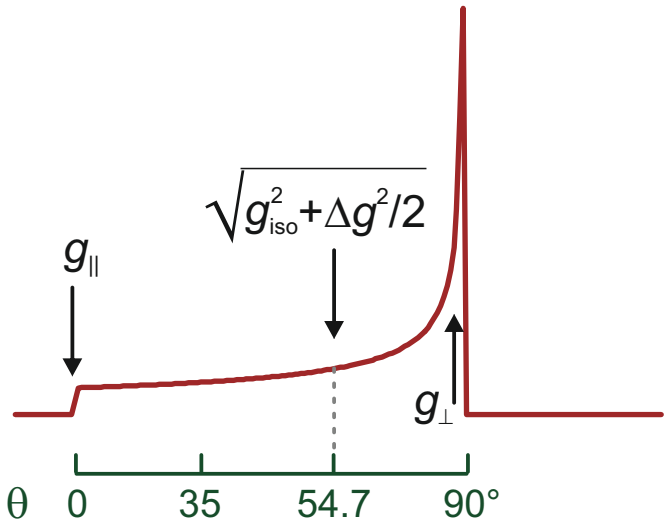

Powder lineshapes for pure electron Zeeman anisotropy

axial symmetry

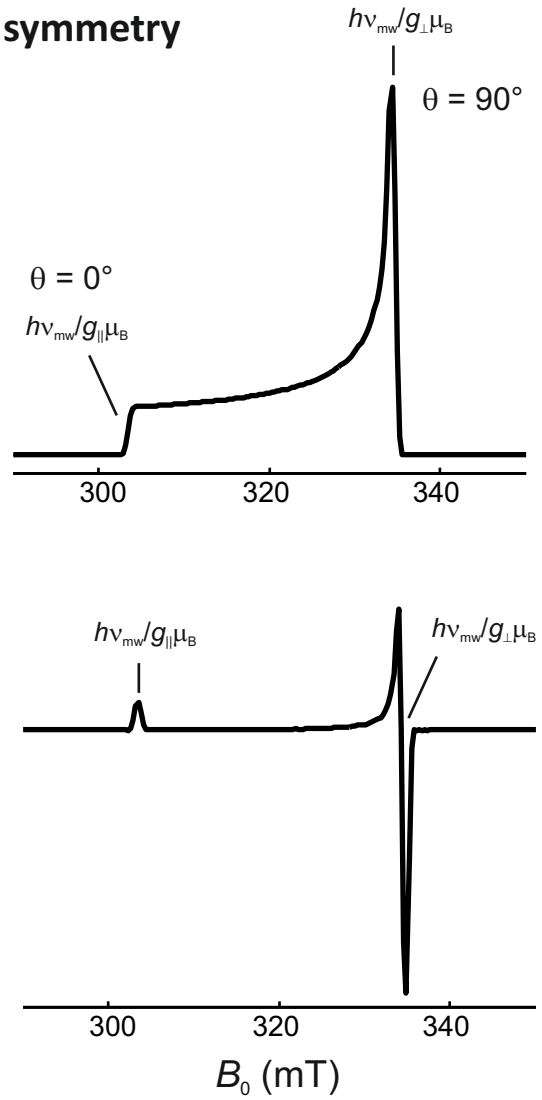

orthorhombic

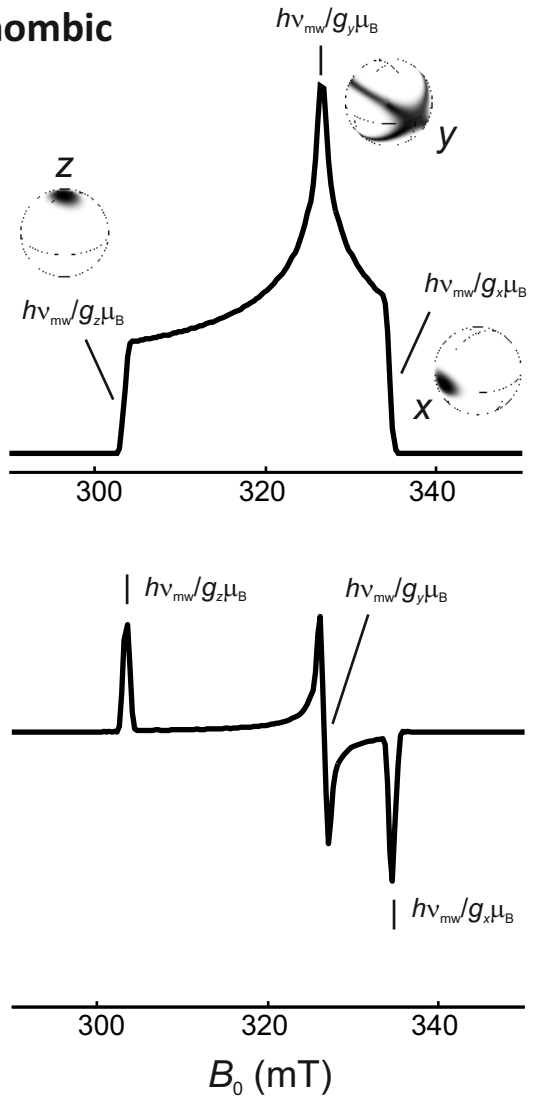

Different topology of typical NMR and EPR spin systems

NMR: a federalistic, democratic spin system

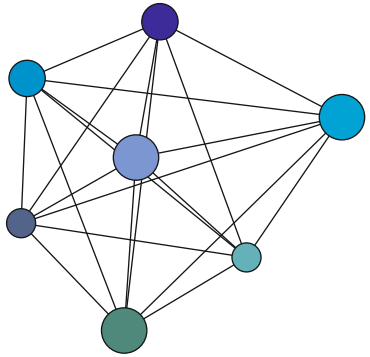

- everybody talks to everybody:
  lots of information, but difficult to disentangle

EPR: a centralistic electron spin dictatorship

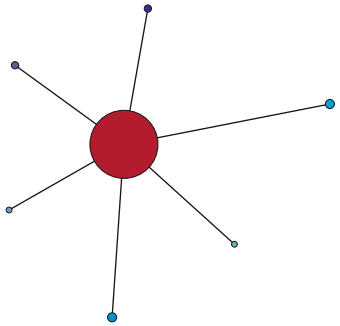

- at least one partner in a talk is an electron spin,
  often there is only one electron spin

Hyperfine coupling is simply...

...the dipole-dipole coupling between the magnetic moments of an electron and a nuclear spin

$$E = -\frac{\mu_0}{4\pi}\frac{1}{r_{12}^3}\left[\boldsymbol{\mu}_1 \cdot \boldsymbol{\mu}_2 - \frac{3}{r_{12}^2}\left(\boldsymbol{\mu}_1 \cdot \boldsymbol{r}_{12}\right)\left(\boldsymbol{\mu}_2 \cdot \boldsymbol{r}_{12}\right)\right]$$

$\mu_1 = \gamma_S \hbar S$ (spin angular momentum)

$\mu_2 = \gamma_I \hbar I$

$$\hat{H}_{\mathrm{dd}} = \frac{1}{r_{SI}^3}\frac{\mu_0 \hbar}{4\pi}\gamma_S\gamma_I\left[\hat{\boldsymbol{S}} \cdot \hat{\boldsymbol{I}} - 3\frac{1}{r_{SI}^2}\left(\hat{\boldsymbol{S}} \cdot \boldsymbol{r}_{SI}\right)\left(\hat{\boldsymbol{I}} \cdot \boldsymbol{r}_{SI}\right)\right]$$

(angular frequency units)

But there are complications...

- r_{SI} is zero at the cusp of *s* orbitals
- electron spin is, in general, distributed in space

...and simplifications in presence of a magnetic field

- spin 1/2 is generally aligned with external magnetic field
  - spin-orbit coupling of electron spins changes that
  - for nuclear spin > 1/2, quadrupole interaction changes that

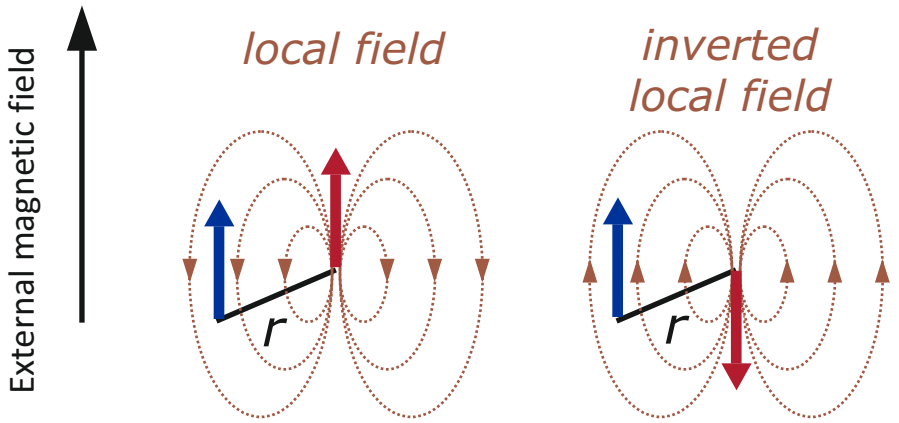

Where does isotropic hyperfine coupling come from?

Fermi contact interaction

$$a_{\mathrm{iso}} = \rho_s \cdot \frac{2}{3}\frac{\mu_0}{\hbar} g_e \mu_{\mathrm{B}} g_{\mathrm{n}} \mu_{\mathrm{n}} \left|\psi_0(0)\right|^2$$

- *Examples:* ^{1}H for $\rho_{1S} = 1$, $a_{\mathrm{iso}} = 1'420$ MHz

  ^{13}C for $\rho_{2S} = 1$, $a_{\mathrm{iso}} = 3'774$ MHz

  ^{19}F for $\rho_{2S} = 1$, $a_{\mathrm{iso}} = 52'831$ MHz

Table: J.R. MORTON, K.F. PRESTON, *J. Magn. Reson.* **1978**, *30*, 577

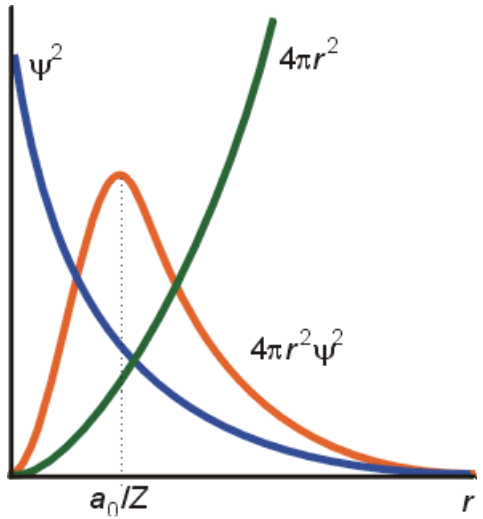

http://home.messiah.edu/~jmelton/361ch1.htm

Contributions to dipolar hyperfine coupling

Point-dipole approximation

- for negligible spin density in *p*, *d*, *f* atomic orbitals of the nucleus under consideration, in particular ^{1}H
- distribute electron spin to a set of points located at nuclei with significant spin density

$$\underline{T}_k = \frac{\mu_0}{4\pi\hbar} g_e \mu_B g_n \mu_n \sum_{j \neq k} \rho_j \frac{3\vec{n}_j \vec{n}_j^{\mathrm{T}} - \vec{1}}{R_j^3}$$

$\vec{n}_j$ unit vector from nucleus to j^{th} center of spin density

- always traceless, but purely axial only if sum runs over a single center *j*

Spin density in *p*, *d*, *f* orbitals of the nucleus under consideration

- often one orbital dominates, axial symmetry contribution
- uniaxial hyperfine constant per isotope, principal values (*T*, *T*, -2*T*)
- *Examples:* ^{13}C for ρ_p = 1, *T* = 107.3 MHz
  ^{19}F for ρ_p = 1, *T* = 628 MHz

Table: J.R. MORTON, K.F. PRESTON, *J. Magn. Reson.* **1978**, *30*, 577

McConnell equation

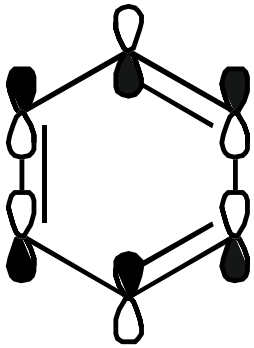

less **electrostatic repulsion** more

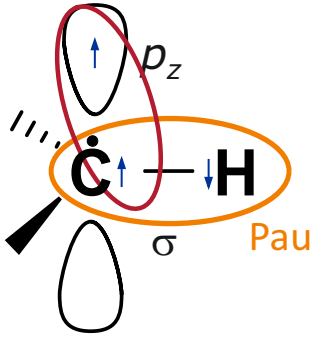

Pauli principle

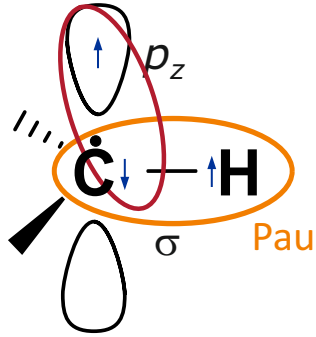

Pauli principle

slightly favoured ⇒ anticorrelation

of spin density on carbon and hydrogen

$$A_{iso,H} = Q_H \rho_\pi \qquad Q_H \approx -2.5 \text{ mT}$$

This is an effect of electron correlation - simple Hartree-Fock computations don't see it!

Characterization of aromatic systems by solution EPR

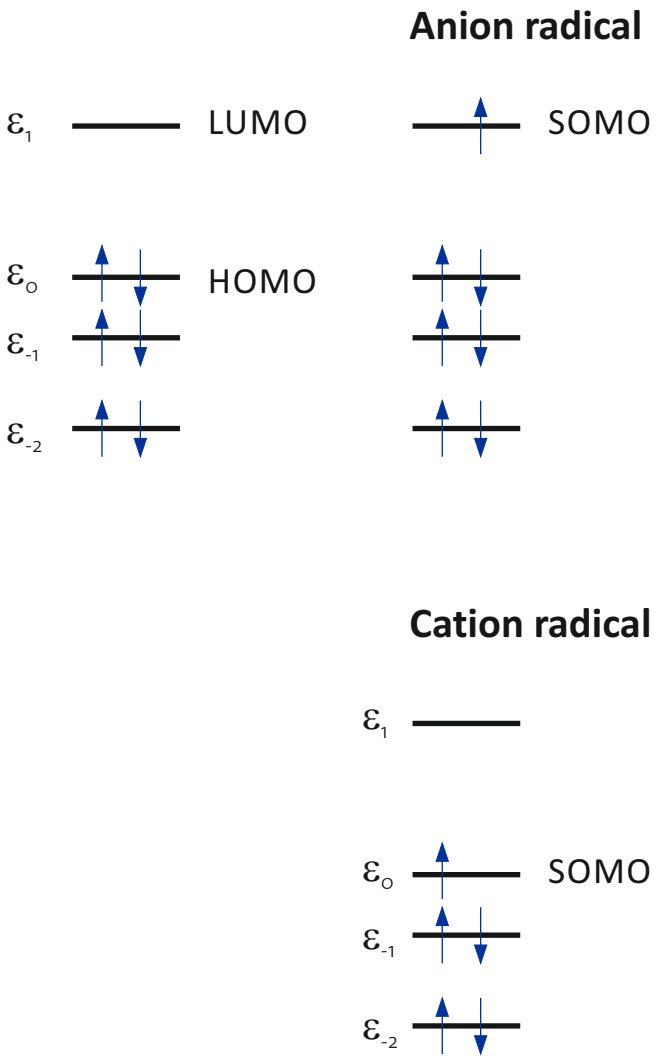

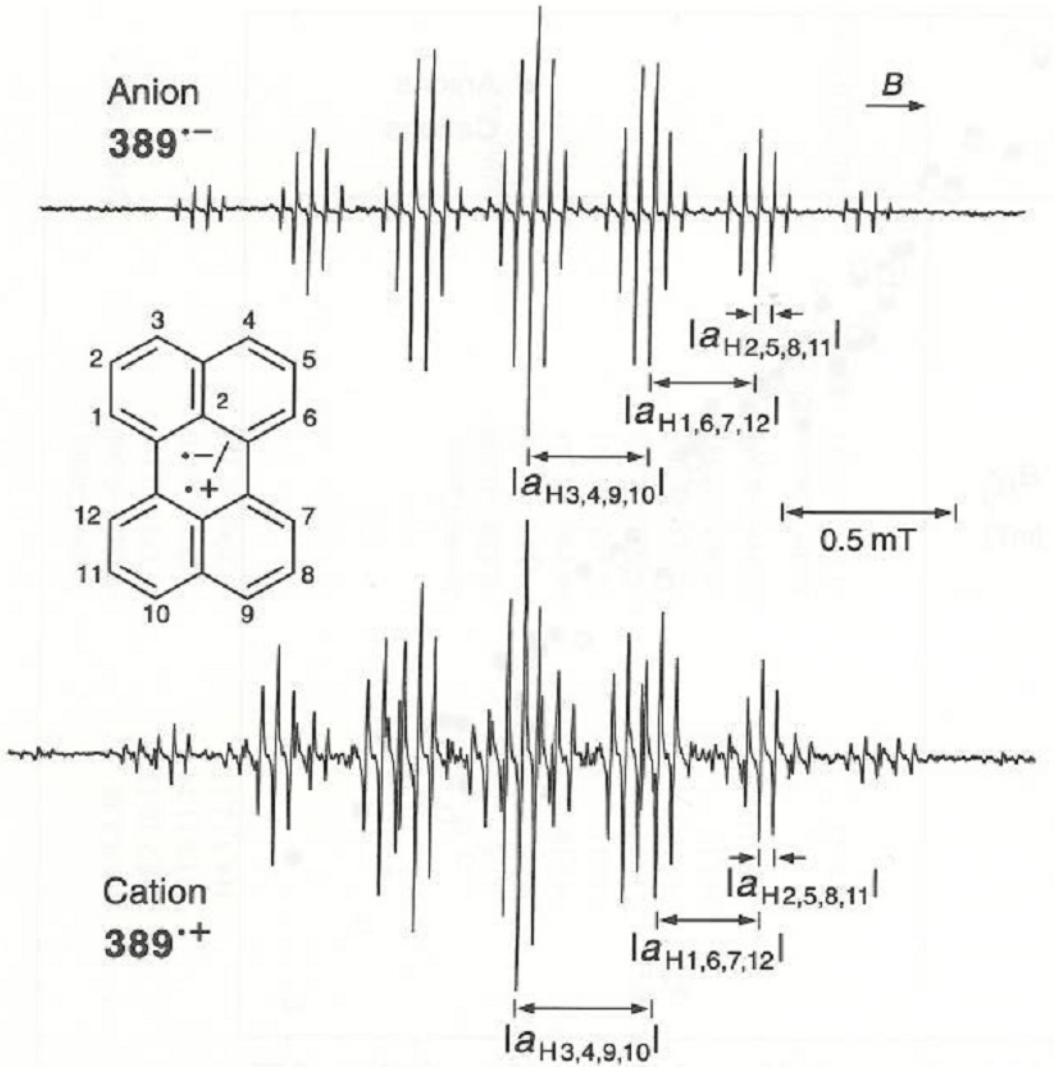

F. Gerson, W. Huber, *Electron Spin Resonance Spectroscopy of Organic Radicals*, Wiley-VCH, 2003

Hyperconjugation

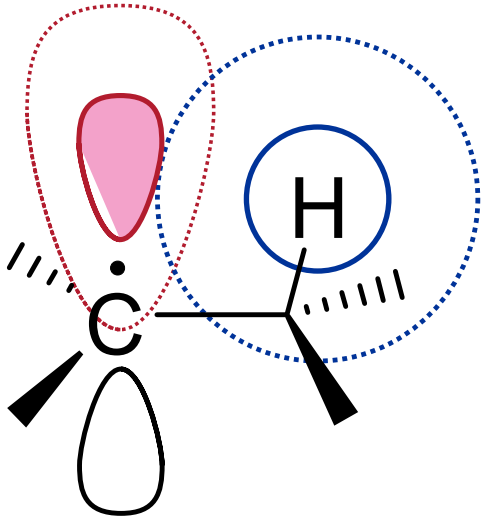

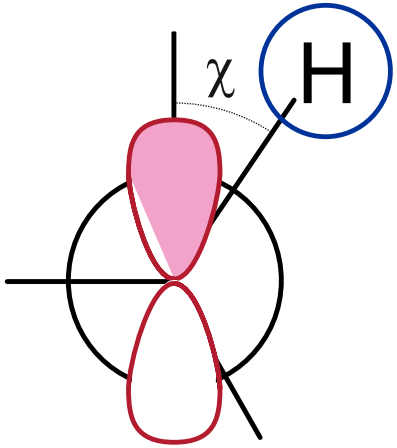

Manifestation of hyperfine couplings in EPR spectra

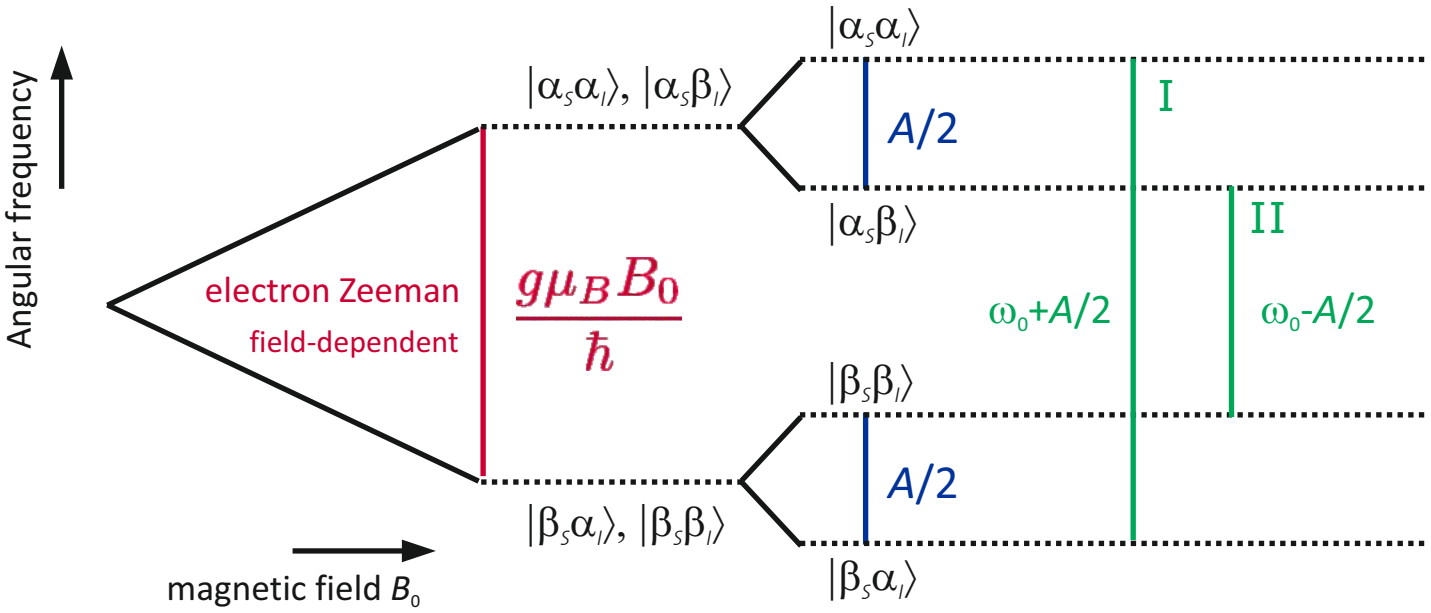

- level shift by hyperfine interaction:
  $m_S m_I A$
- selection rules:
  $|\Delta m_S| = 1$, $\Delta m_I = 0$

Field-swept EPR spectrum

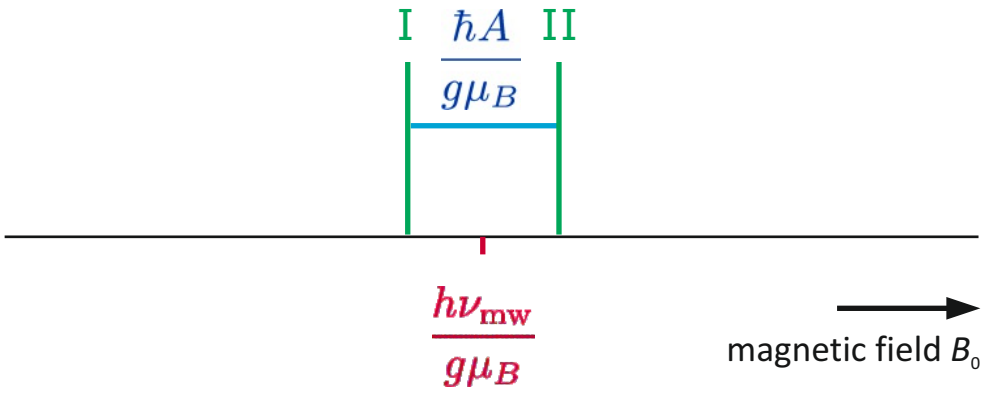

- be aware: hyperfine couplings are given in
  - field units (G, mT)
  - frequency units (MHz, $A/2\pi$)
  - wave numbers (cm^{-1}, $A/2\pi c$)

  1 G = 0.1 mT ≈ 2.8 MHz ≈ 10^{-4} cm^{-1} (at $g=g_e$)

Hyperfine multiplets in solution

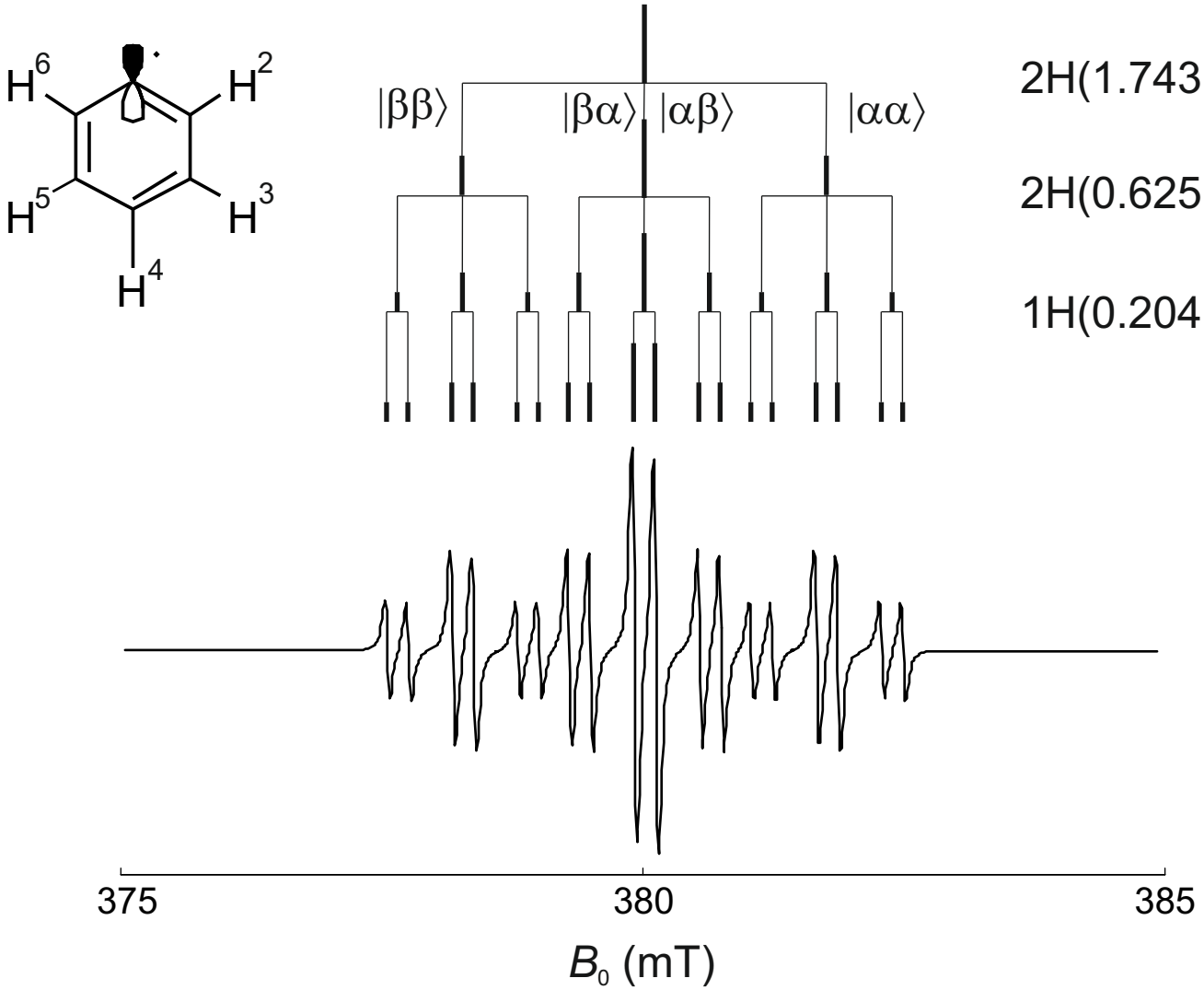

Hyperfine multiplets in solution (II)

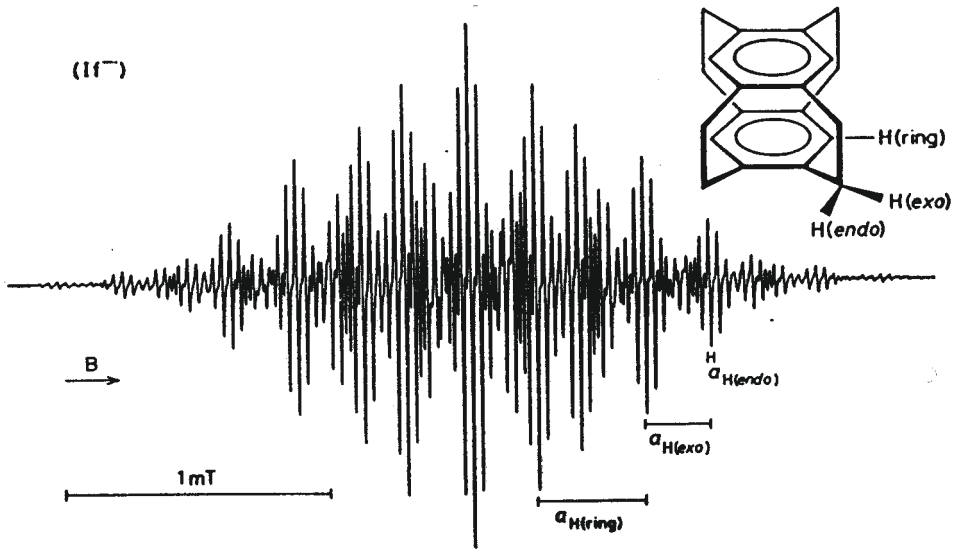

4 equivalent aromatic protons

8 equivalent *exo* protons

8 equivalent *endo* protons

5·9·9 = 405 lines

$$n_{EPR} = \prod_{i} (2\,k_i\,I_i + 1)$$

multiplicity

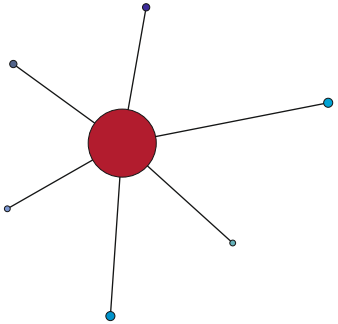

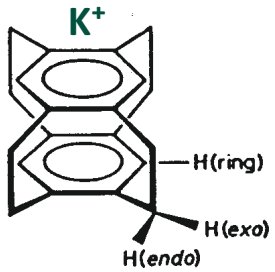

+ ^{39}K (I = 3/2)

2×2 equivalent aromatic protons

2×4 equivalent *exo* protons

2×4 equivalent *endo* protons

4·3·3·5·5·5·5 = 22'500 lines

Manifestation of hyperfine couplings in nuclear frequency spectra

ENDOR and ESEEM

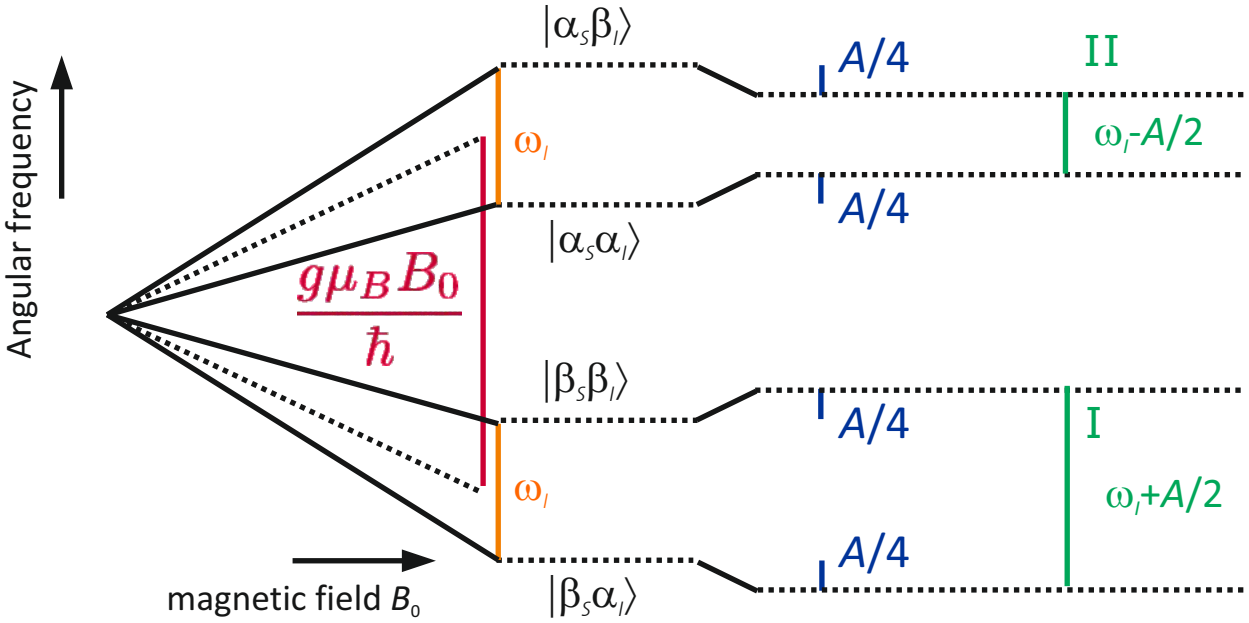

- selection rules: $\Delta m_s = 0$, $|\Delta m_I| = 1$
- ω_I is characteristic for a given element and isotope

ENDOR spectra *S*=1/2, *I*=1/2 for weak coupling ($A/2 < \omega_I$)

Liquid or single orientation

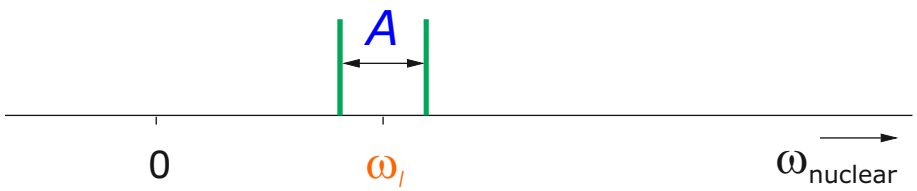

For strong coupling, one line is ‘mirrored’ at zero frequency

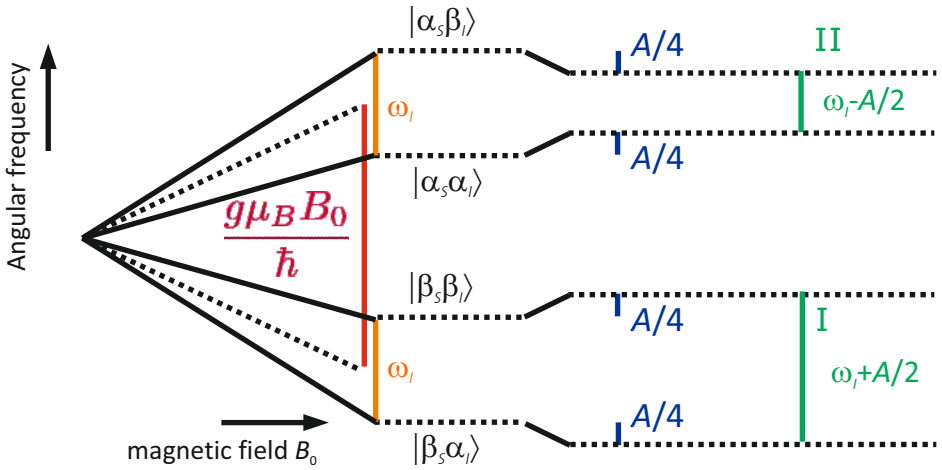

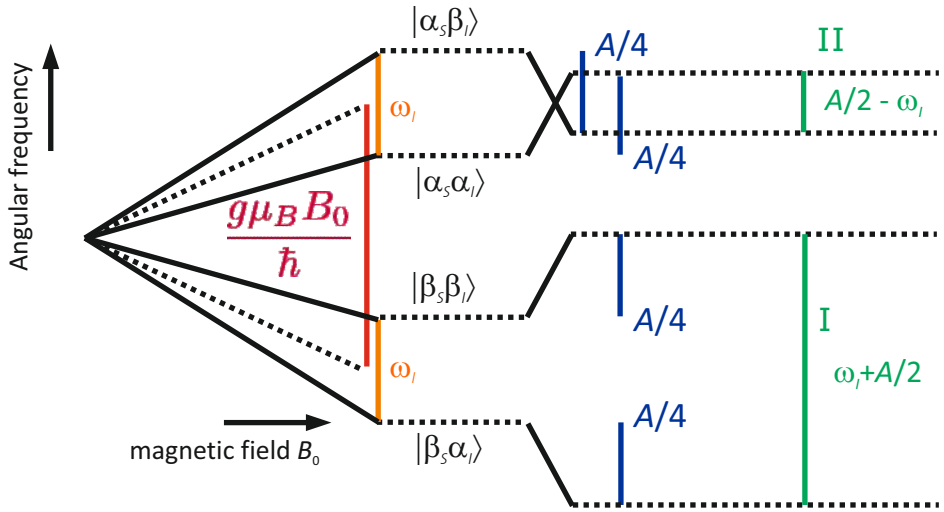

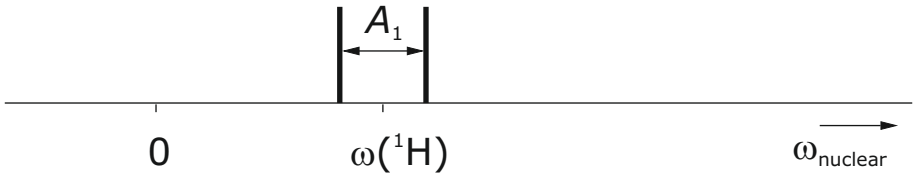

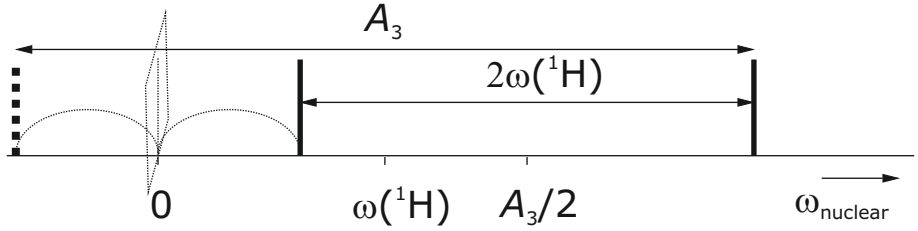

Comparison of EPR and ENDOR spectra

$$n_{\mathrm{EPR}} = \prod_i (2k_i I_i + 1)$$

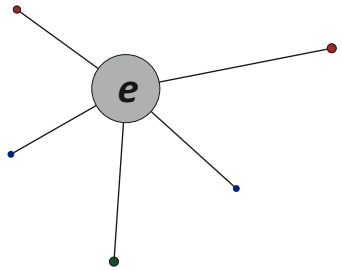

$$n_{\mathrm{NMR,liq}} = \sum_i 2S + 1 \qquad n_{\mathrm{NMR,sol}} = \sum_i 2I_i\,(2S + 1)$$

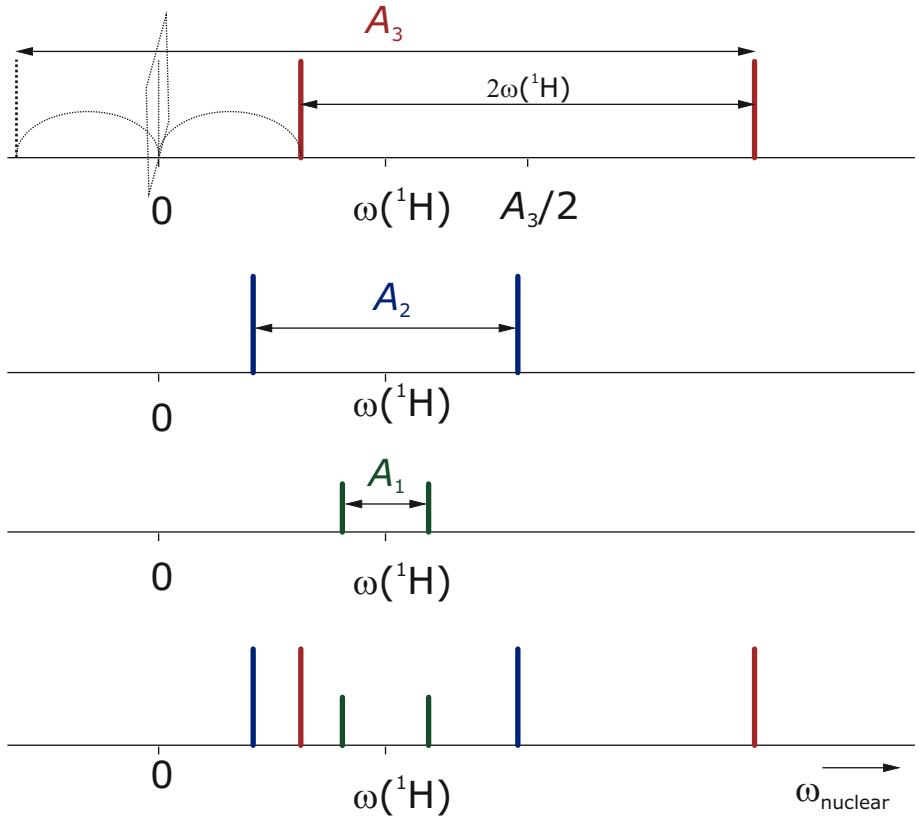

$$\omega = |\omega_I + A_{\mathrm{eff}}/2|$$

Comparison of EPR and ENDOR spectra

Real-life example

recently seen in our lab

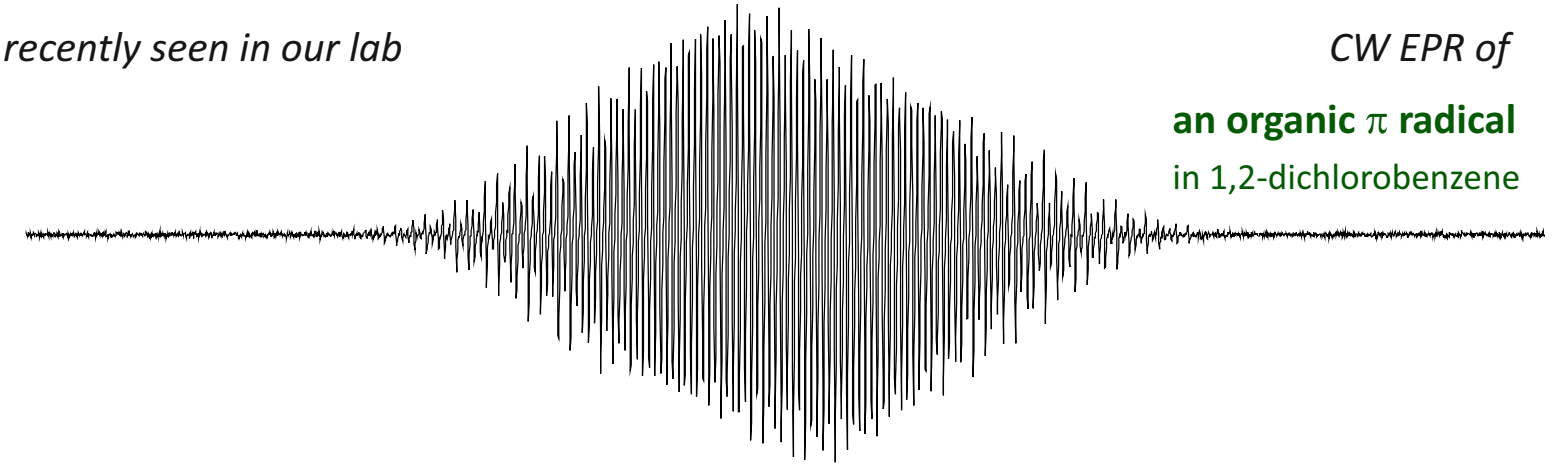

CW EPR of

an organic π radical

in 1,2-dichlorobenzene

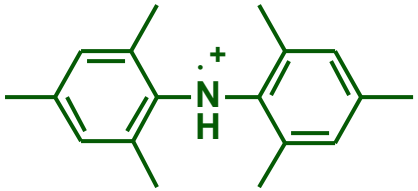

sample courtesy Agnes Kütt, University of Tallinn

Mims ENDOR

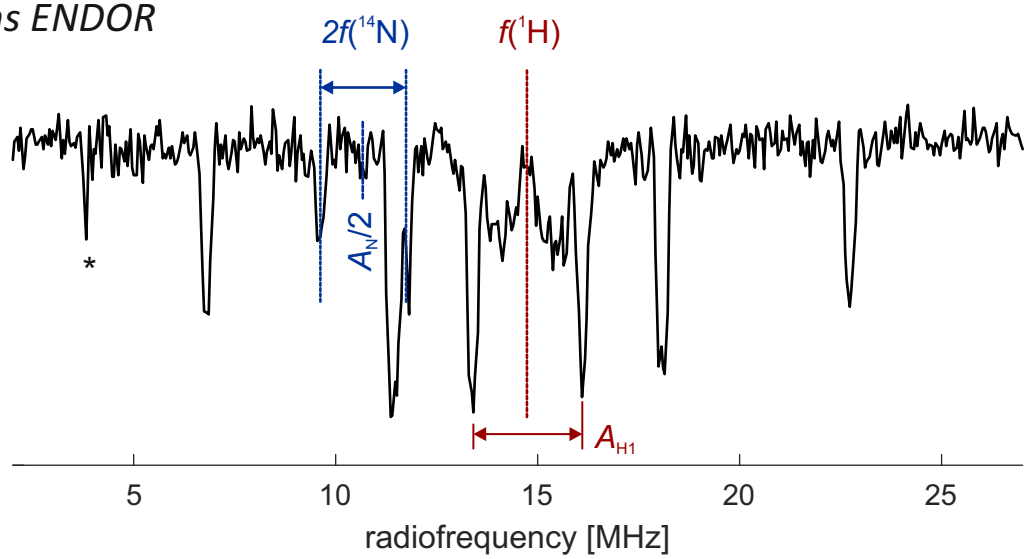

⊕ identity of the nuclei (^{1}H, ^{14}N)

⊕ direct read-off of hyperfine couplings

Powder spectra in the absence of hyperfine coupling

Repetition

Absorption spectra

(echo detected EPR)

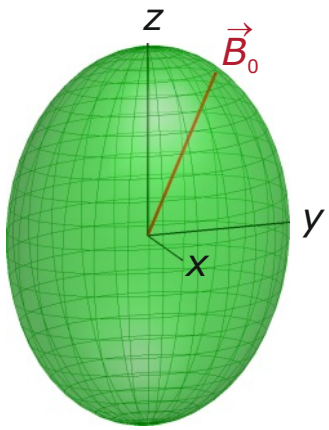

First derivative

(CW EPR)

axial symmetry

$\omega(\theta) \propto 3\cos^2\theta - 1$

$p(\theta) \propto \sin\theta$

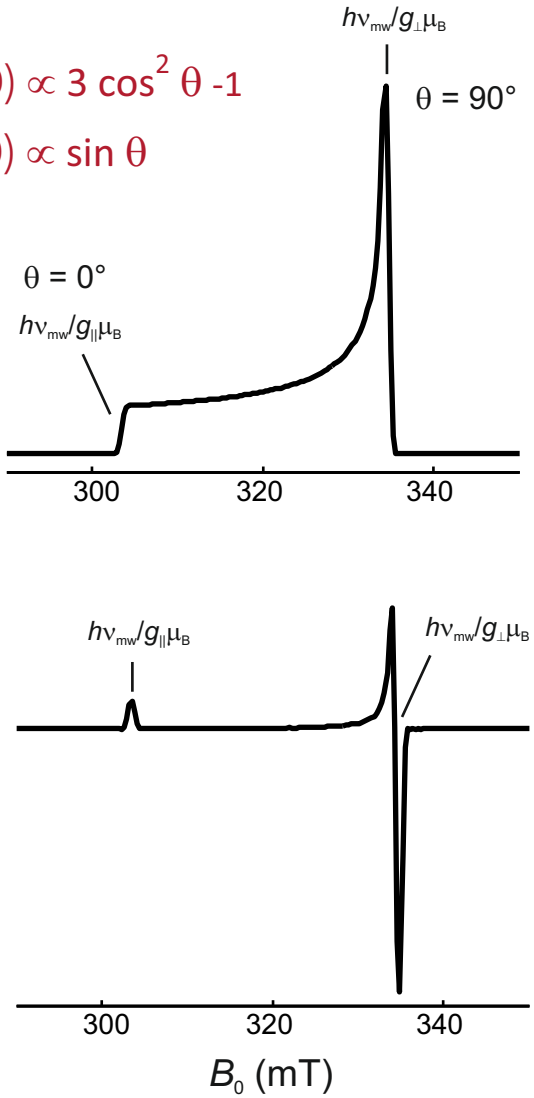

orthorhombic

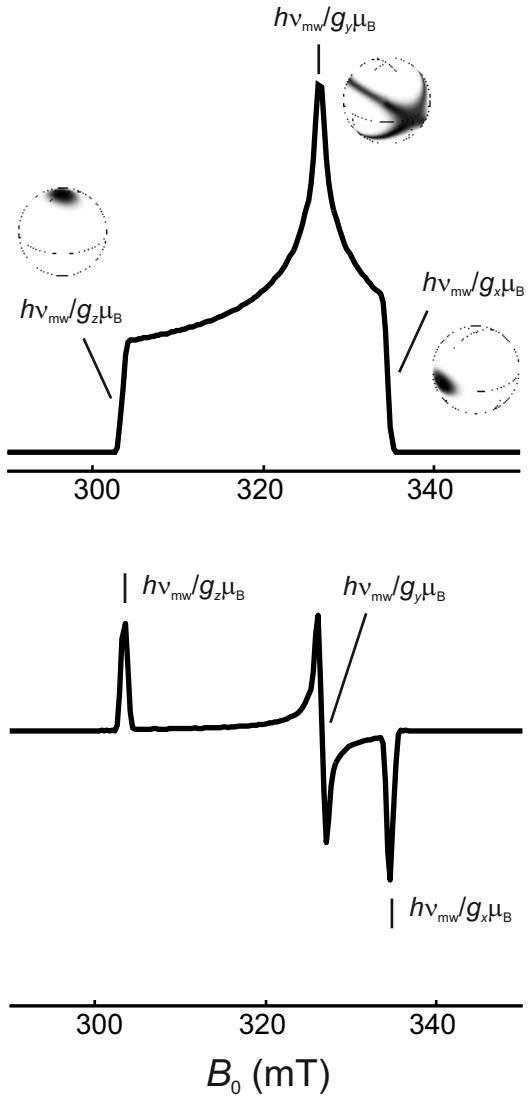

Manifestation of hyperfine couplings in EPR powder spectra

Example: Cu(II), S =1/2, I = 3/2, axially symmetric g- and hyperfine tensor

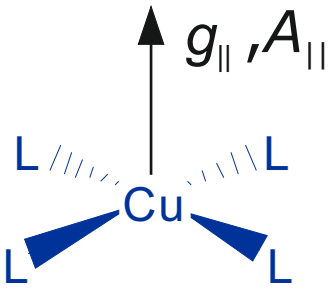

Spectra of individual nuclear states

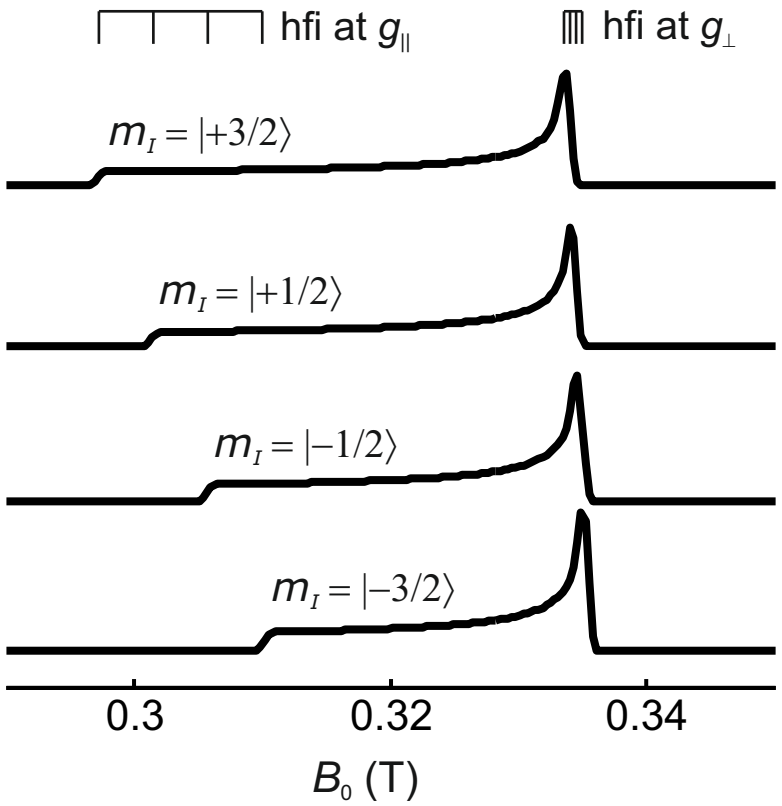

Total spectrum

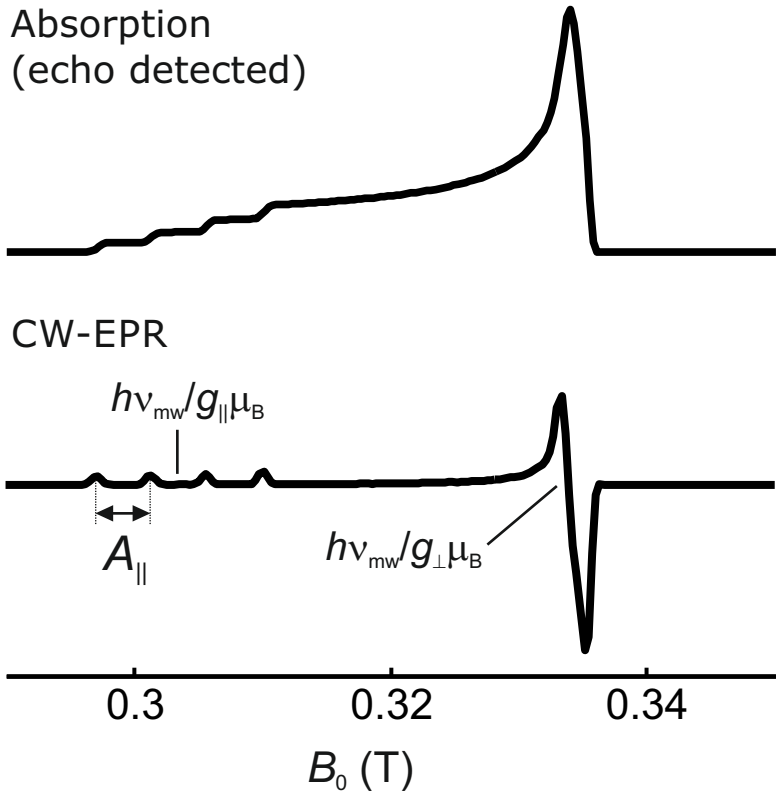

Solid-state nuclear frequency spectra

$A_{iso} > 0$, weak coupling

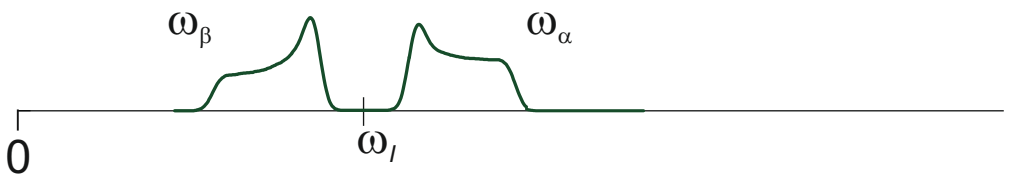

$A_{iso} < 0$, weak coupling

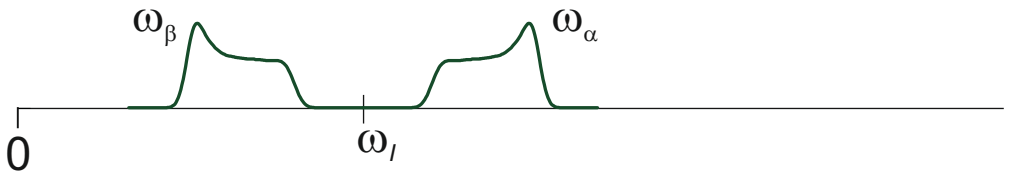

$A_{iso} > 0$, strong coupling

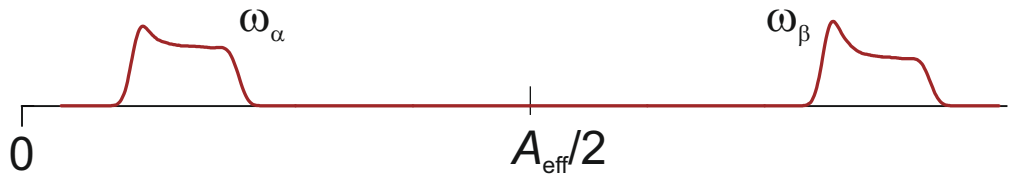

$A_{iso} < 0$, strong coupling

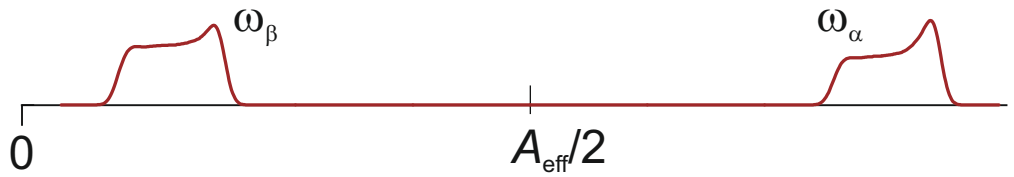

Manifestation of exchange coupling in the presence of hyperfine coupling

Example:

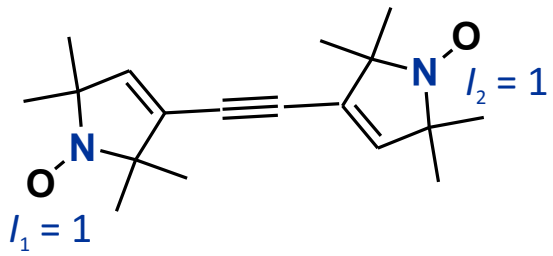

Simulated spectra for different exchange/hyperfine ratios

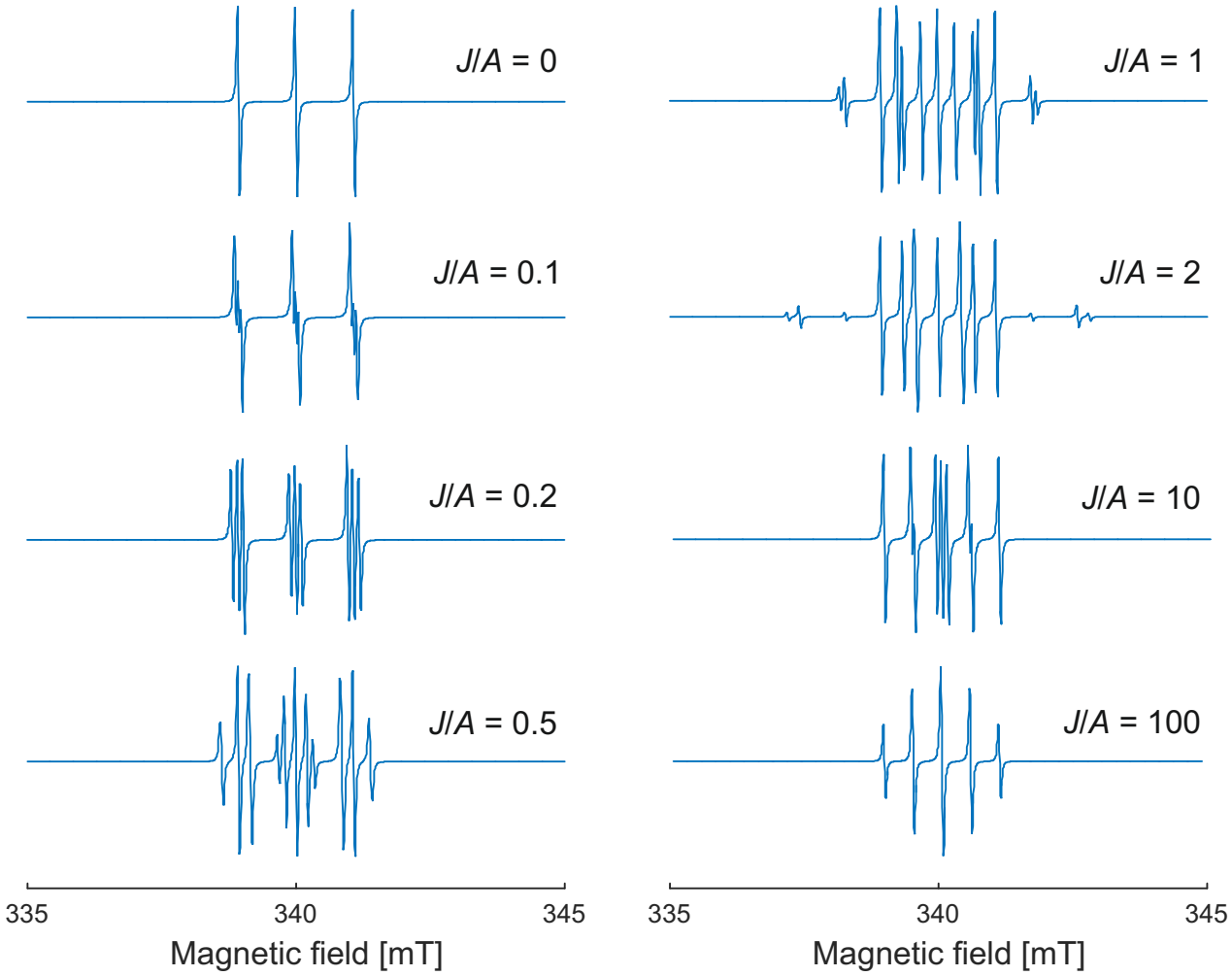

Two-spin system and the electron-electron coupling

Like spins 1/2 (two electrons)

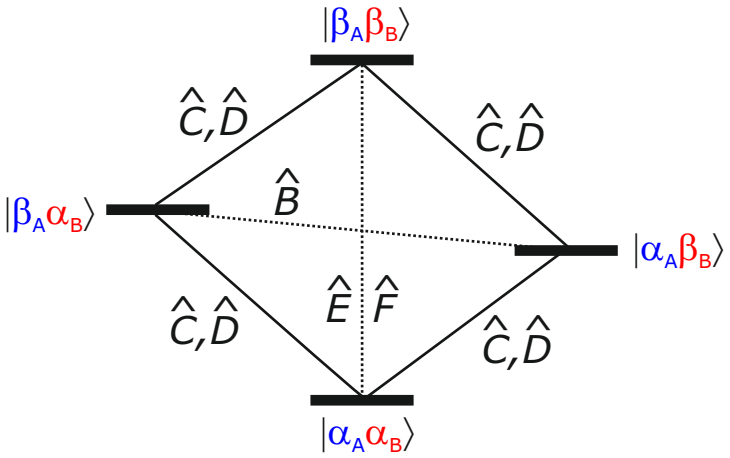

$$\mathcal{H}_0 = \omega_A S_{Az} + \omega_B S_{Bz} + \mathcal{H}_{dd} + J(S_x I_x + S_y I_y + S_z I_z)$$

$$S_x I_x + S_y I_y = ½(S^+ I^- + S^- I^+)$$

Weak coupling

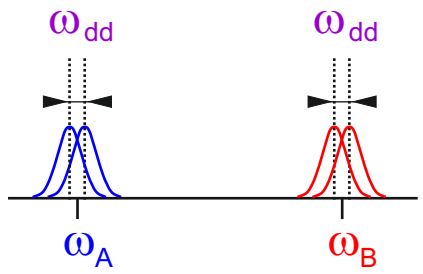

Strong coupling

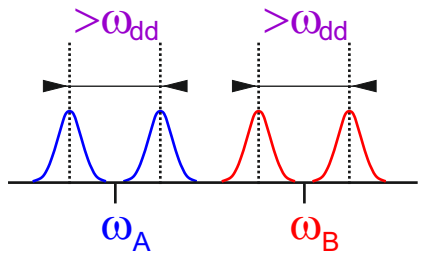

Dipolar alphabet $\hat{\mathcal{H}}_{dd} = \frac{1}{r_{SI}^3}\frac{\mu_0\hbar}{4\pi}\gamma_S\gamma_I\left[\hat{A}+\hat{B}+\hat{C}+\hat{D}+\hat{E}+\hat{F}\right]$

secular $\hat{A} = \hat{S}_z\hat{I}_z\left(1-3\cos^2\theta\right)$,

pseudo-secular $\hat{B} = -\frac{1}{4}\left[\hat{S}^+\hat{I}^- + \hat{S}^-\hat{I}^+\right]\left(1-3\cos^2\theta\right)$

non-secular $\hat{C} = -\frac{3}{2}\left[\hat{S}^+\hat{I}_z + \hat{S}_z\hat{I}^+\right]\sin\theta\cos\theta e^{-i\phi}$,

non-secular $\hat{D} = -\frac{3}{2}\left[\hat{S}^-\hat{I}_z + \hat{S}_z\hat{I}^-\right]\sin\theta\cos\theta e^{i\phi}$,

non-secular $\hat{E} = -\frac{3}{4}\hat{S}^+\hat{I}^+\sin^2\theta e^{-2i\phi}$,

non-secular $\hat{F} = -\frac{3}{4}\hat{S}^-\hat{I}^-\sin^2\theta e^{-2i\phi}$.

G. JESCHKE, H. W. SPIESS, Lect. Notes Phys. 2006, 684, 21-63.

How the Pake pattern arises

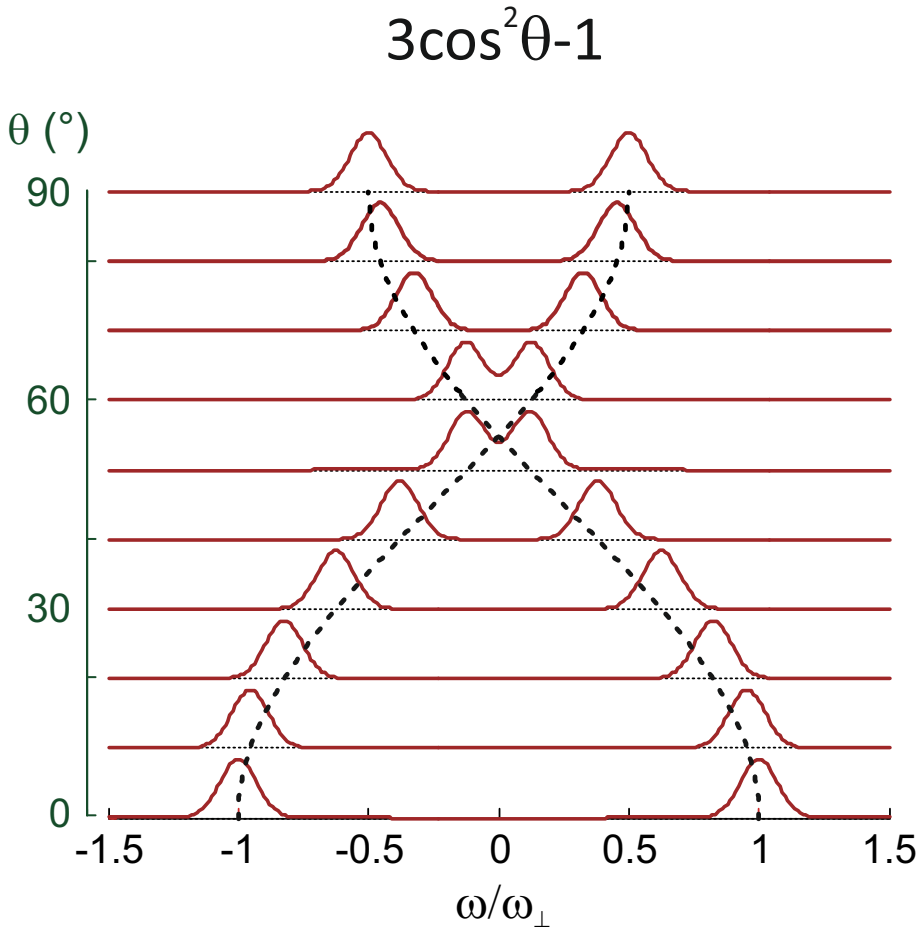

$P(\theta) \propto \sin\theta$

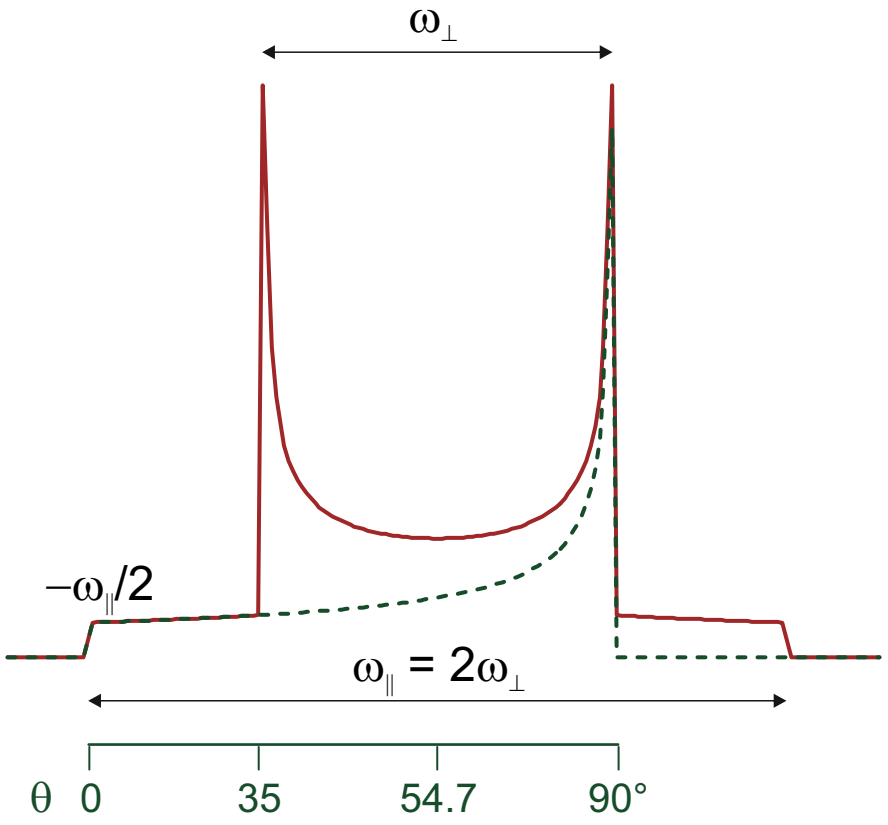

High-spin systems

Example: $3d^5$ (Fe^{3+})

Isolated ion
(Hund's rule)

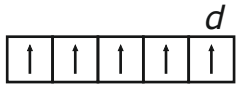

$S = 5/2$

Weak ligand field
(high-spin case)

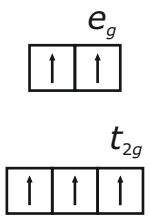

as in $[FeF_6]^{3-}$

$S = 5/2$

Strong ligand field
(low-spin case)

as in $[Fe(CN)_6]^{3-}$

$S = 1/2$

Large zero-field splitting effective spin $S' = 1/2$
$E/D = 0$

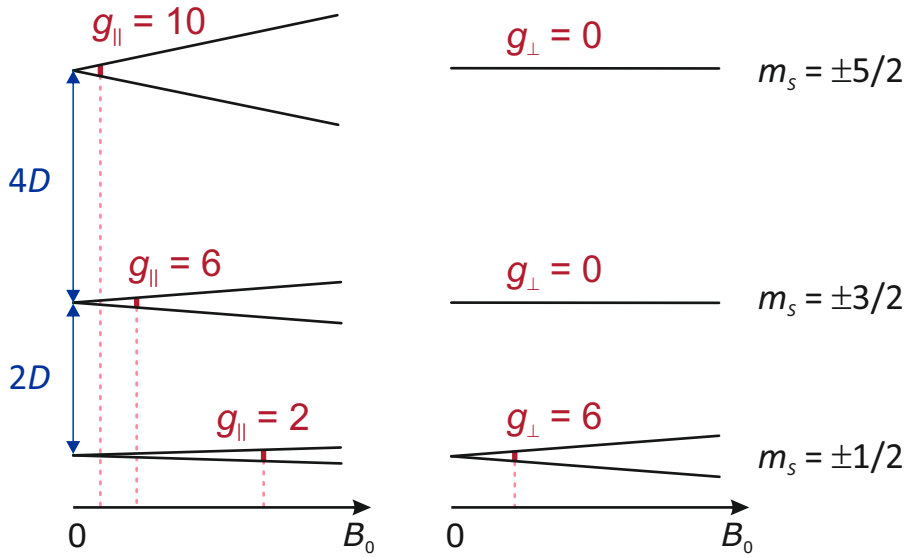

- high-spin and low-spin iron have very different *g* tensors

⇒ EPR is a reliable technique for determining the spin state

- for $E/D = 1/3$, zero-field splittings are 3.53 D and the $m_s = \pm 3/2$ pair has an isotropic effective *g* value of 4.3

Spectra for triplet species (S = 1)

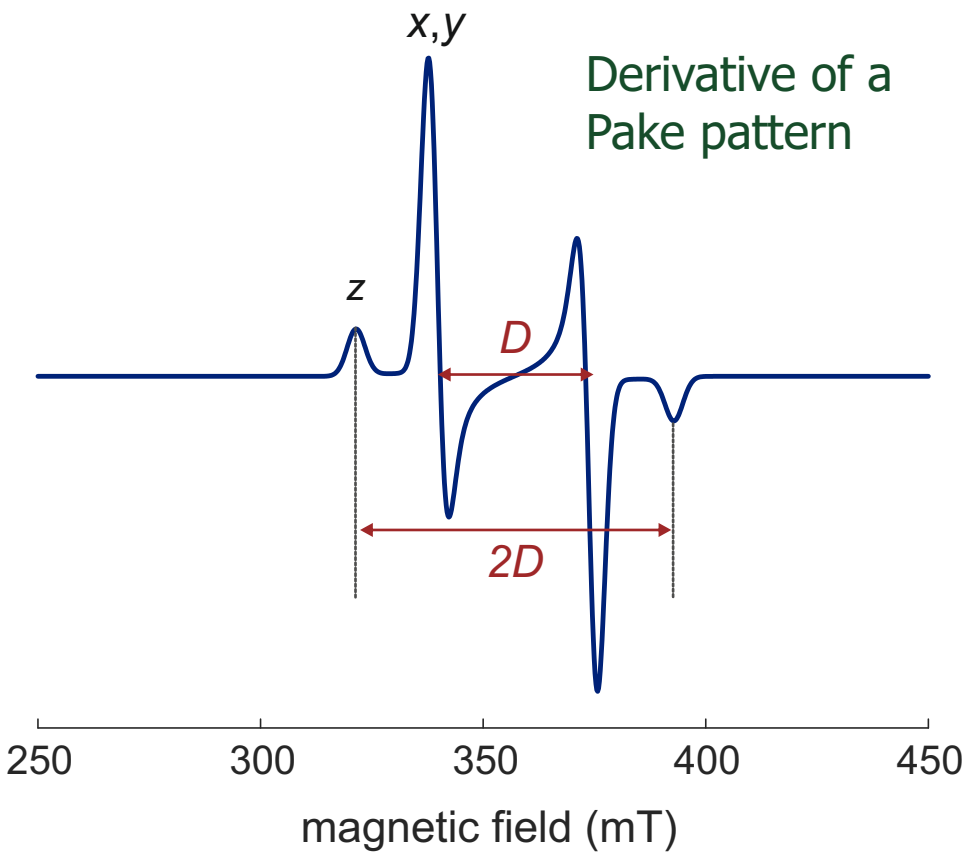

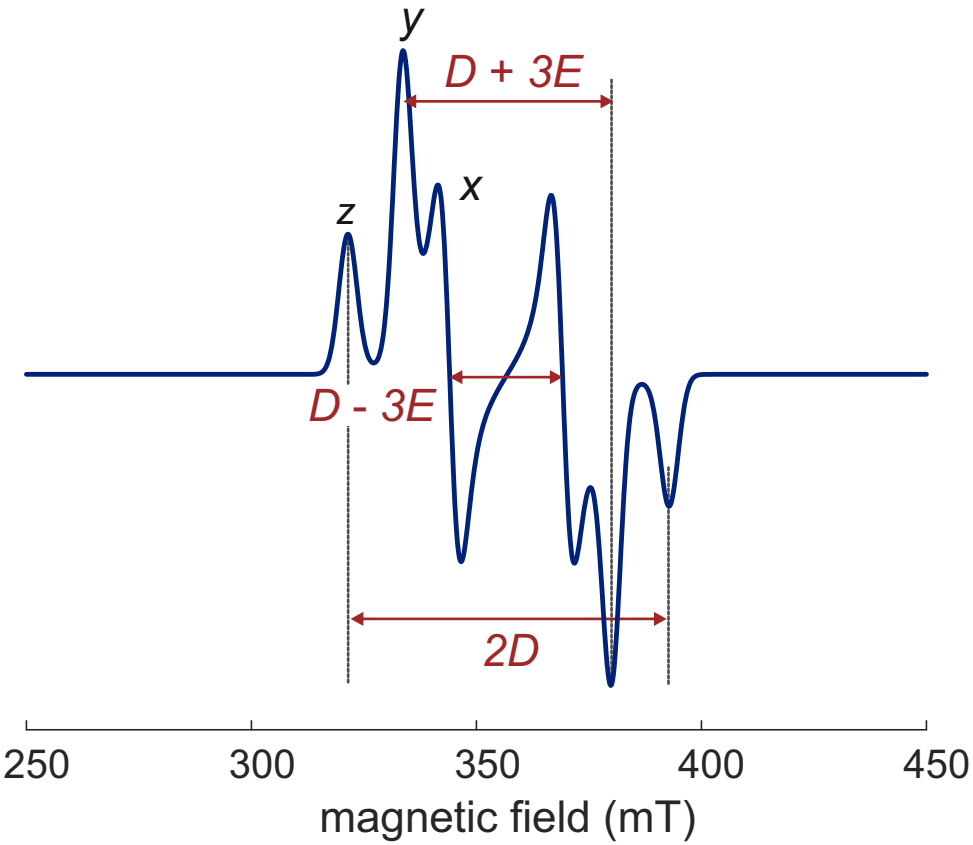

D = 1000 MHz
E = 0 MHz

D = 1000 MHz
E = 100 MHz

Forbidden electron-nuclear transitions

Selection rules do not strictly apply

$$\hat{H}_{\mathrm{dd}} = \omega_{\mathrm{dd}} \left[\underbrace{\left(1 - 3\cos^2\theta\right) \hat{S}_z \hat{I}_z}_{A} - \underbrace{3\sin\theta\cos\theta \hat{S}_z \hat{I}_x}_{B} \right]$$

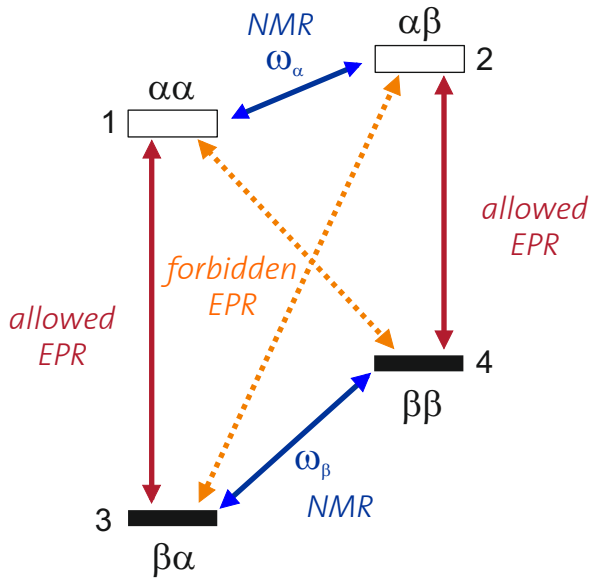

Local fields at the nuclear spin

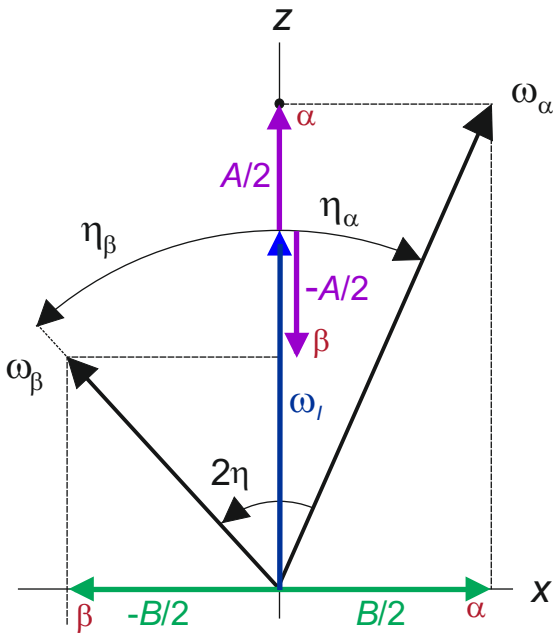

- nuclear spin quantization axis not parallel to B_0
- nuclear spin quantization axis depends on electron spin state

EPR spectrum (schematic)

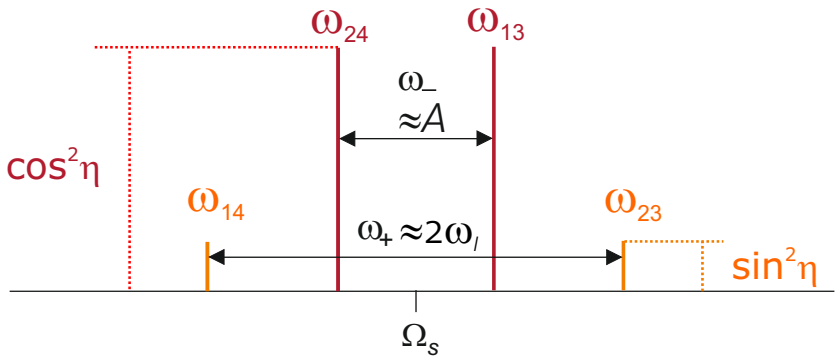

Continuous-wave EPR measurements - Detection

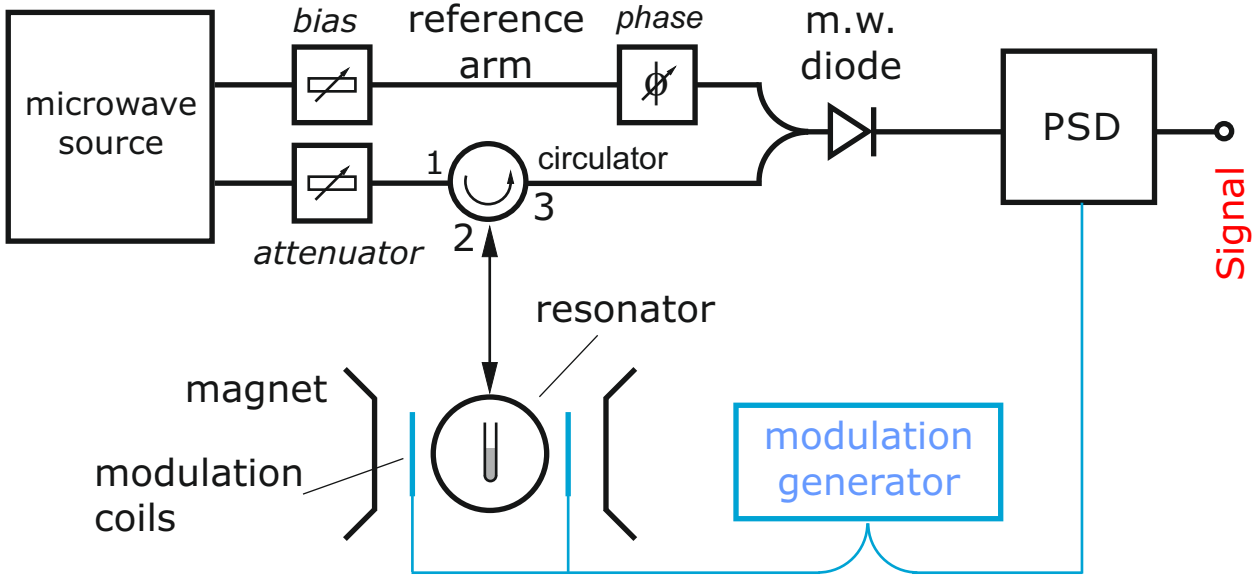

Field modulation

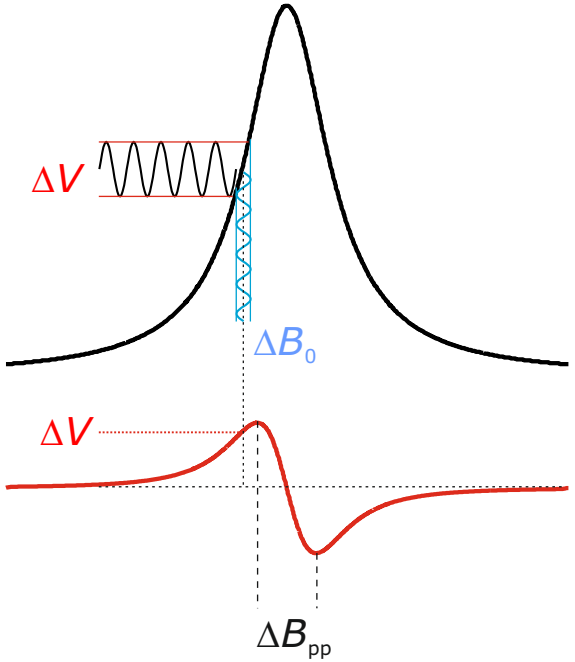

Characteristic curve of an m.w. diode

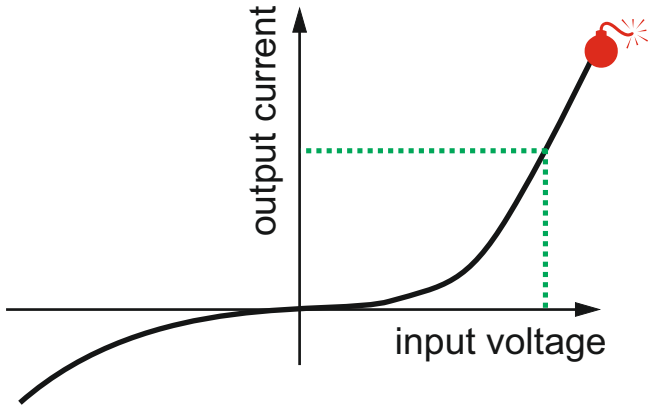

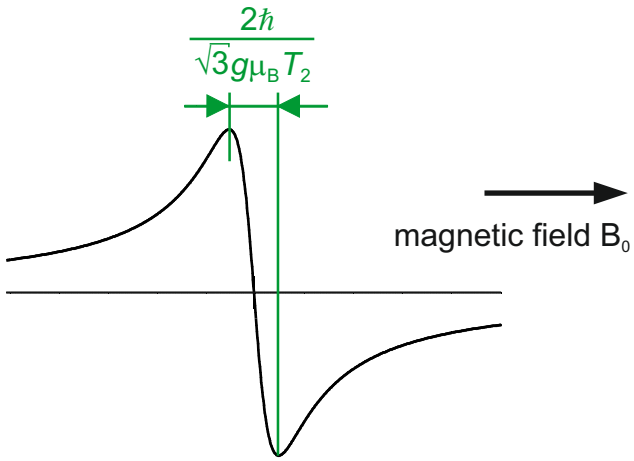

Relaxation via collisional exchange

Diffusing paramagnetic species

before **during** **and after**

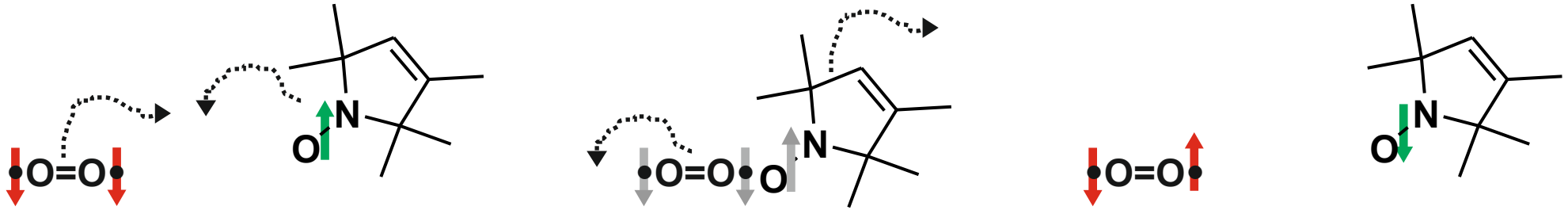

observer spin up ↑

electrons in overlapping orbitals are indistinguishable

observer spin down ↓

collision

$\Rightarrow$ relaxation time T_1 decreases with increasing exchange rate W_{ex}

- most easily detected via saturation curves (CW EPR)

$$\Delta P_{1/2} \propto W_{ex}/T_{2e}$$

ALTENBACH et al., *Proc. Natl. Acad. Sci. USA* **91**, 1667-1671 (1994)

Oxygen accessibility measurement in plant light harvesting complex

Accessibility measurements via relaxation enhancement

Spin-labeled major plant light harvesting complex II (V229C labeled with IA-Proxyl)

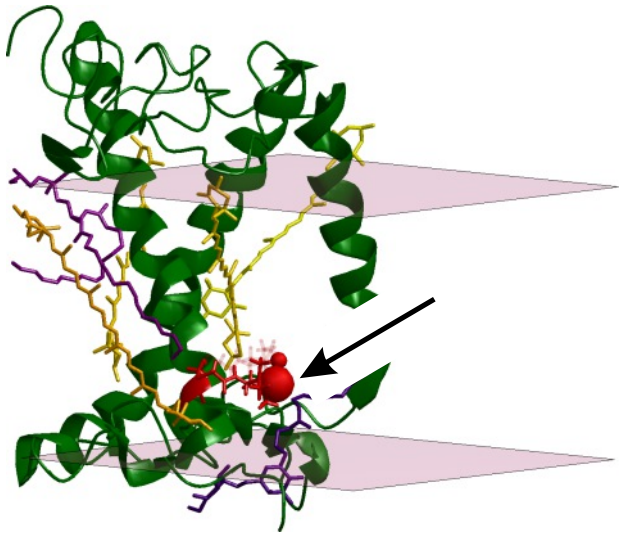

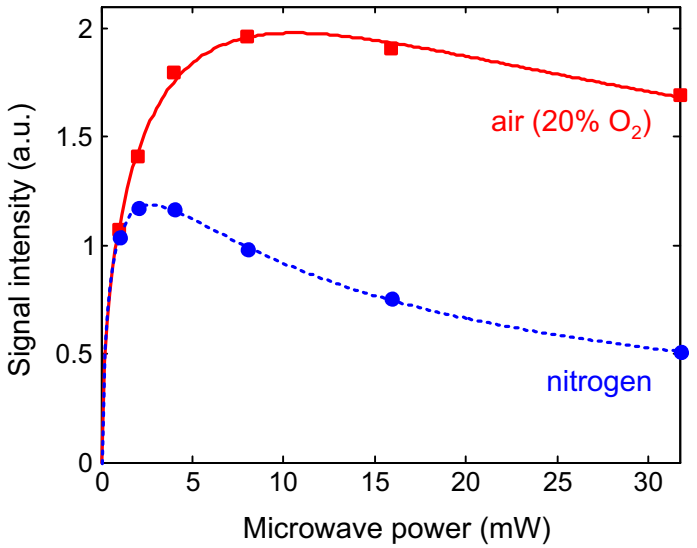

Measuring hyperfine couplings

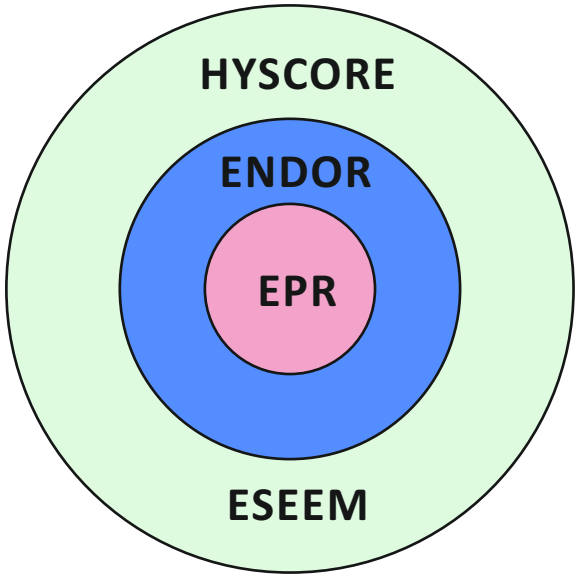

Example: Cu(II) in a protein

Remote nuclei:
ENDOR, ESEEM & HYSCORE
(nuclear Zeeman, hyperfine nuclear quadrupole)

Directly coordinated nuclei:
EPR & ENDOR
(nuclear Zeeman, hyperfine nuclear quadrupole)

Transition metal ion:
EPR
(g tensor,
metal hyperfine coupling)

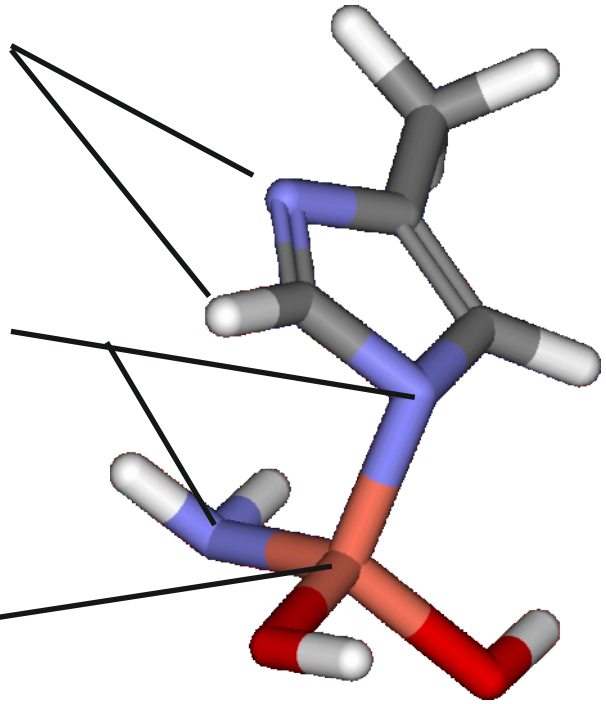

Thermal electron and nuclear spin polarization

Boltzmann distribution

populations: $p_\alpha = \exp(-g_e\mu_B B_0/2kT)/Z$ $p_\beta = \exp(g_e\mu_B B_0/2kT)/Z$ partition function: $Z = \exp(-g_e\mu_B B_0/2kT) + \exp(g_e\mu_B B_0/2kT)$

High-temperature approximation: $g_e m_B B_0 << kT$

$p_\alpha = 1-\varepsilon$ $p_\beta = 1+\varepsilon$ $\varepsilon_e = g_e\mu_B B_0/2kT$ polarization: 2ε

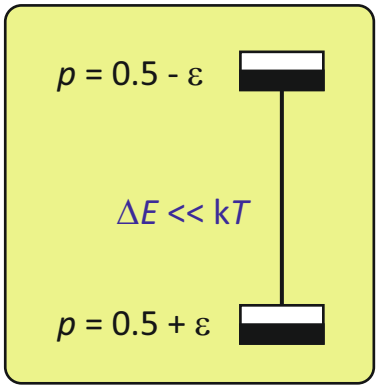

- polarization is much smaller for nuclear spins due to lower resonance frequency at the same field (factor >660)

Consequence: NMR is much less sensitive

Approximation:

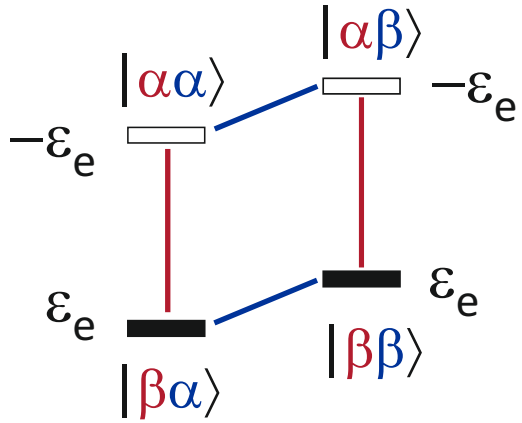

Davies ENDOR

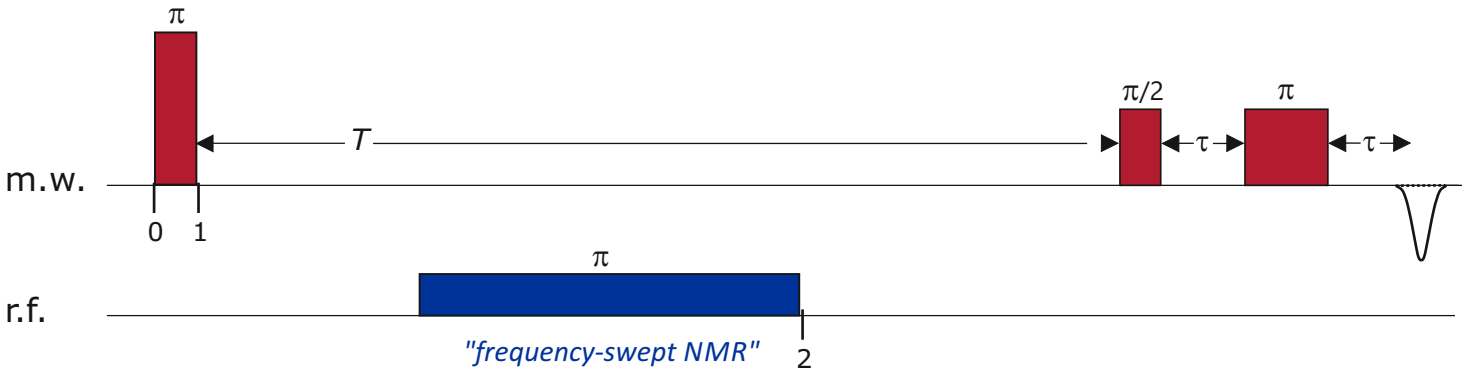

thermal equilibrium

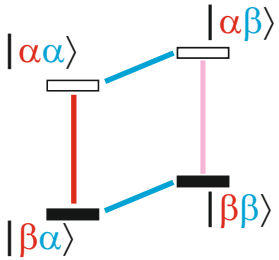

before r.f. pulse

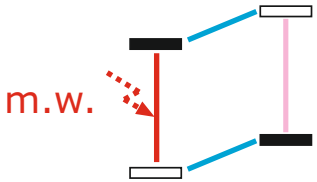

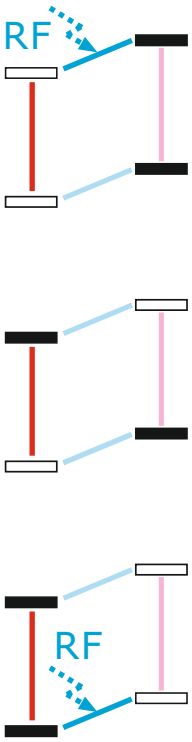

after r.f. pulse

Davies ENDOR

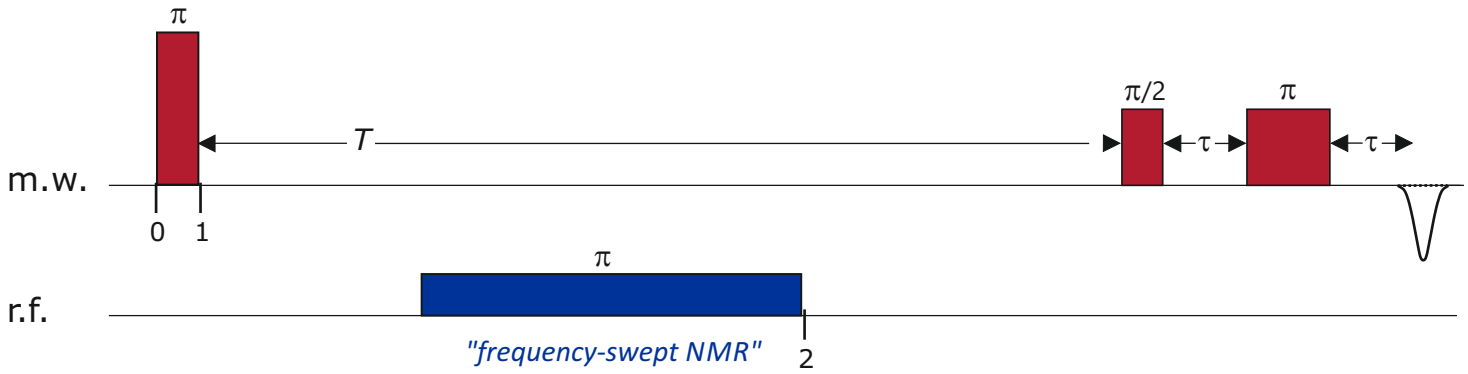

Inhomogeneous line & hole burning

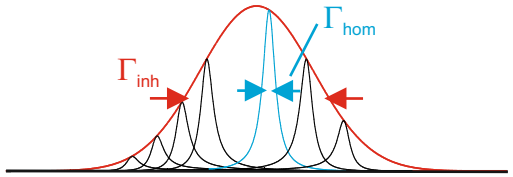

thermal equilibrium

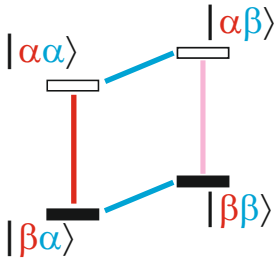

before r.f. pulse

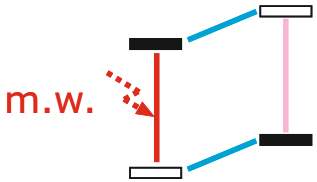

hole pattern

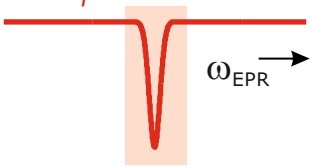

detection bandwidth

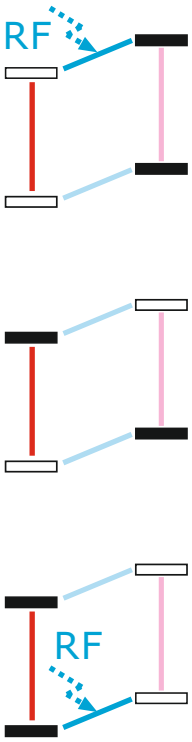

after r.f. pulse

hole pattern

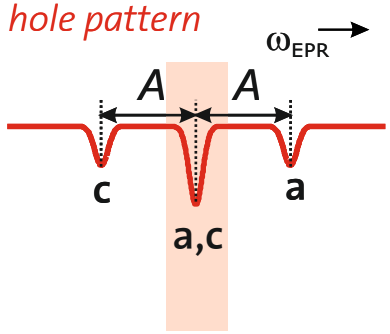

detection bandwidth

Hyperfine contrast selectivity in Davies ENDOR

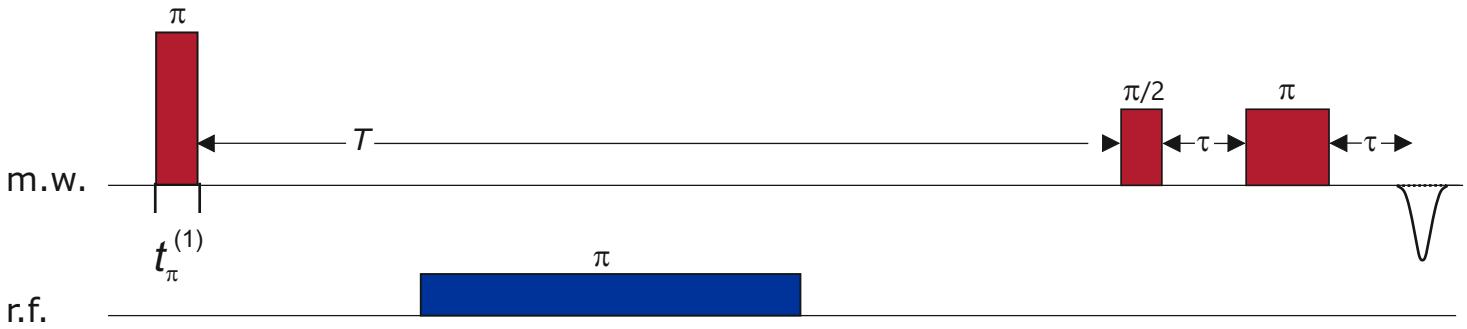

$t_\pi^{(1)}$ = 400 ns

$t_\pi^{(1)}$ = 20 ns

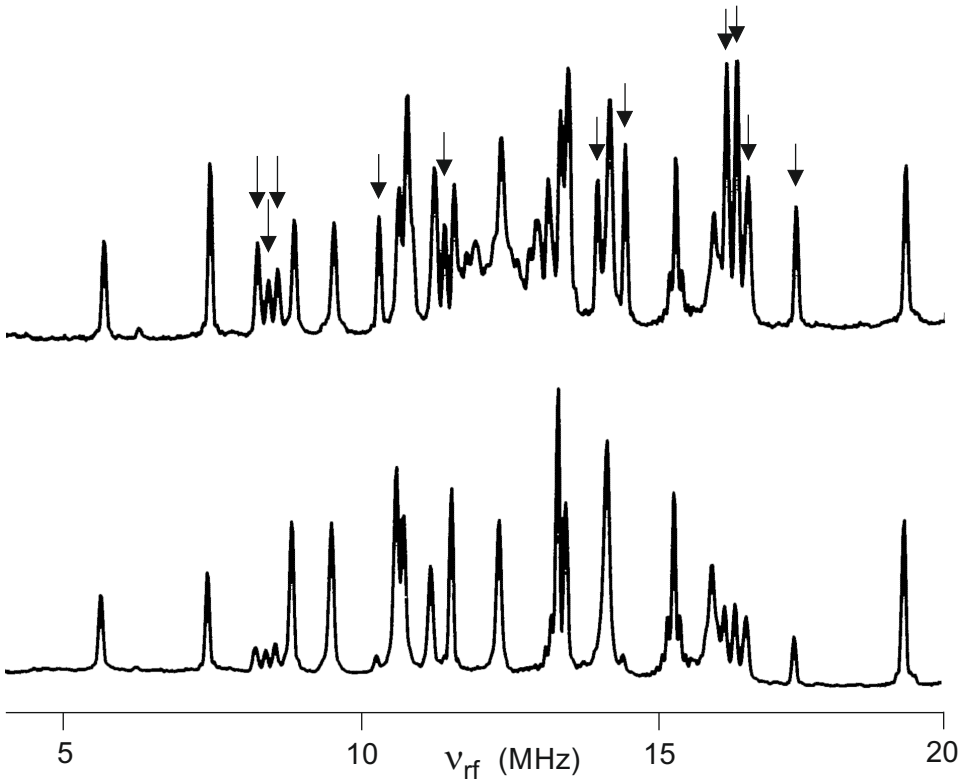

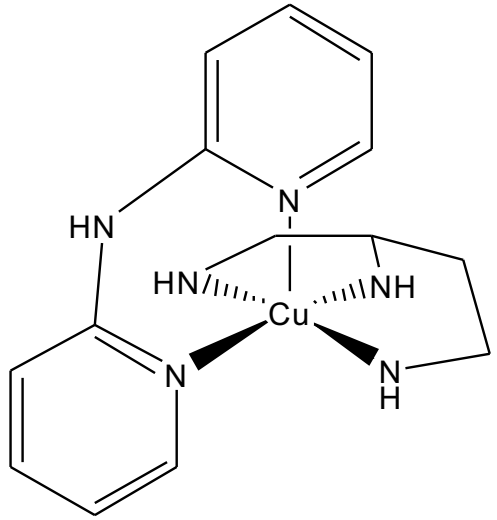

Mims ENDOR

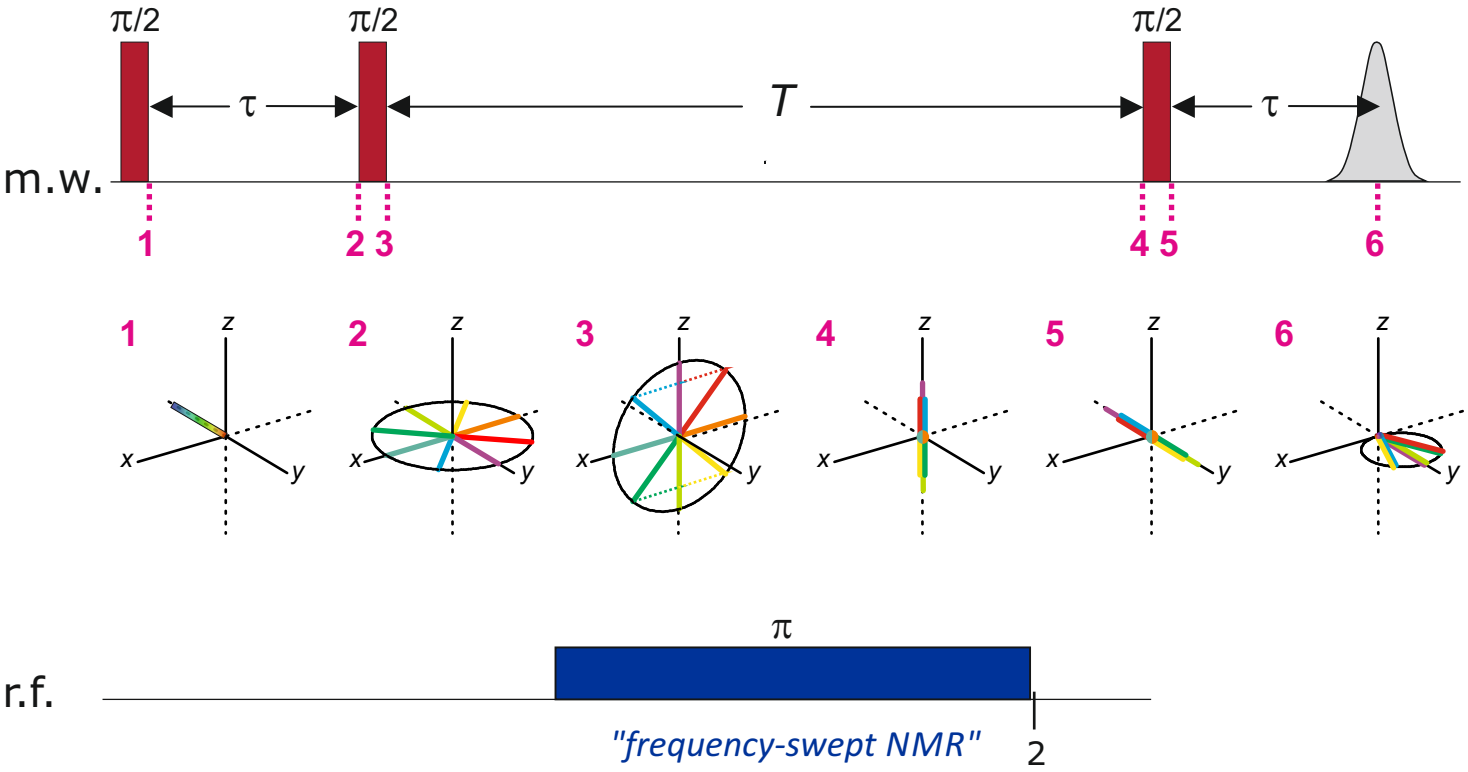

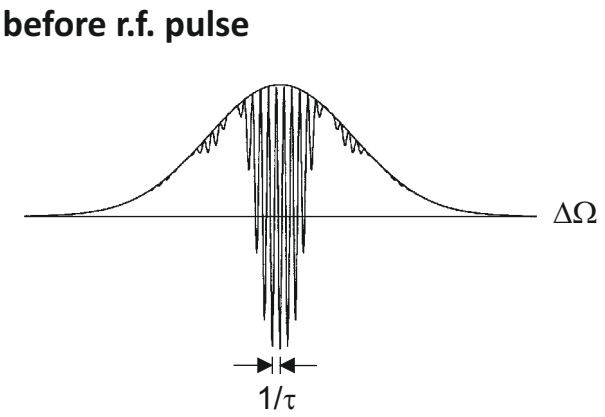

Blind spot behaviour

Mims ENDOR efficiency as a function of interpulse delay τ

$$F_{ENDOR} = \frac{1}{4}[1-\cos(A_{eff}\,\tau)]$$

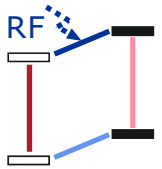

up to 50% destructive interference

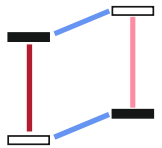

no change

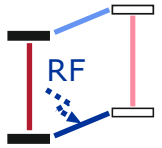

up to 50% destructive interference

Electron-electron coupling

Exchange coupling

- arises from overlap of the SOMO's of two electrons
  - binding overlap ↔ antiferromagnetic coupling ↔ $\Delta E_{\alpha\beta}=\Delta E_{\beta\alpha} < \Delta E_{\alpha\alpha}=\Delta E_{\beta\beta}$
  - anti-binding overlap ↔ ferromagnetic coupling ↔ $\Delta E_{\alpha\beta}=\Delta E_{\beta\alpha} > \Delta E_{\alpha\alpha}=\Delta E_{\beta\beta}$
- strong exchange coupling ($J > g\mu_B B_0/\hbar$)
  - antiferromagnetic: diamagnetic singlet ground state
  - ferromagnetic: paramagnetic triplet ground state

Weak coupling: J, $\omega_{dd} << \omega_0$

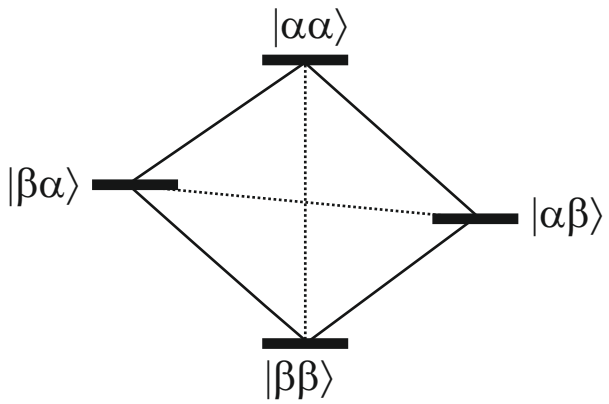

Dipole-dipole coupling

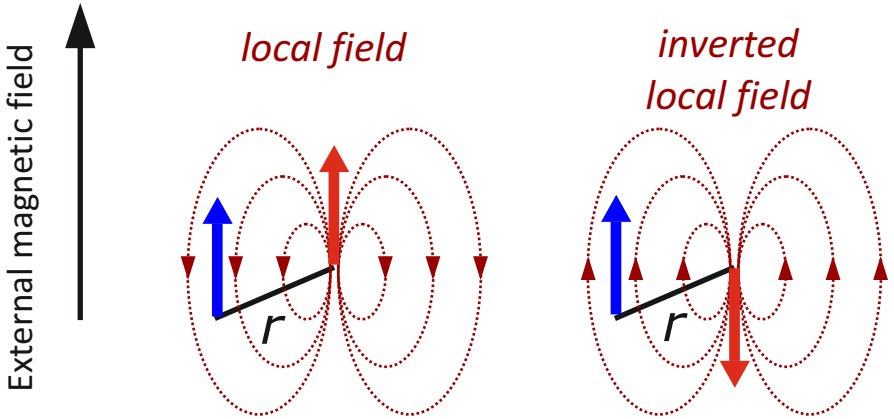

for weak g anisotropy

$$\omega_{dd} = \frac{1}{r_{12}^3}\frac{\mu_0}{4\pi\hbar} g_1 g_2 \mu_B^2$$

$\omega_{dd}/2\pi \approx 52.04$ MHz at $r_{12} = 1$ nm

for strong g anisotropy

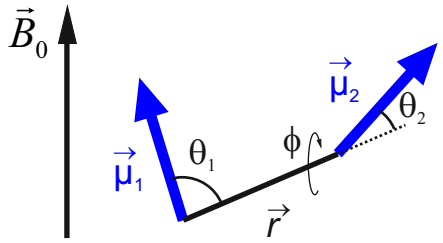

Origin of the Pake pattern

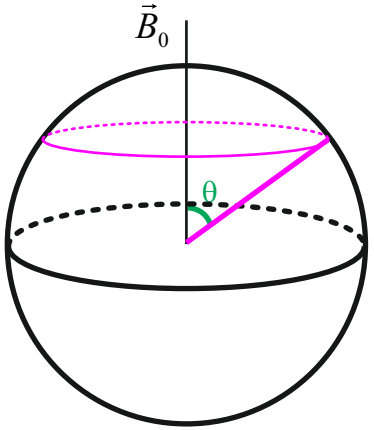

circumference:
$2\pi \sin\theta\, r$

$$\mathcal{H}_{dd} = d\, 2S_z I_z$$

$$d(\theta) = \tfrac{1}{2}\left(1 - 3\cos^2\theta\right)\omega_\perp$$

$$\omega_\perp = \frac{1}{r^3}\frac{\mu_0}{4\pi\hbar} g_1 g_2 \mu_B^2$$

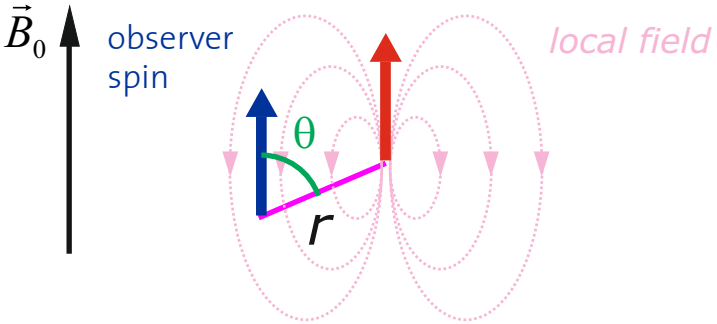

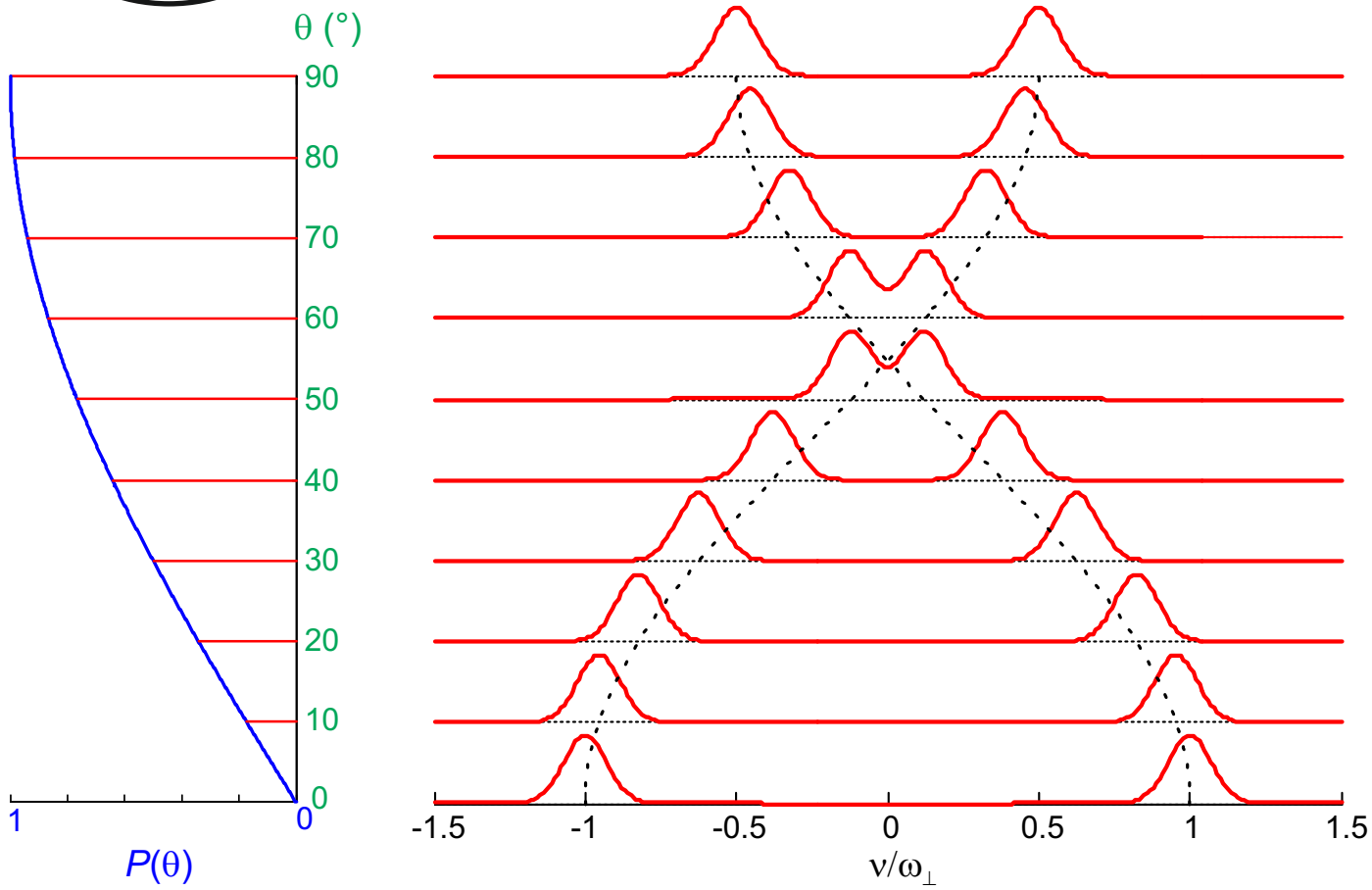

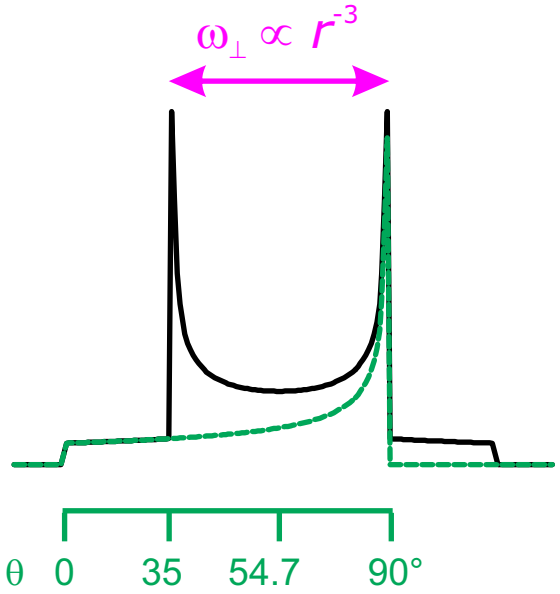

Neglect of exchange coupling at long distances

Distance is computed from dipole-dipole coupling only

- exchange coupling *cannot be separated* from dipole-dipole coupling *by spin manipulation*
- *purely isotropic for r > 0.5 nm* (5 Å) in most cases

  ⇒ no contribution to intensity of half-field transitions

  ⇒ distinguishable from purely anisotropic dipolar coupling

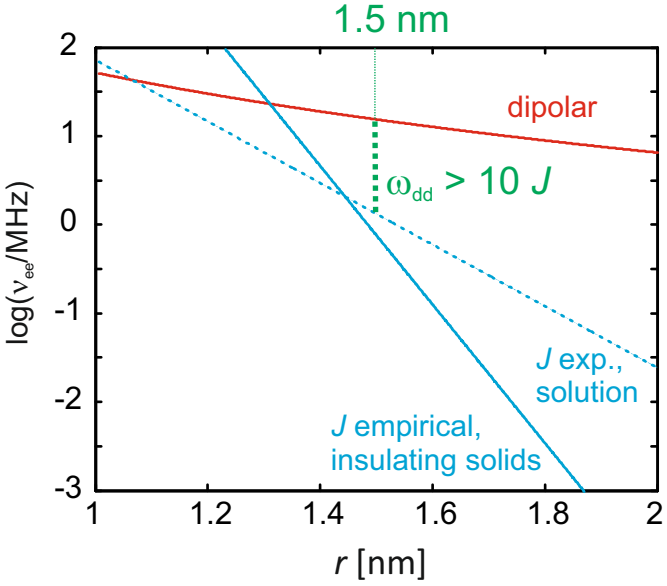

> 1.5 nm safe for nitroxides in proteins

Beware of through-bond couplings in conjugated systems!

$J > \omega_{dd}$ at 3.6 nm: $J \approx 40$ MHz

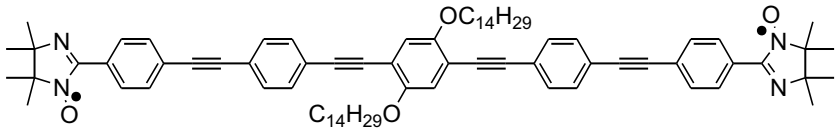

P. WAUTELET, A. BIEBER, P. TUREK, J. LEMOIGNE, J. J. ANDRE, *Mol. Cryst. Liq. Cryst*. **1997**, *305*, 55.

see also: C. RIPLINGER, J. P. Y. KAO, G. M. ROSEN, V. KATHIRVELU, G. R. EATON, S. S. EATON, A. KUTATELADZE, F. NEESE, *J. Am. Chem. Soc.* **2009**, *131*, 10092-10106.

Distance measurements by CW EPR

Dipolar interaction of aligned spins

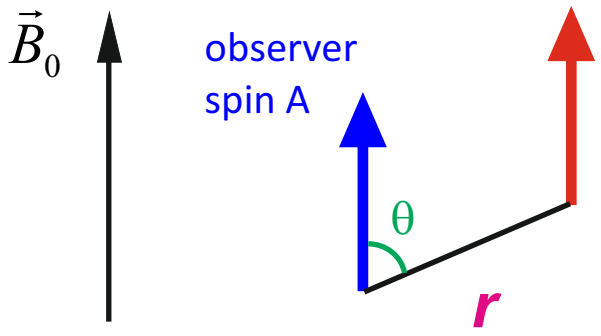

Pake pattern

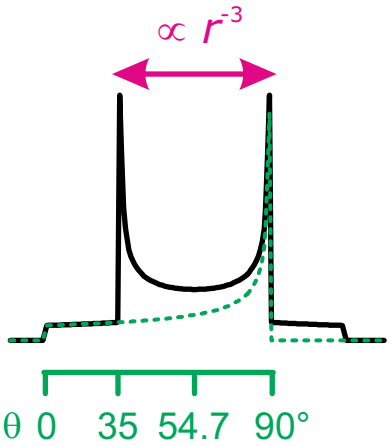

Nitroxide EPR spectrum & Pake patterns

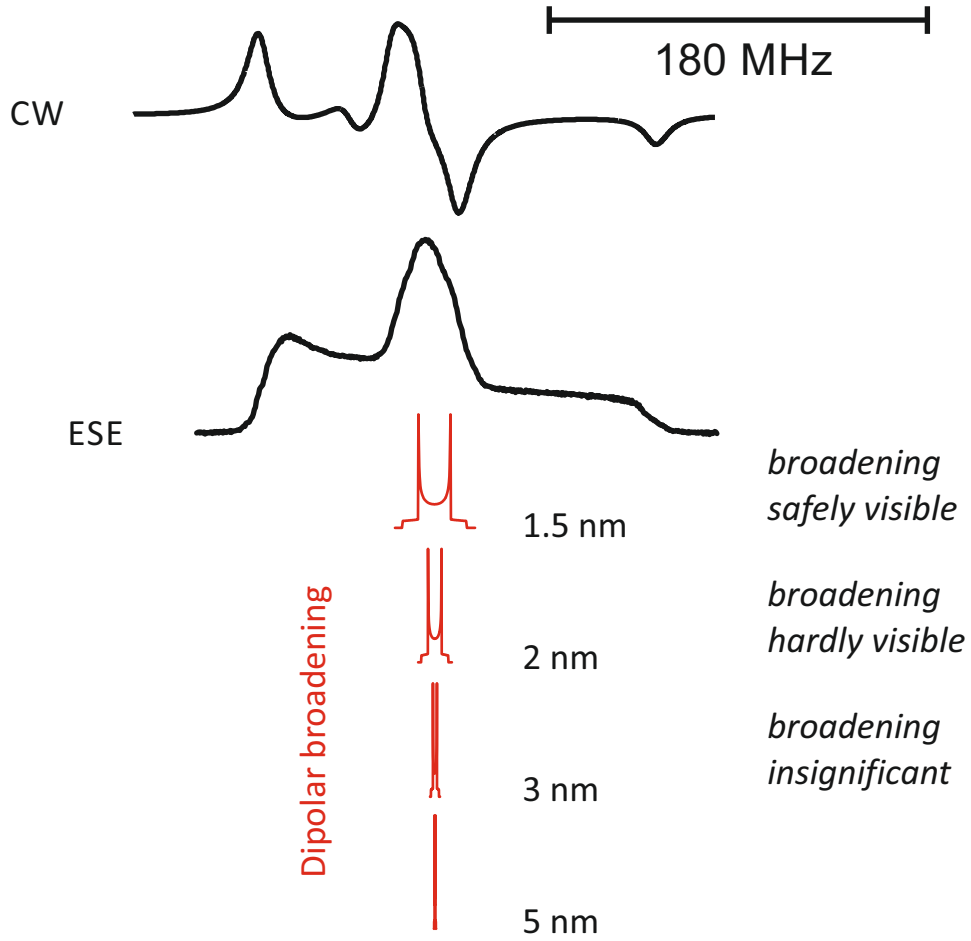

Distance measurements by CW EPR

- dipole-dipole coupling in a doubly labeled molecule is manifest as line broadening

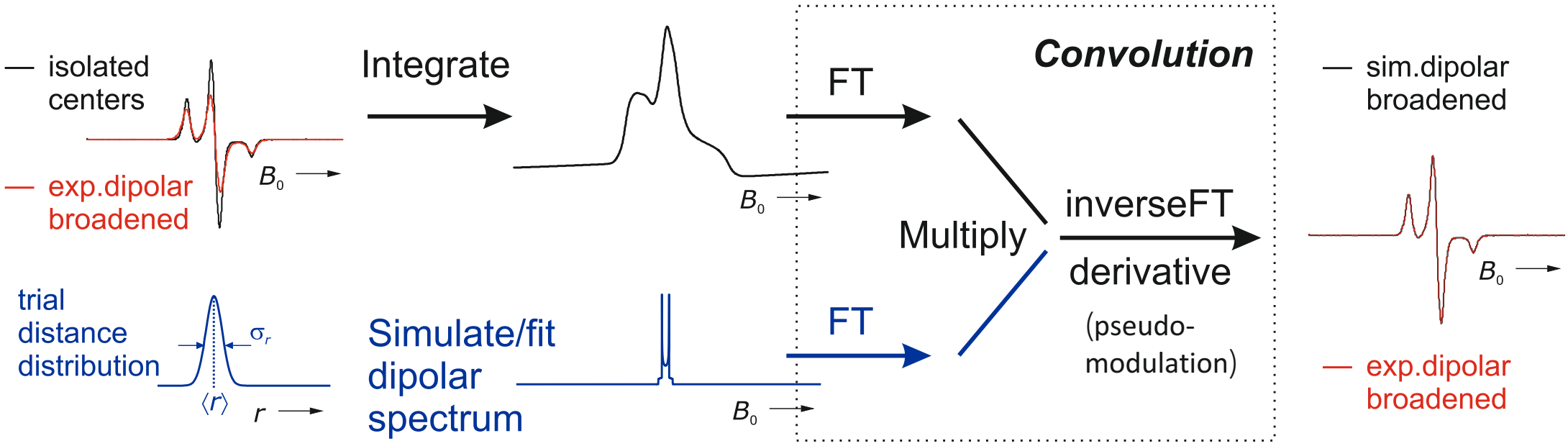

- works very well between 1.3 and 1.8 nm
- longer distances: uncertainty from other broadening mechanisms
- shorter distances: uncertainty from exchange coupling

Separation of the electron-electron coupling from other interactions

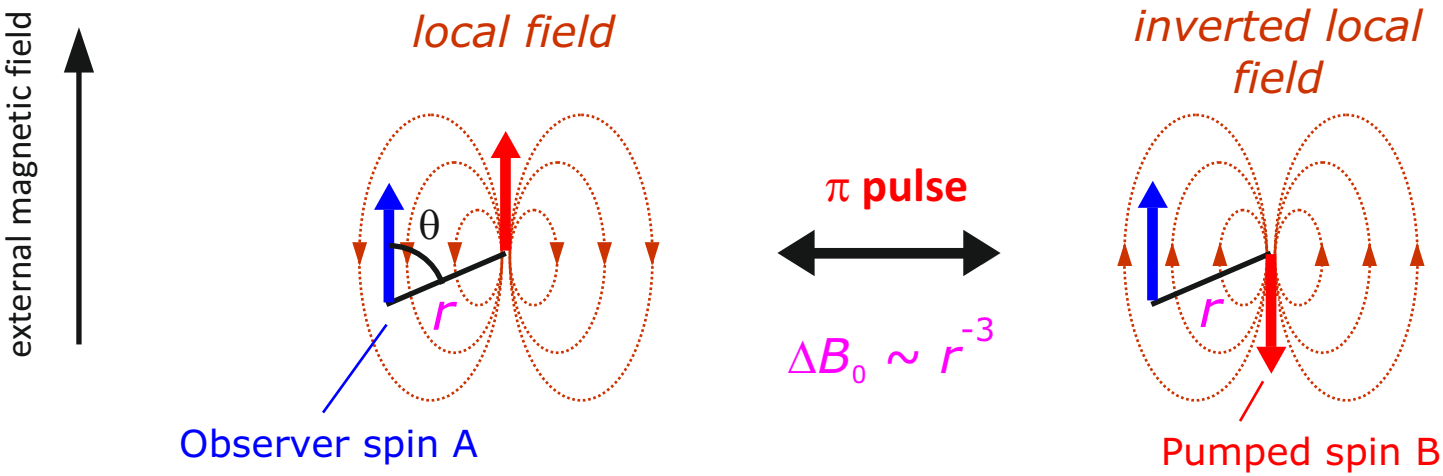

1. Signal is labeled with resonance frequency $\nu = g\mu_B B_o / h$

2. Pumped spin is inverted, field shifts

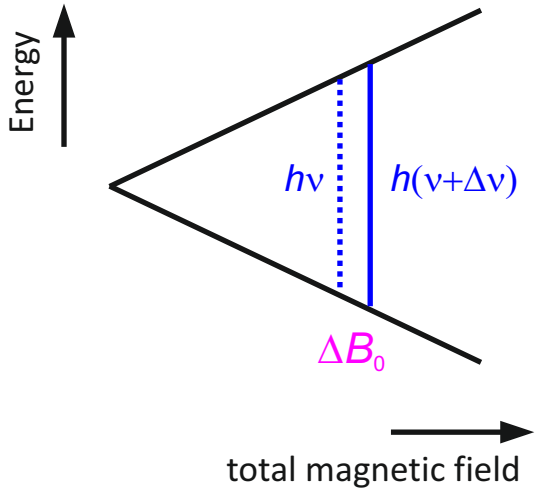

3. Field shift ΔB_0 is measured via change $\Delta\nu$ of resonance frequency

4. Distance r is computed from $\Delta\nu$

$r^3 = (52.04\ \text{MHz}/\Delta\nu)\ \text{nm}$

Separating the dipole-dipole interaction by a spin flip

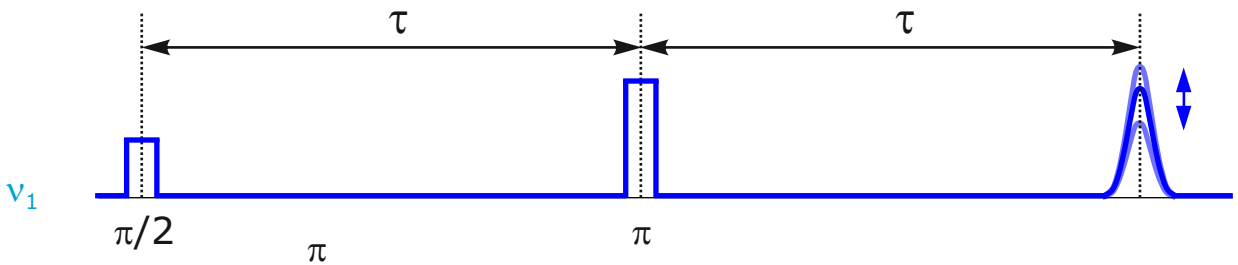

- constant delay τ:
  no echo variation
  due to relaxation
- variable delay *t*:
  resonance frequency
  is changed at different times

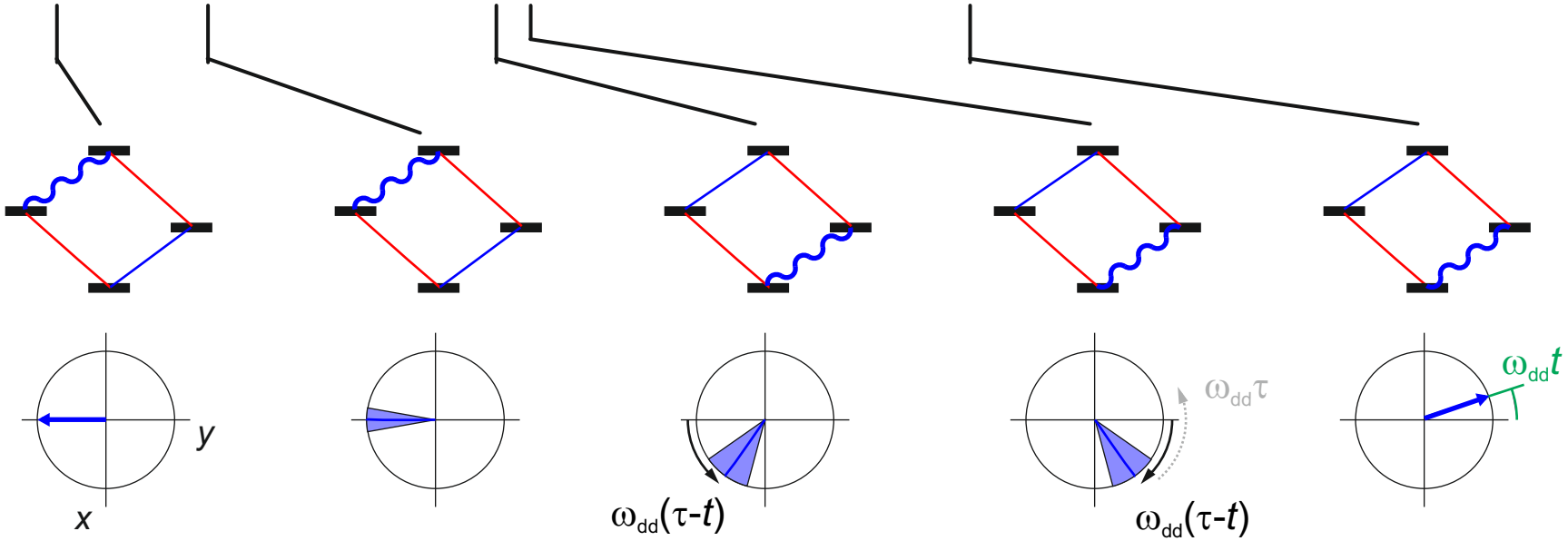

Ultimate resolution by a constant-time experiment

- if the total length of the pulse sequence changes, dipolar evolution is damped by relaxation
- for distances larger than ~3-4 nm, dipolar modulation is overdamped

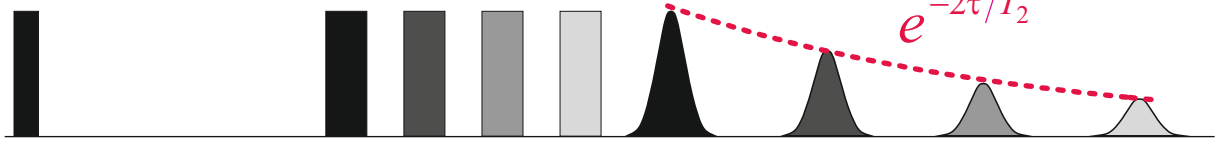

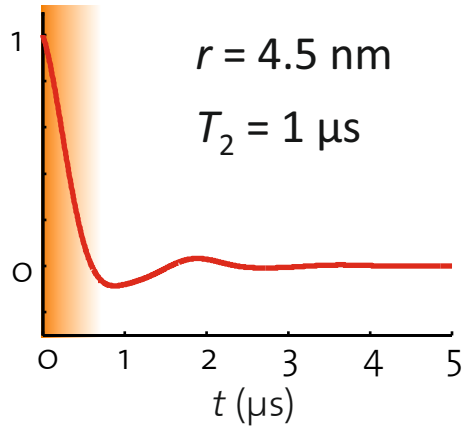

Keep τ fixed, vary only *t*, pulse sequence has constant length

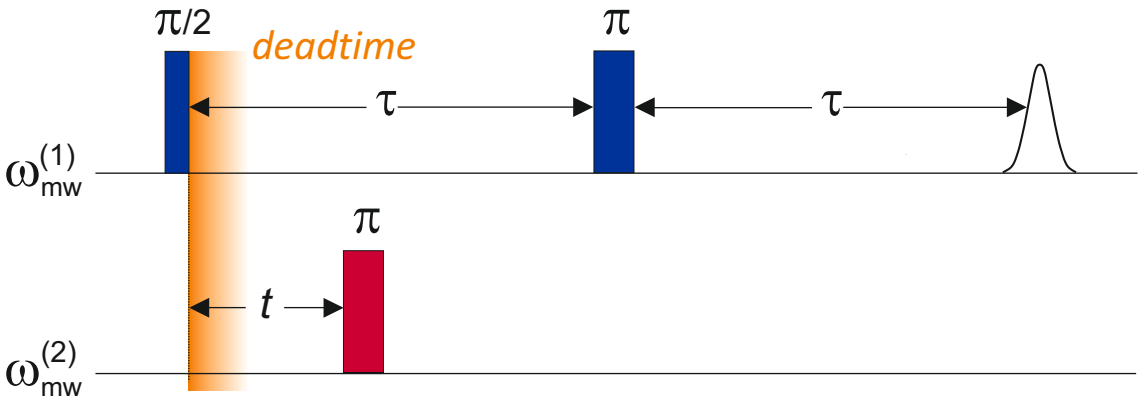

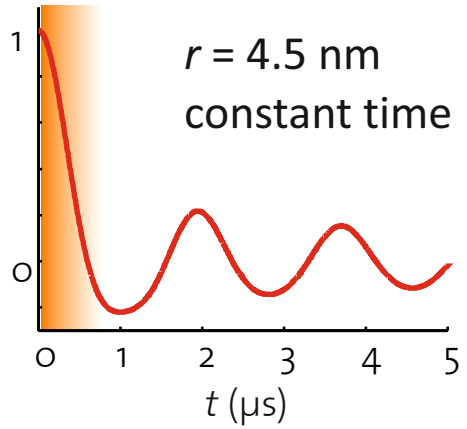

Eliminating dead-time by the four-pulse DEER experiment

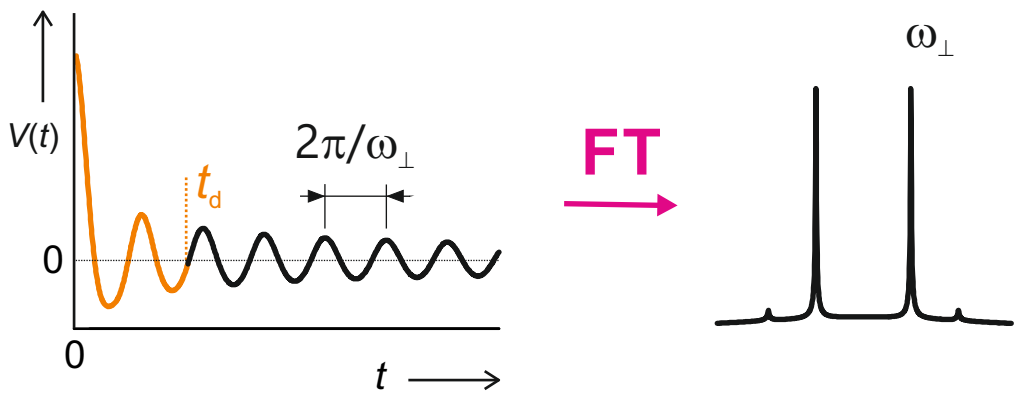

unreliable results due to deadtime for

- distributions with $r < 2.2$ nm
- direct extraction of distance distributions

sensitivity loss for small r

Remedy: Refocusing of the echo $\Rightarrow$ accessible t: $-\tau_1+t_d < t < \tau_2-t_d$

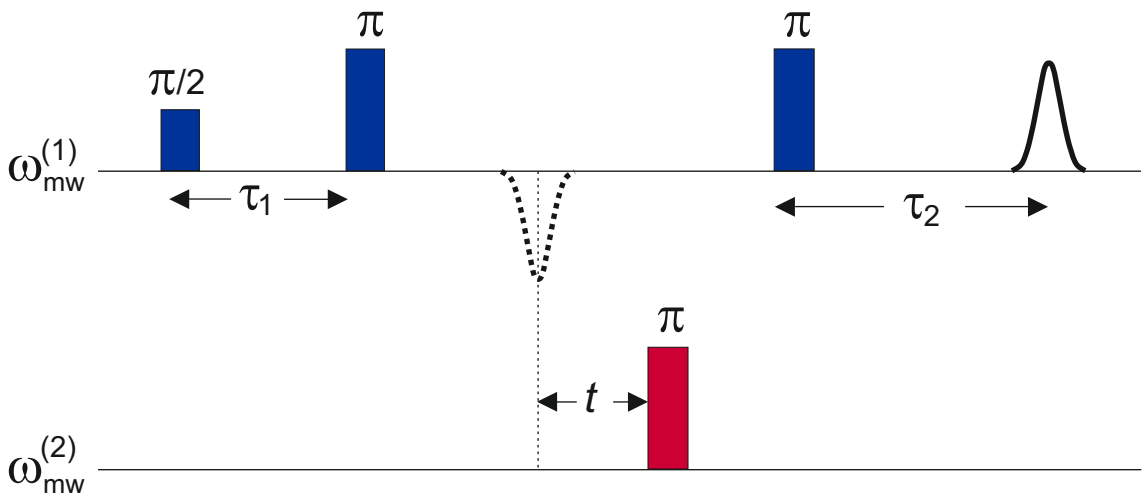

Typical values (nitroxides):

$\tau_1 \approx$ 120...200 ns, 400 ns with deuterated matrix

$\tau_2 \approx$ 1 µs (2 nm)... 6 µs (5-8 nm)

$t_p(1)$ = 32 ns

$t_p(2)$ = 12 ns (opt. sensitivity)

The spectrum of nitroxides

Liquid state (or single orientation)

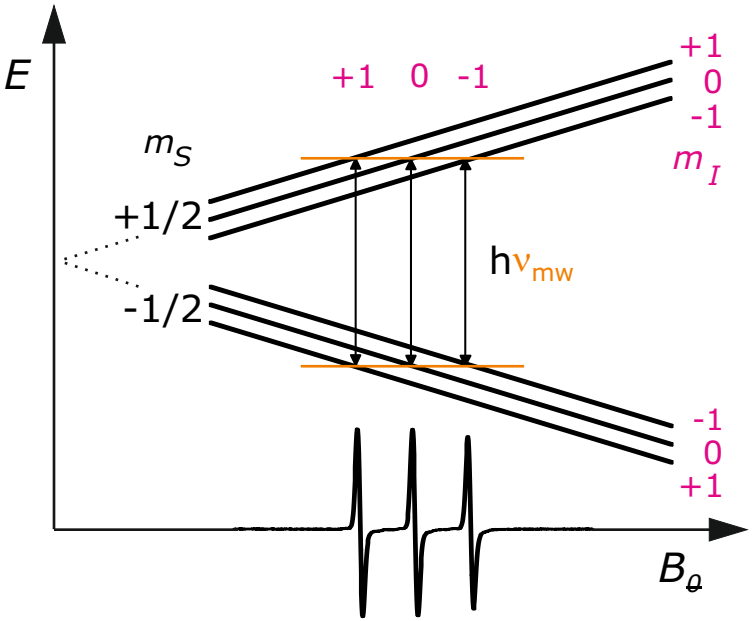

Molecular frame and orientation dependence

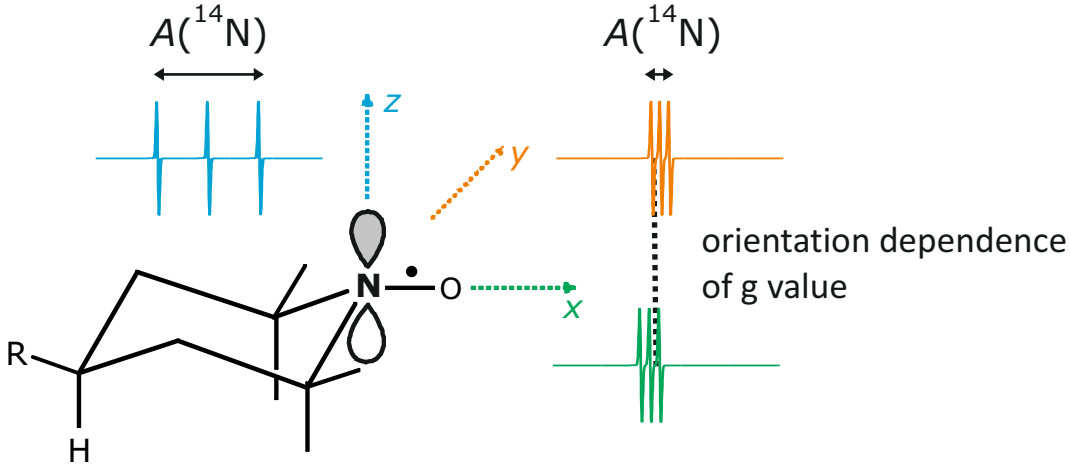

Solid state

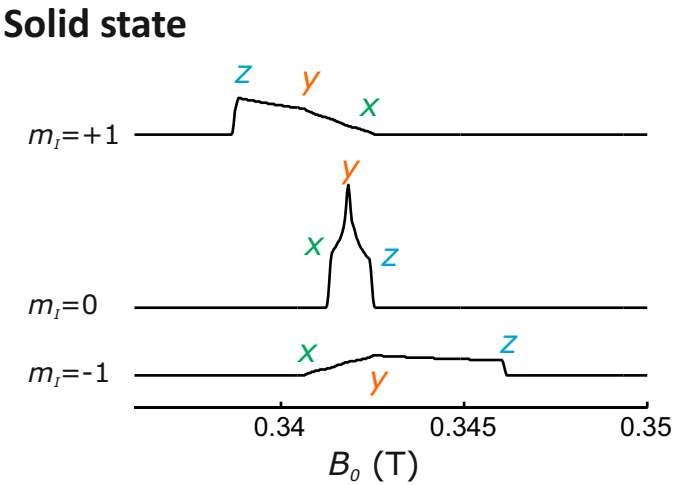

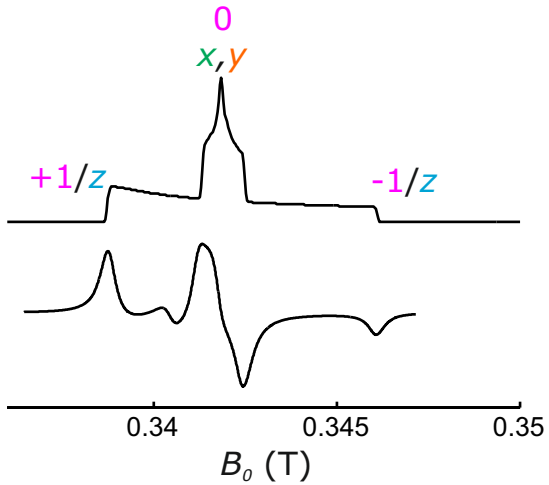

Why can we excite two nitroxide labels with two frequencies?

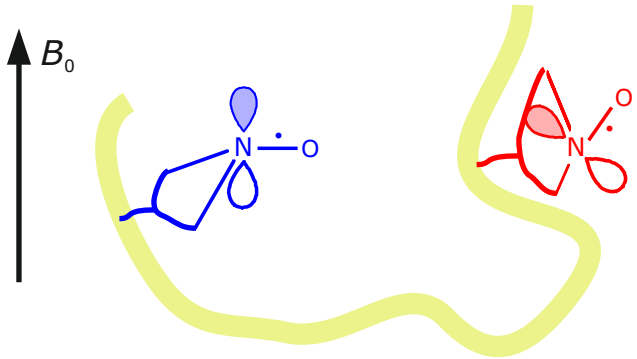

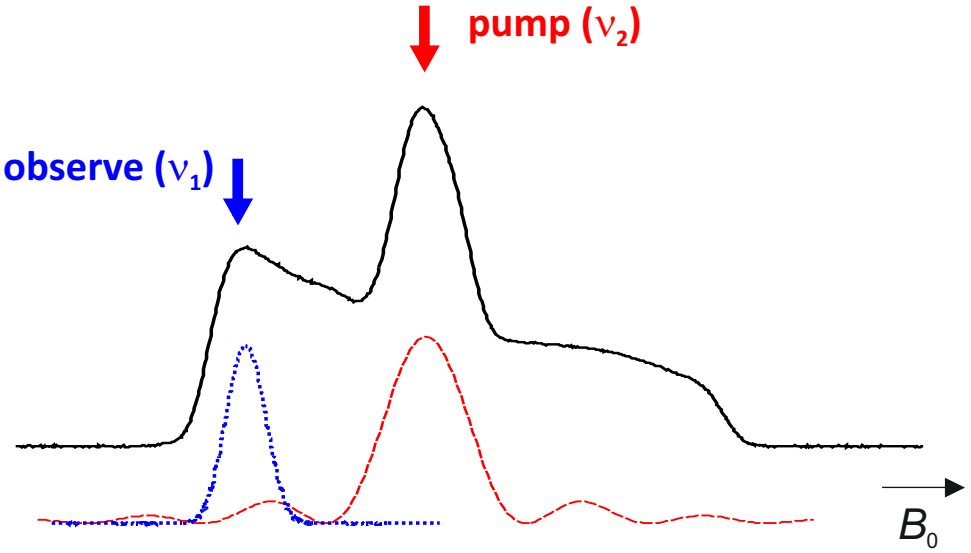

excitation bands

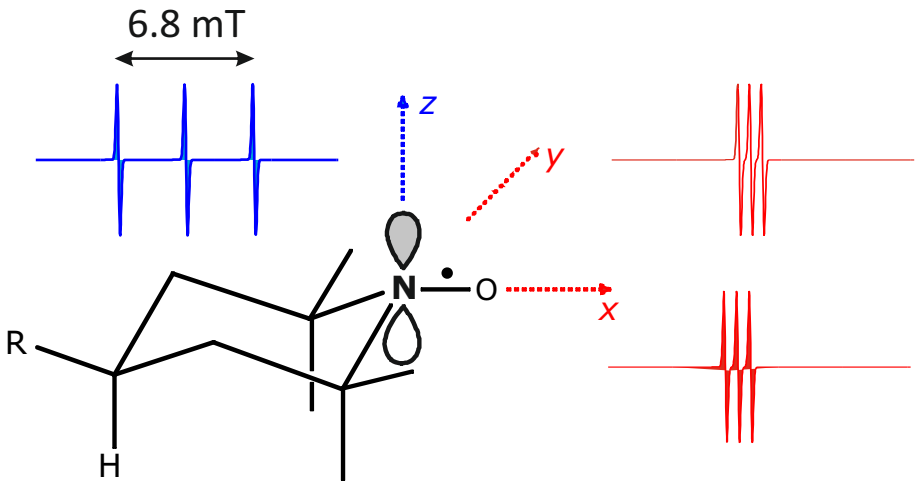

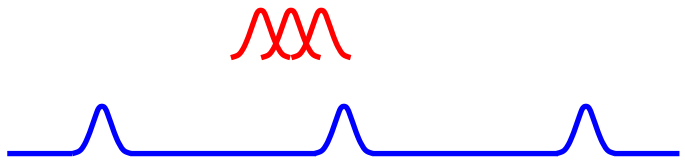

schematic spectra

- only for a fraction λ of all spin pairs of the observed spin A the coupled spin B is indeed excited (pumped)

Information content of the DEER signal

Primary experimental data

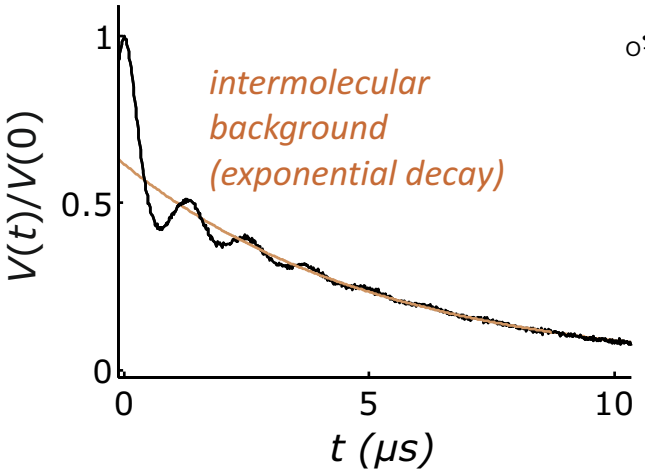

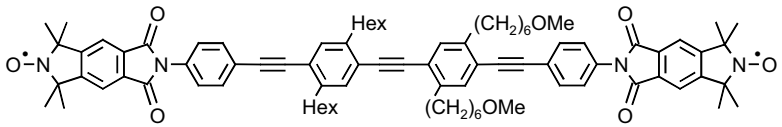

background

correction

Form factor (intramolecular)

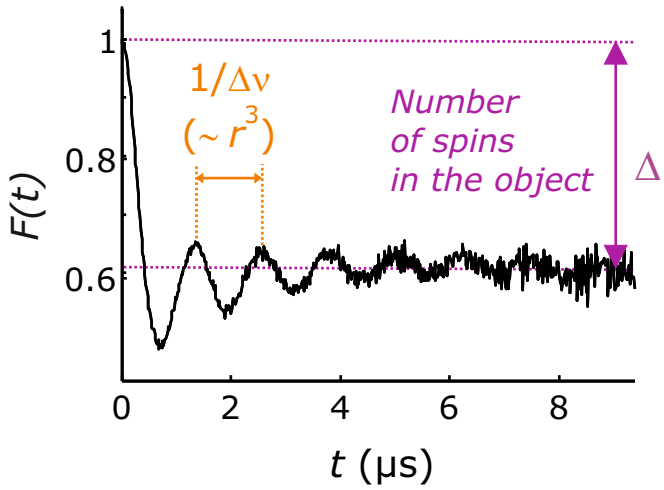

- decay envelope depends on distance distribution: fast decay of modulation ⇒ broad distribution

Dipole-dipole interaction $\omega_{dd} = \frac{1}{r^3}\frac{\mu_0}{4\pi h} g_1 g_2 \mu_B^2$

Dipolar frequency $d(\theta) = \left(1 - 3\cos^2\theta\right)\omega_{dd}$

Form factor of an isolated spin pair $F(r,t) = \frac{V(t)}{V(0)} = 1 - \int_0^{\pi/2} \lambda(\theta)\left\{1 - \cos\left[2\pi\nu_{dd}(\theta)\right]\right\}\sin\theta\, d\theta$

Data analysis by Fourier transformation

Dipolar evolution function (form factor)

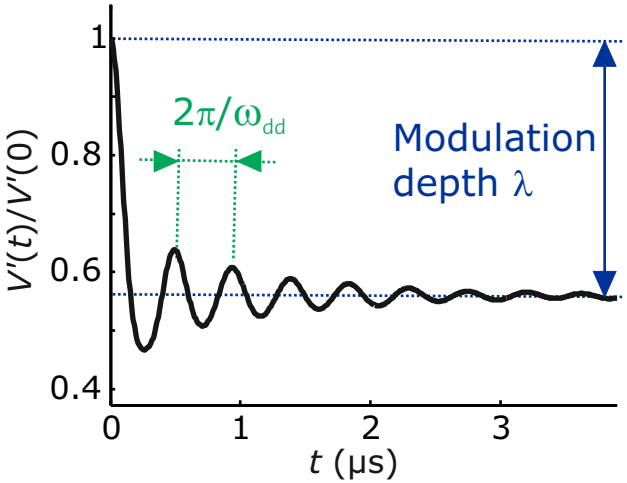

Fourier transformation

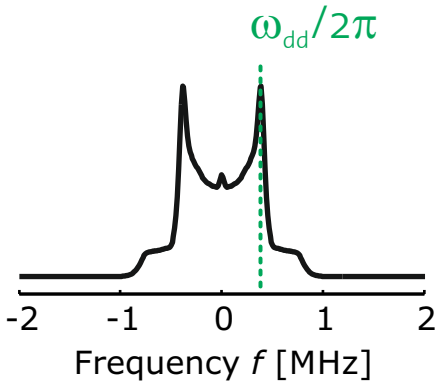

Normalized echo modulation

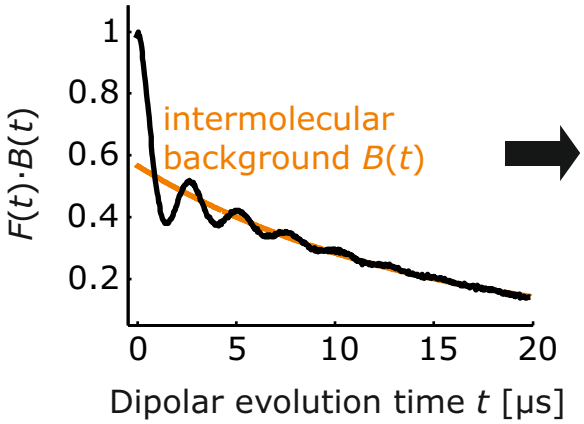

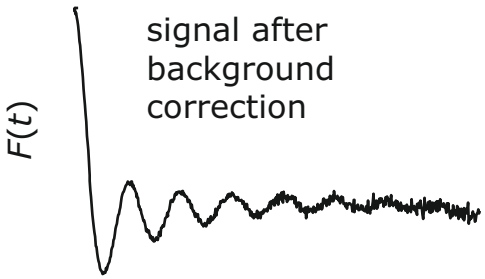

FT

$\omega_{dd}/2\pi$ = 380 kHz

$\Rightarrow r$ = 5.05 nm

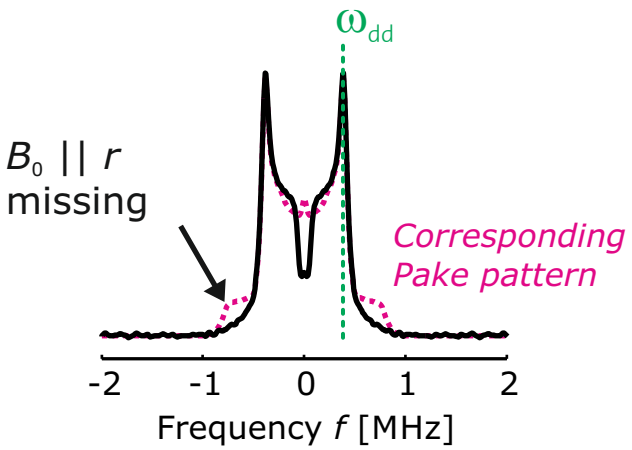

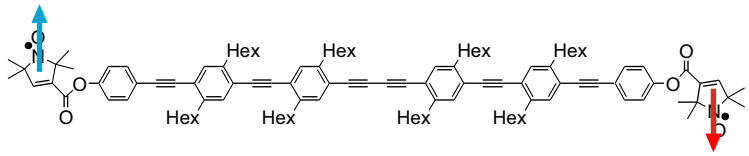

Average distance is not the full information

Molecular dynamics causes distribution of *r*

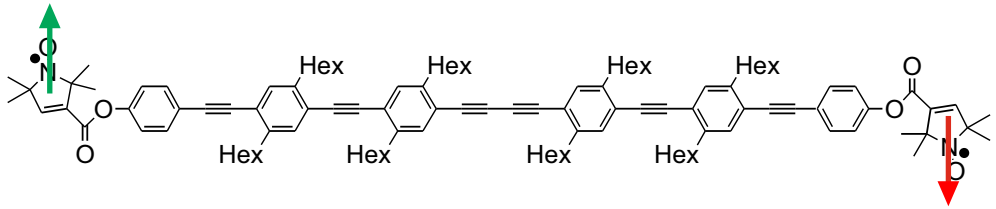

Expectation:

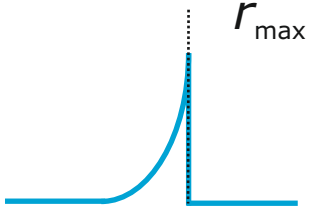

bent, higher energy, lower population, smaller *r*

stretched, min. energy, max. population, max. *r*

Experimental distance distribution

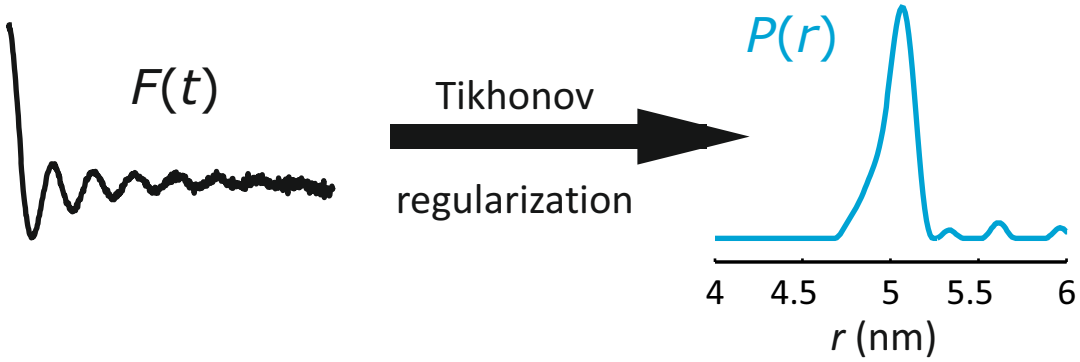

Basic mathematics

fit simulated dipolar evolution function $S(t)=K\,P(r)$

Minimize

$$G_\alpha(\mathrm{P}) = \| KP(r) - F(t) \|^2 + \alpha \left\| \frac{d^2}{dr^2} P(r) \right\|^2$$

mean square deviation

smoothness of 2nd derivative

regularization parameter α

G. JESCHKE, A. KOCH, U. JONAS, A. GODT A, *J. Magn. Reson.* 155, 72-82 (2002)

G. JESCHKE et al. *Appl. Magn. Reson.* 30, 473-498 (2006)

Why regularization is required and how to do it

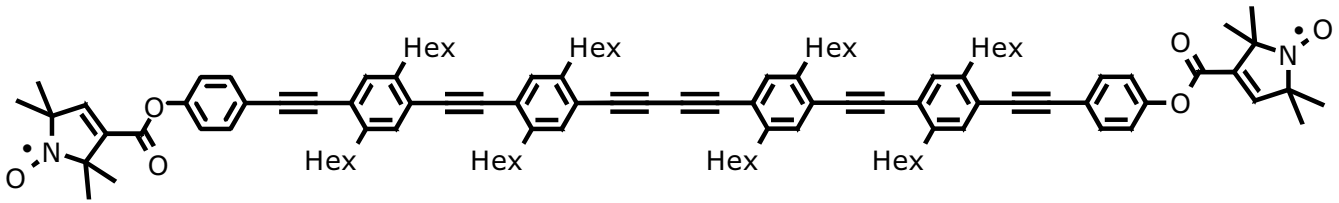

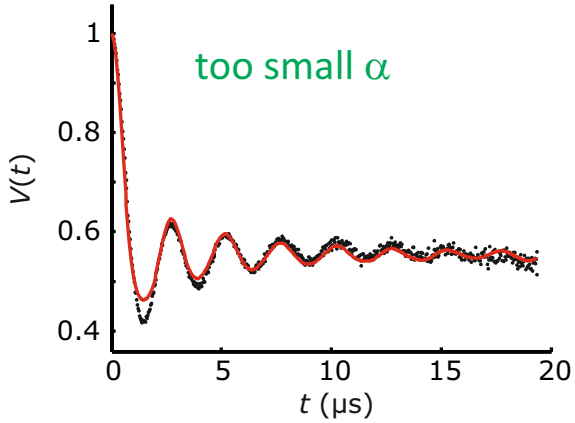

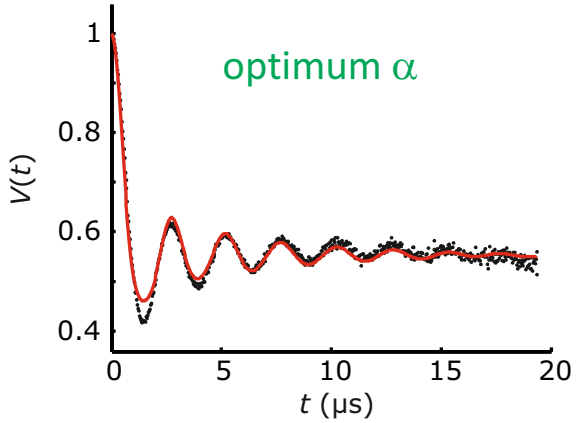

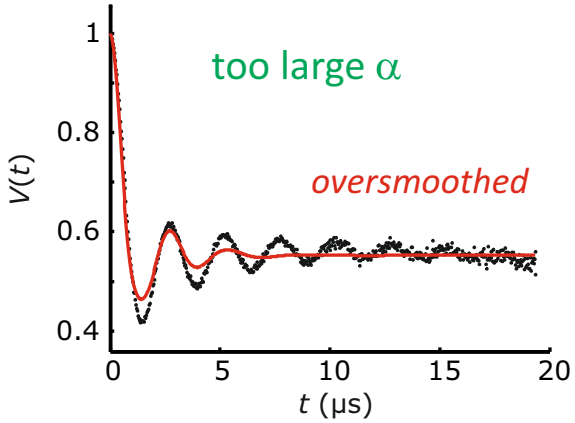

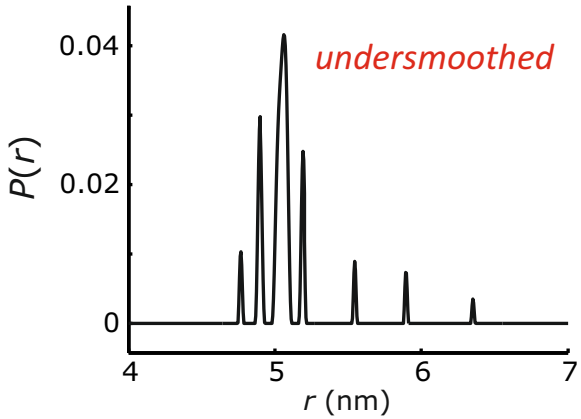

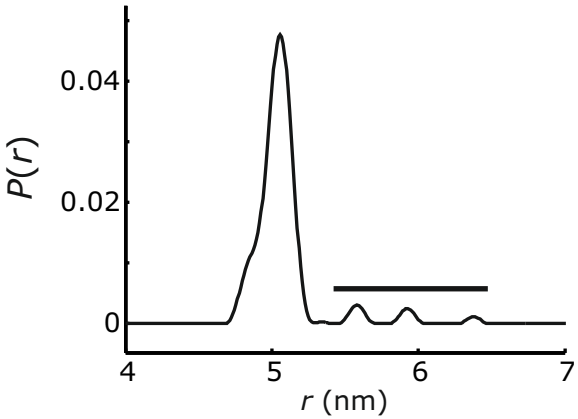

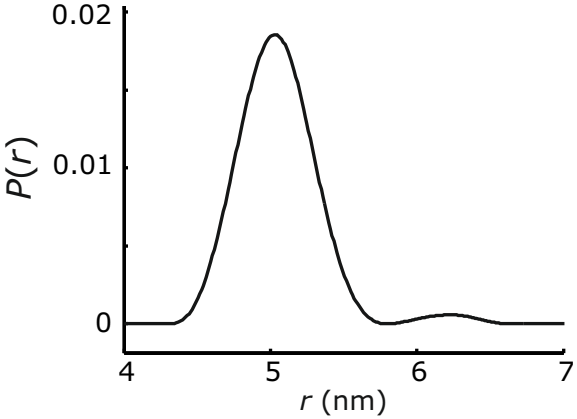

Two-pulse ESEEM: Spin physics

Level scheme

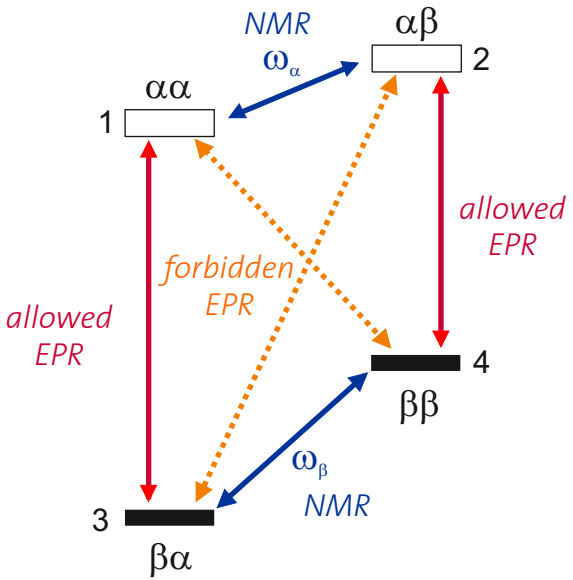

Pulse sequence

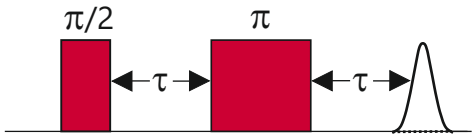

- interpulse delay τ is varied

Coherence branching

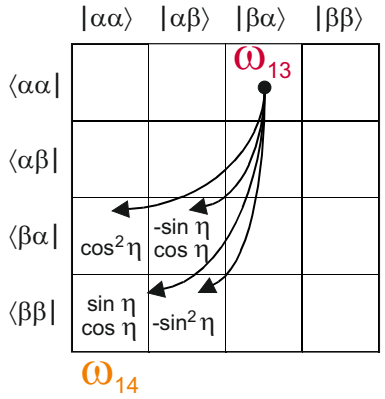

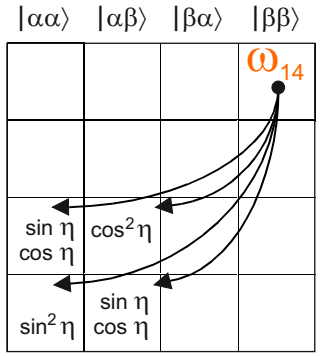

- transverse magnetization (coherence) that evolved on one transition during first interpulse delay τ is distributed to all four transitions

EPR spectrum (schematic)

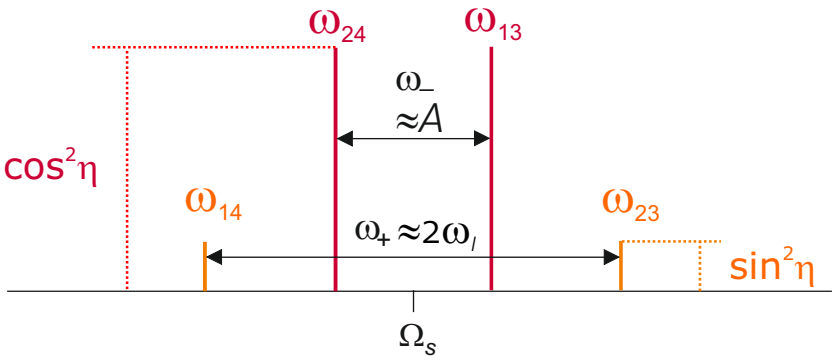

Defocusing with ω_{13}, refocusing with ω_{14}:
echo oscillates with ω_{14}-ω_{13} = ω_β

Three-pulse ESEEM

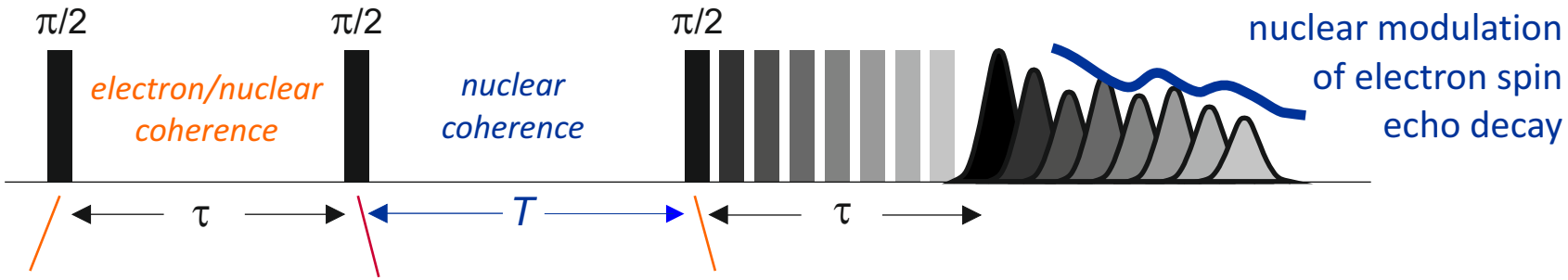

forbidden *e/n* transition $\propto r^{-3}$

allowed *e* transition

forbidden *e/n* transition $\propto r^{-3}$

Coherence branching

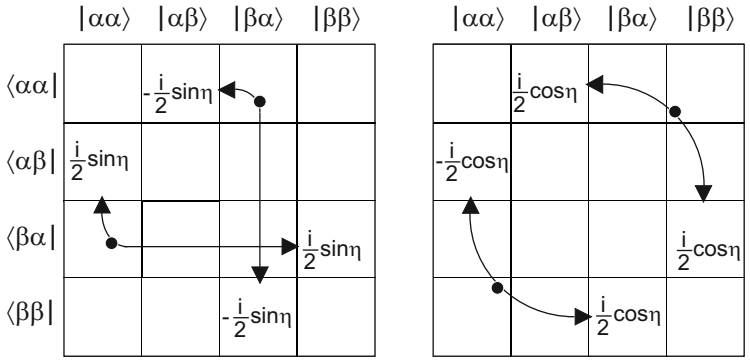

- electron coherence is transferred to nuclear coherence
- lines only at ω_α and ω_β

Main advantage

narrower lines, as nuclear coherence relaxes more slowly

Main disadvantage

blindspot behaviour as a function of τ

The HYSCORE experiment

HYperfine Sublevel CORrElation
(P. Höfer et al.)

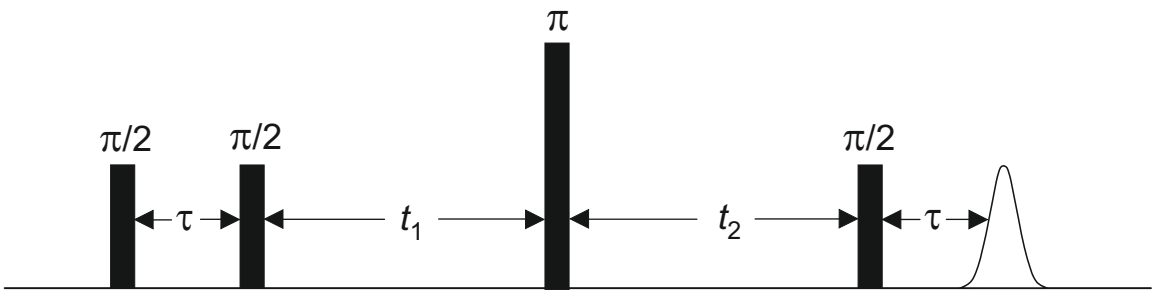

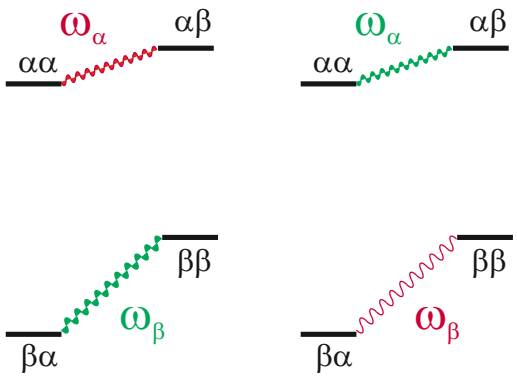

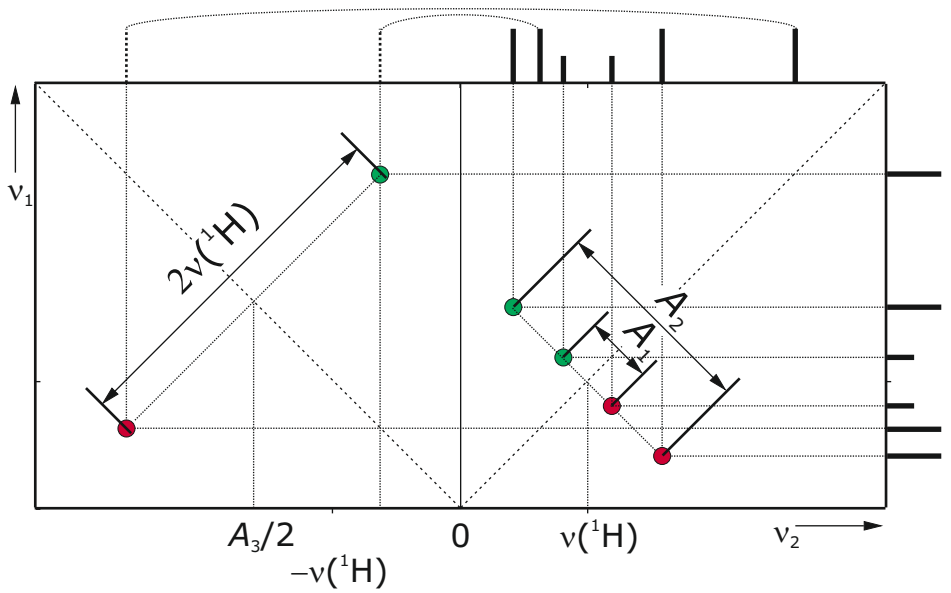

- correlates frequencies of the same nucleus for the α and β state of the electron spin

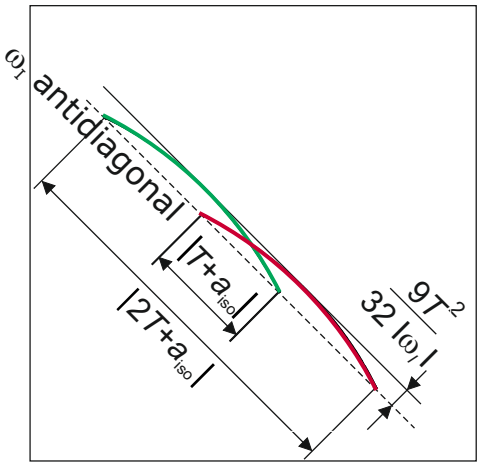

Binding mode of an inhibitor to methyl-coenzyme M reductase

Active center of the enzyme

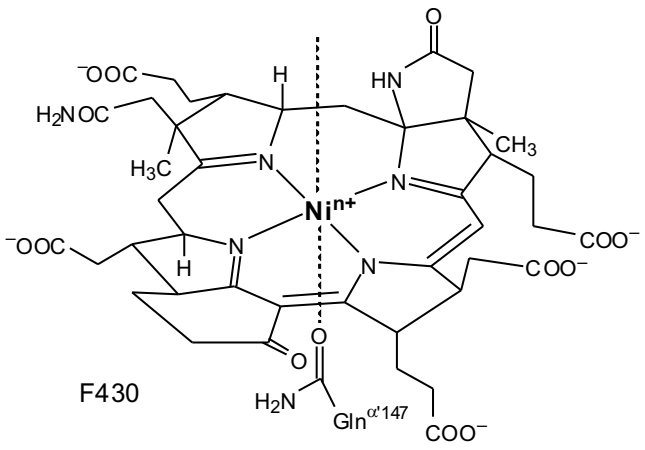

Inhibitor

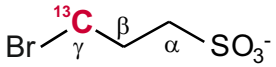

3-bromopropane sulfonate

- binds to the enzyme (step 1)
- cannot be reduced to methane (step 2 blocked)

^{13}C signals in HYSCORE: hyperfine coupling

Experiment

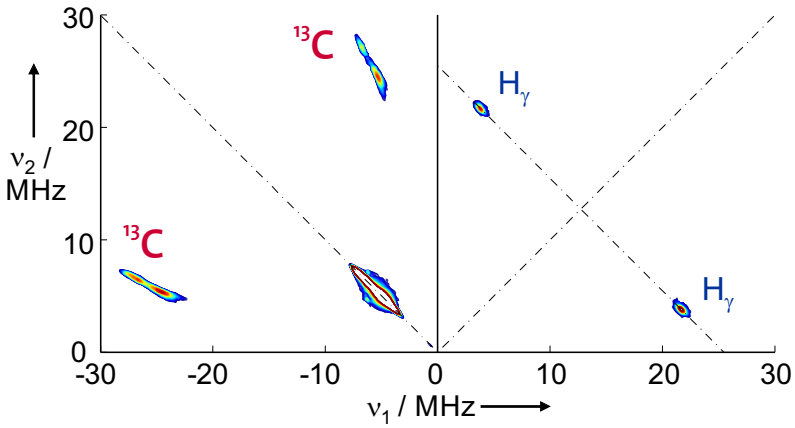

Simulation

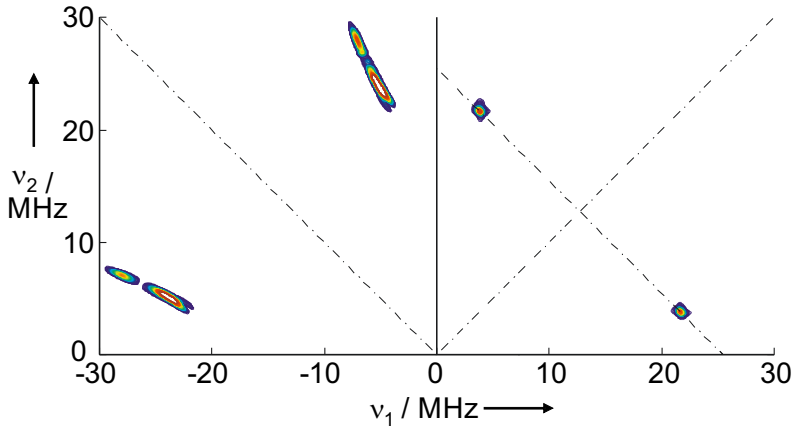

Hyperfine coupling reveals the binding mode

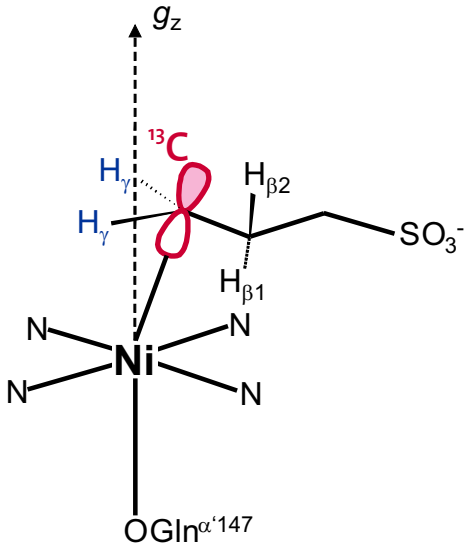

⇒ relative orientation of hyperfine and *g* tensor can be determined

HINDERBERGER D. *et al.*, Angew. Chem. Int. Ed. **2006**, *45*, 3602-3607

EPR- the little big sister of NMR

The little sister

chemical bonding is electron pairing, spins compensate

EPR signals ⇔ Chemical reactivity

- transition metal catalysis
- metalloproteins
- radical reactions
- electron transfer reactions (e.g. photosynthesis)

Defect-based function of solid-state materials

- color centres
- semiconductors
- conducting polymers

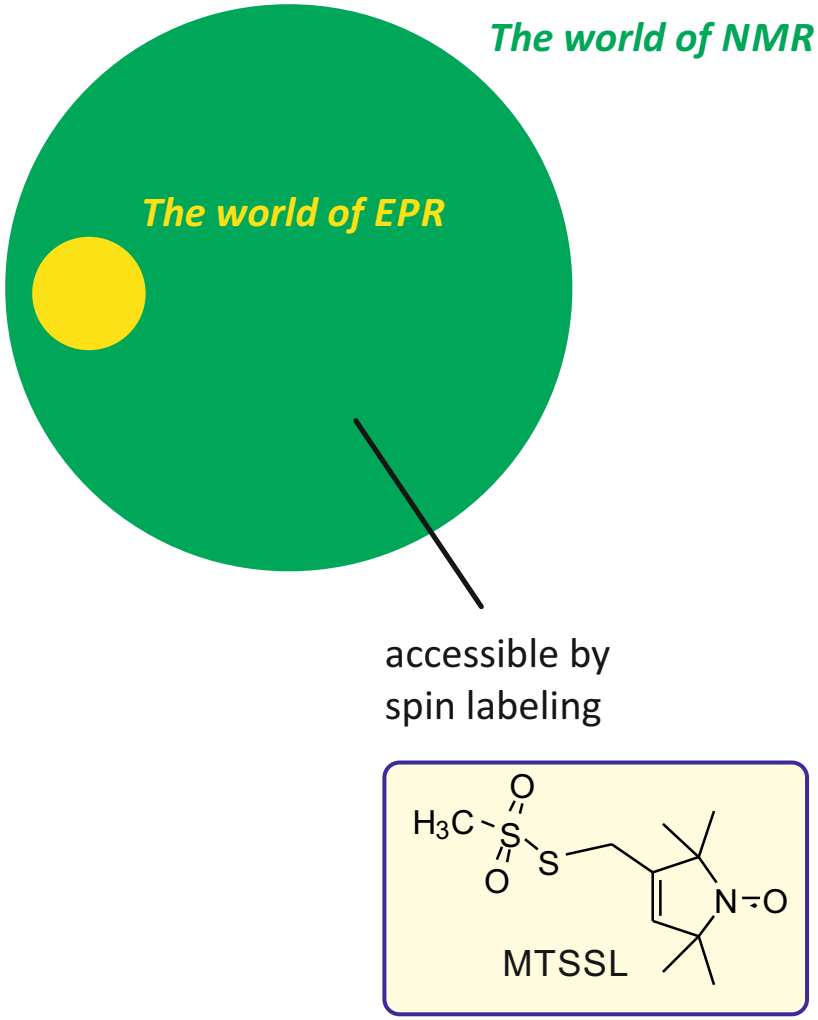

Exploring the diamagnetic world

Spin probes and labels

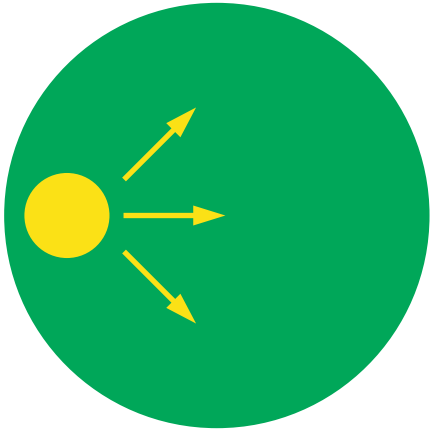

- by attaching stable free radicals to a site of interest in a complex system

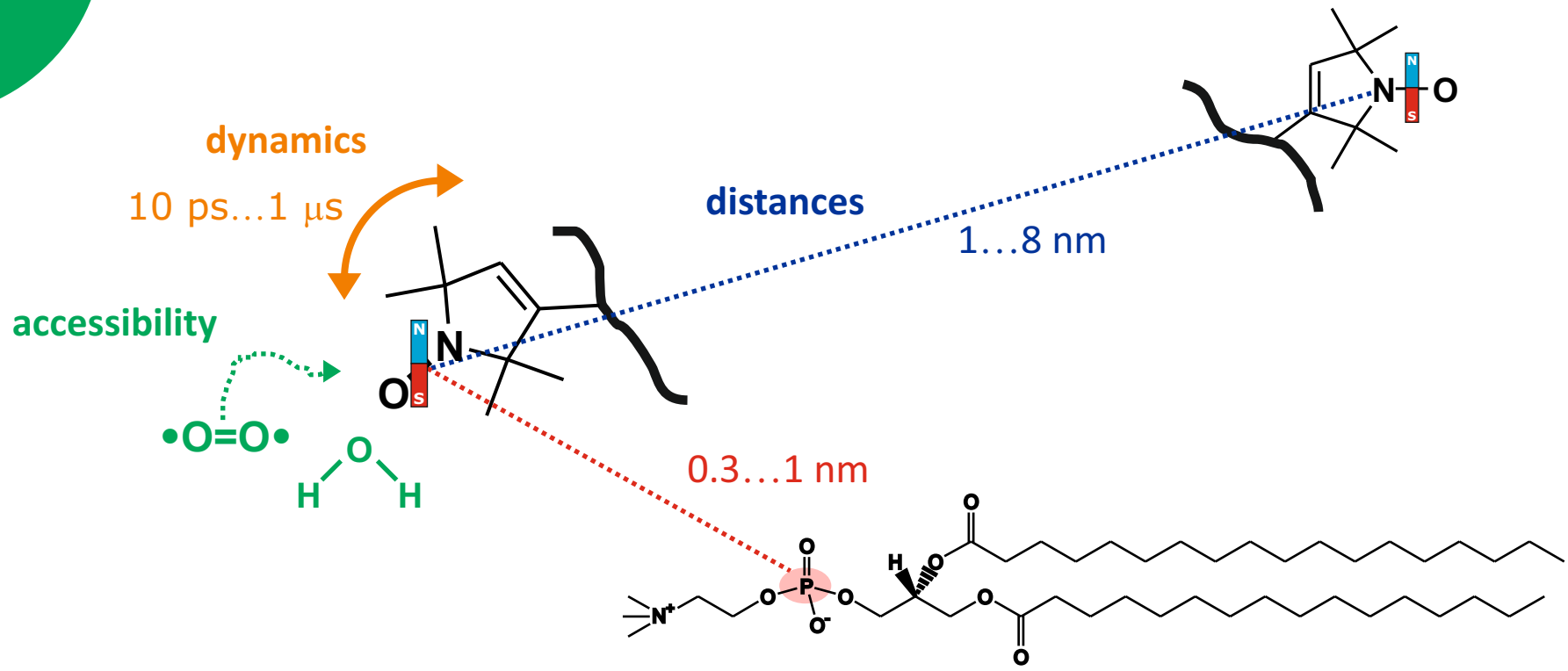

Spin probes and labels

Spin probes

- stable paramagnetic compounds are added to a system

Spin labels

- stable paramagnetic compounds are covalently bound to a molecule

Nitroxides as stable free radicals

- most common class of spin probes and labels
- stable for years at ambient temperature in solids
- thermally stable up to about 140 °C
- sensitive to strong acids and reducing conditions

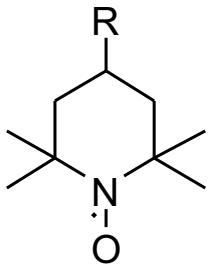

TEMPO derivatives

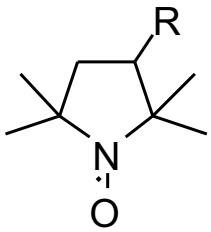

PROXYL derivatives

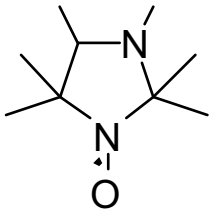

imidazoline nitroxide

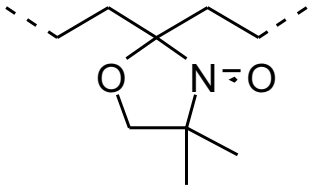

DOXYL derivatives

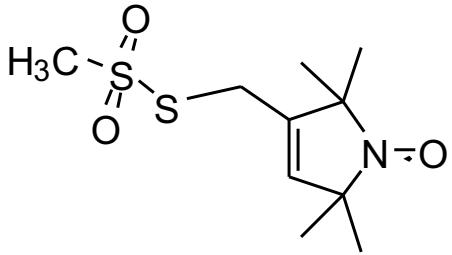

MTSSL

Site-directed spin labeling of proteins and RNA

Proteins

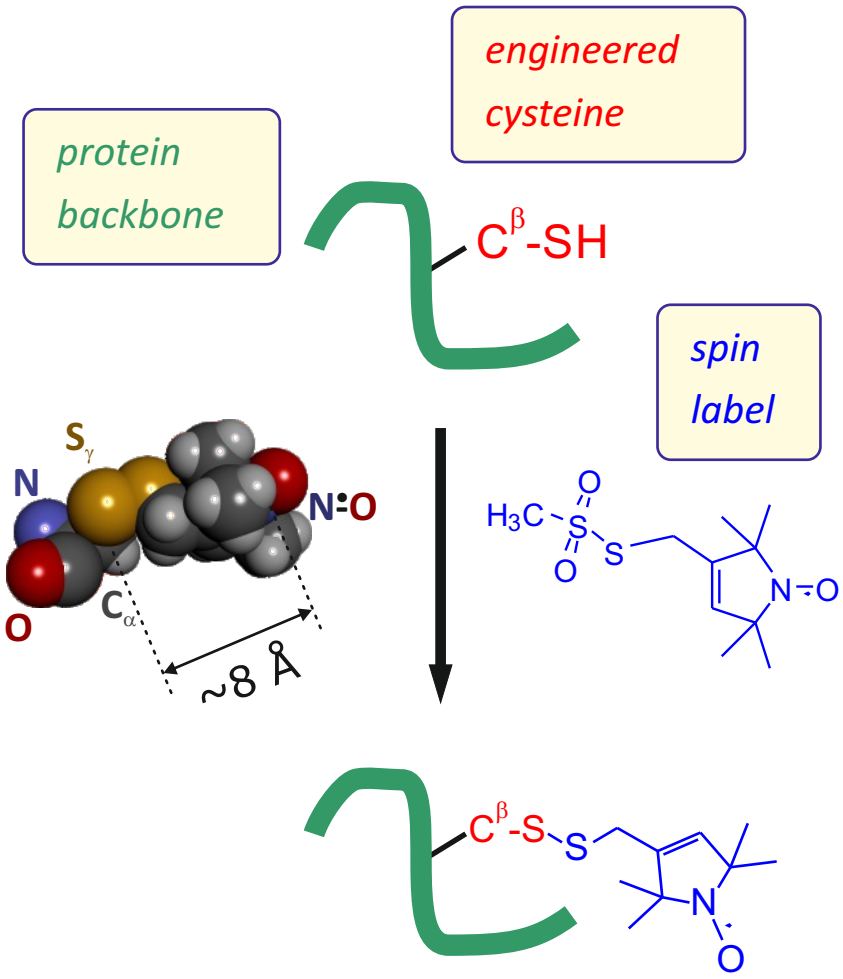

W.L. Hubbell, C. Altenbach, et al.

RNA

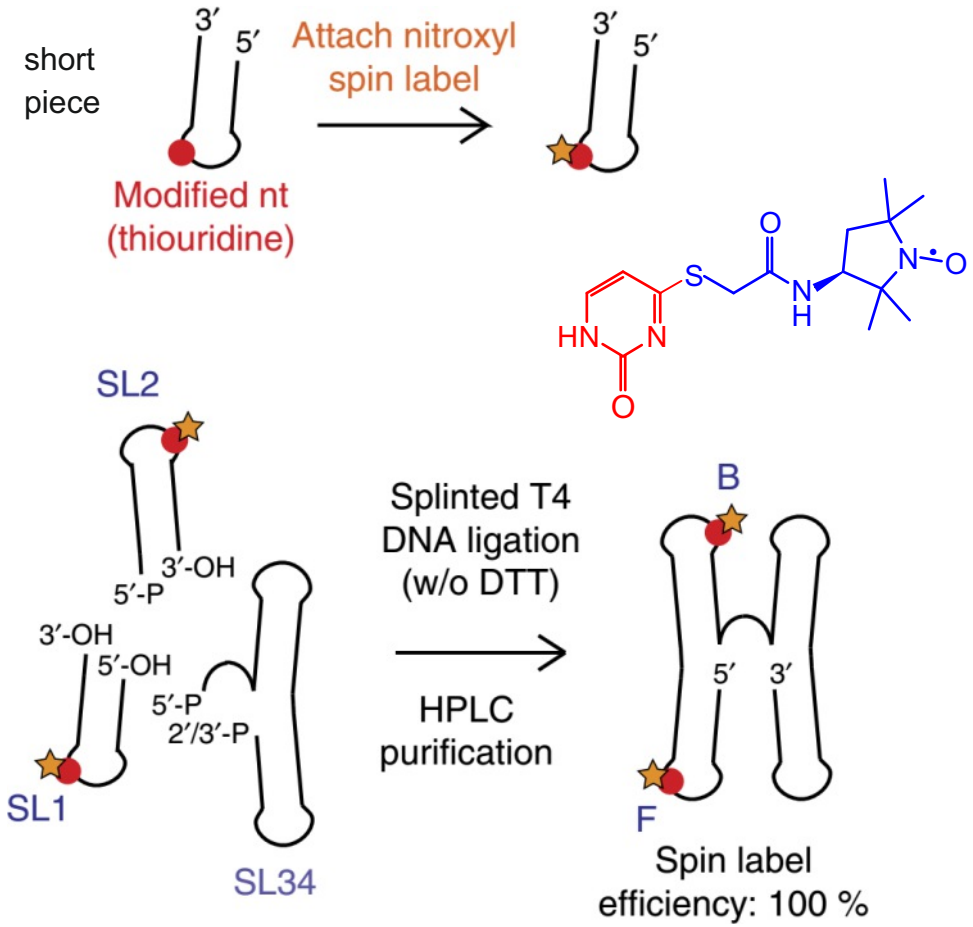

O. Duss, M. Yulikov, G. Jeschke, F. H.-T. Allain *Nature Comm.* **5**, 3669 (2014)

The spectrum of nitroxides

Liquid state (or single orientation)

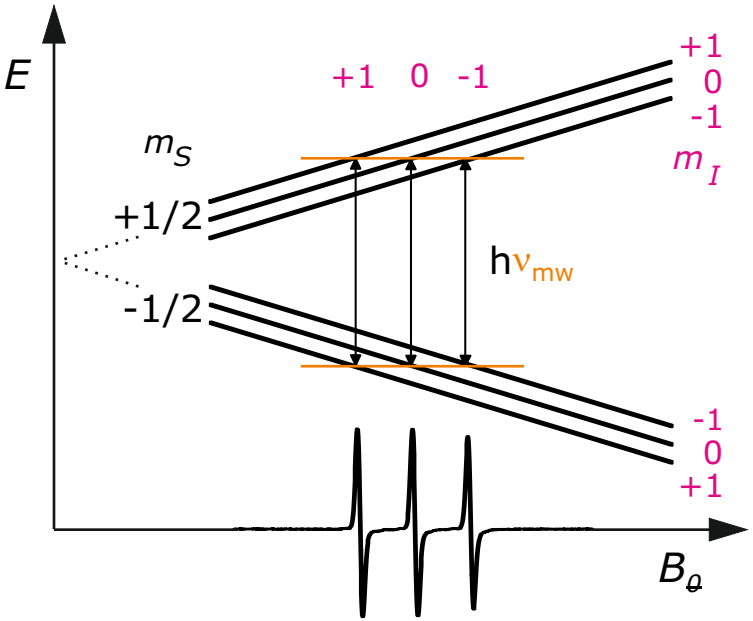

Molecular frame and orientation dependence

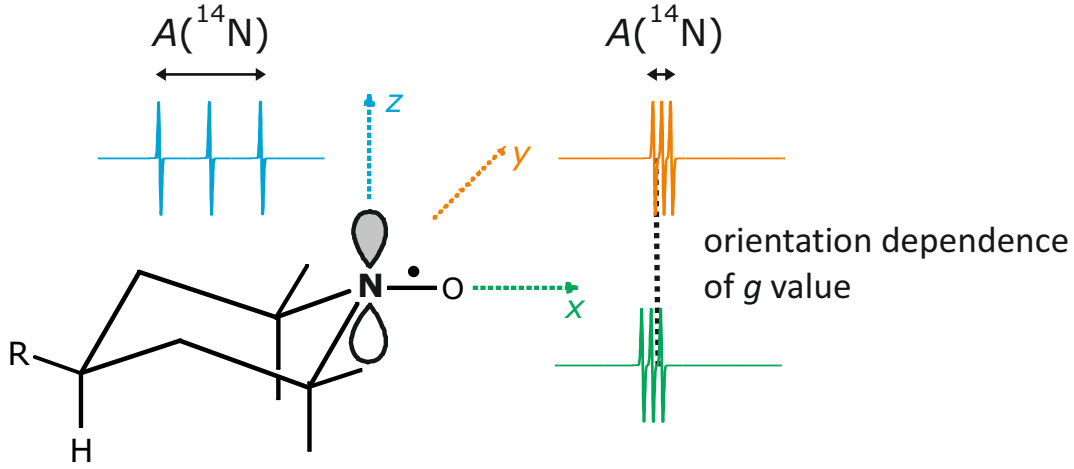

Solid state

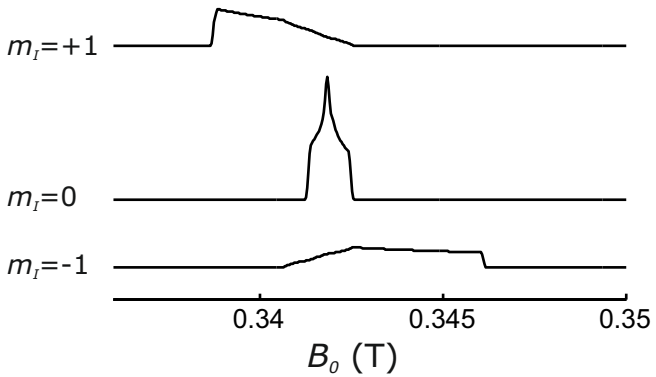

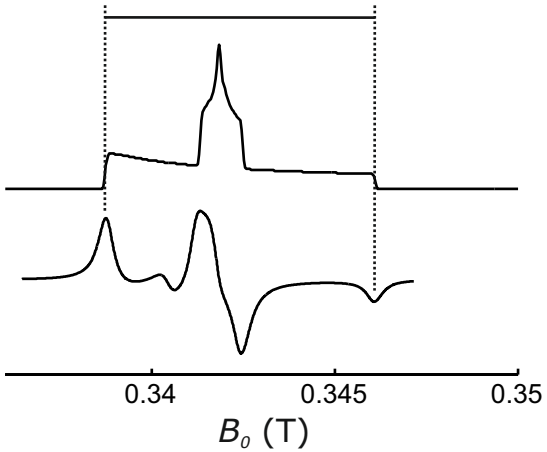

- ideal liquid state: rotational averaging in less than 10 ps
- ideal solid state: rotational averaging in more than 1 µs

Polarity of environment and hydrogen bonding

- both *g* tensor and ^{14}N hyperfine tensor are sensitive to intermolecular interactions

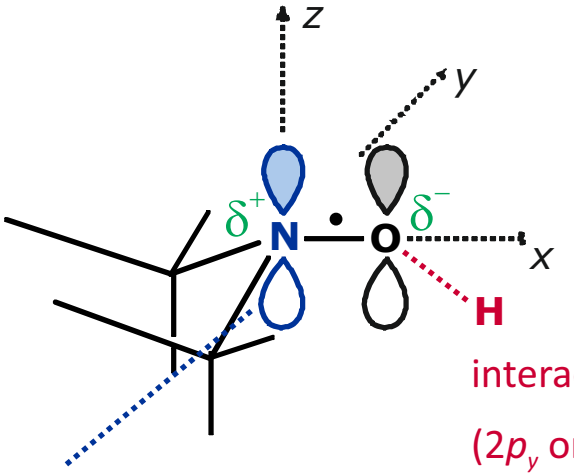

interacts with lone pair ($2p_y$ orbital)

spin population ρ_N influenced by solvent polarity and H bonding

$$\rho_O \approx 1 - \rho_N$$

$$N{-}O^{\bullet} \leftrightarrow N^{+\bullet}{-}O^{-}$$

$$g_{xx} = g_e + \frac{2\zeta_O \left(C_{O,y}^{(n)}\right)^2 \rho_O}{E_p - E_n}$$

KAWAMURA et al., *Bull. Chem. Soc. Jpn.* **40**, 1111 (1967)

$a_{iso} \propto \rho_N$ (good approximation)

KARPLUS & FRAENKEL, *J. Chem. Phys.* **35**, 1312 (1961)

$A_{zz} \propto a_{iso}$ (good approximation)

KURAD et al., *Biophys. J.* **86**, 264 (2004)

Polarity profile of a lipid bilayer: Spin probing

5-DOXYL-P-Lipid

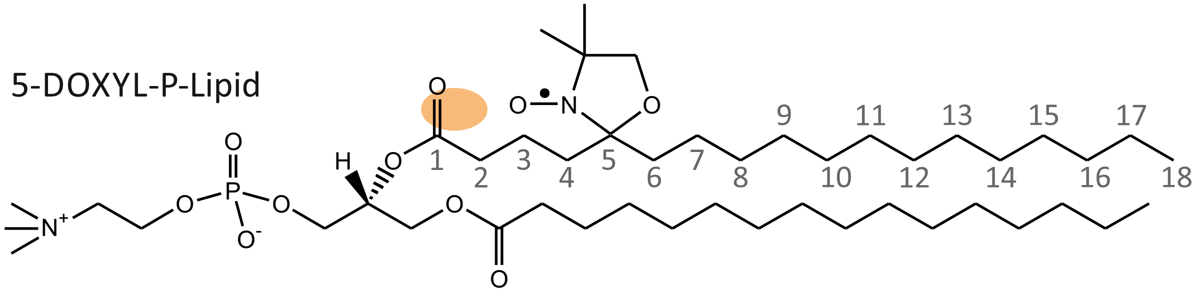

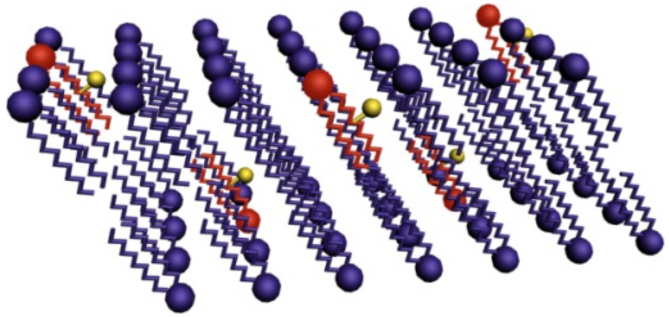

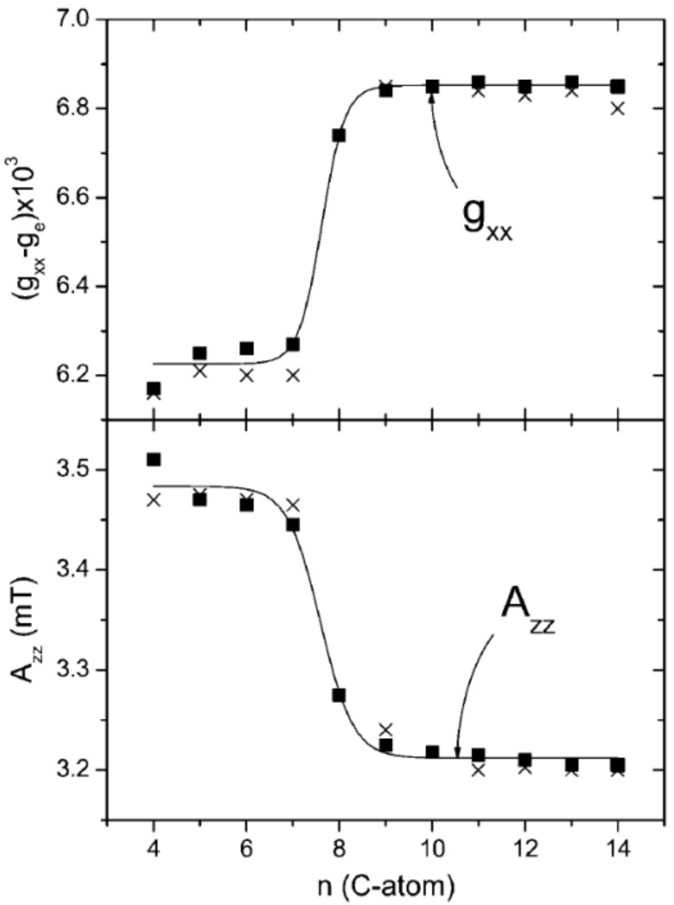

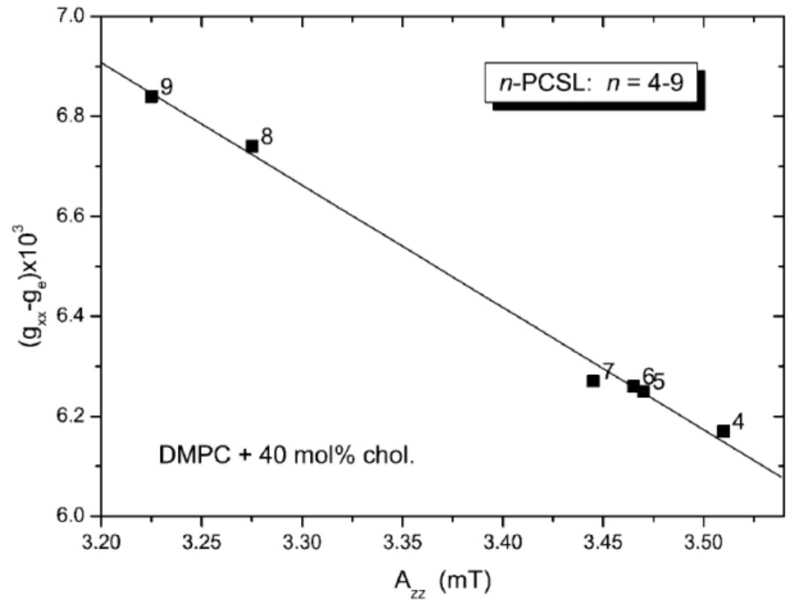

- measurement at high field (W-band frequency of 94 GHz)

Spectral changes by chemical exchange

McConnell equations

- Bloch equations for each exchanging species
- exchange terms are added:

$$\left(\frac{d}{dt}\mathbf{M}_1\right)_{exch} = k_2\,\mathbf{M}_2 - k_1\,\mathbf{M}_1$$

$$\left(\frac{d}{dt}\mathbf{M}_2\right)_{exch} = k_1\,\mathbf{M}_1 - k_2\,\mathbf{M}_2$$

- symmetric exchange ($k_1 = k_2$), free evolution

  (M_{1x}, M_{2x}, M_{1y}, M_{2y} treated separately from M_{1z}, M_{2z})

  analytical solution for eigenvalues of the 4 × 4 matrix,

  if transverse relaxation is negligible

$$\Lambda_{1,2} = \frac{i}{2}(\Omega_1 + \Omega_2) - k \mp \left(k^2 - \frac{1}{4}(\Omega_1 - \Omega_2)^2\right)^{1/2}$$

imaginary parts are the frequencies

real parts are decay time constants

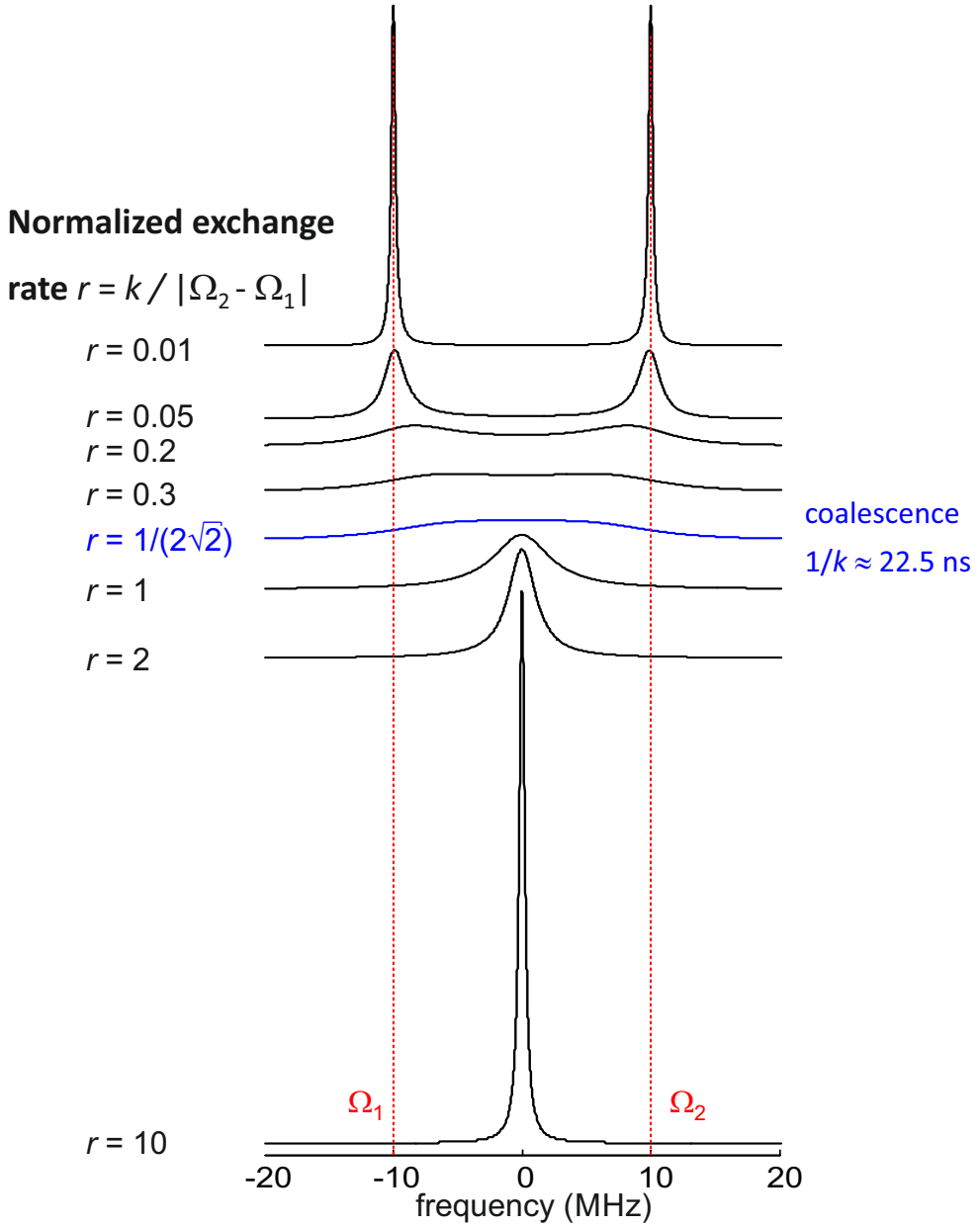

Hypothetical two-site orientation exchange for a nitroxide

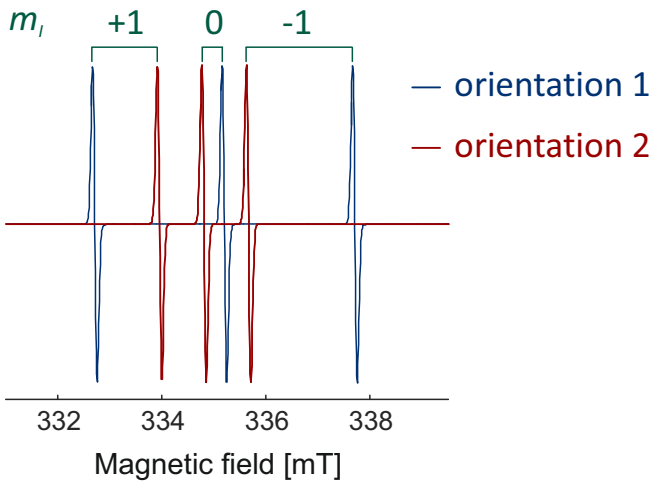

Fast exchange

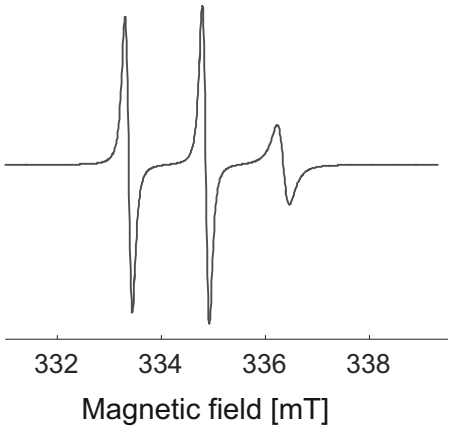

Three separate two-site exchange problems

- m_I does not change (unless nitroxides collide)
- $|\omega_1^{(0)} - \omega_2^{(0)}| < |\omega_1^{(+1)} - \omega_2^{(+1)}| < |\omega_1^{(-1)} - \omega_2^{(-1)}|$

since $r = k / |\omega_2 - \omega_1| \Rightarrow$

$r^{(0)}$ > $r^{(+1)}$ > $r^{(-1)}$

less more broadening in fast regime

The real situation

- exchange between infinitely many orientations $\Omega_i(\theta_i,\rho_i)$
- exchange rates k are a function $k(\Omega_i,\Omega_j)$
- the function $k(\Omega_i,\Omega_j)$ encodes the type of dynamics and the rate

Isotropic Brownian rotational diffusion

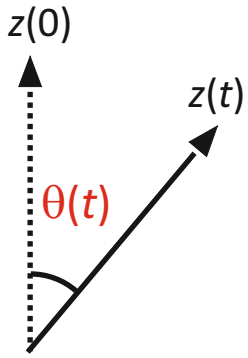

rotational correlation time τ_r

Ensemble average $\langle \cos\theta(t) \rangle$

$\langle \cos\theta(t) \rangle = 1$ for $t = 0$

$\langle \cos\theta(t) \rangle \rightarrow 0$ for $t \rightarrow \infty$

Brownian rotational diffusion:

$\langle \cos\theta(t) \rangle = \exp(-t/\tau_r)$

- a single parameter (τ_r) for dynamics

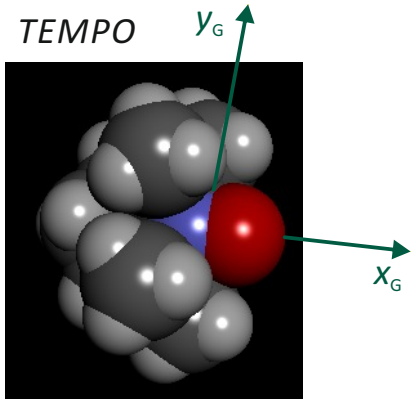

almost spherical

Laboratory frame

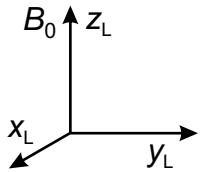

$\Omega_{LG}(t)$

g-tensor frame
molecule-fixed

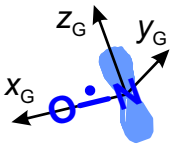

Example: Thermally activated Brownian diffusion

$E_A = 22.9$ kJ·mol^{-1}

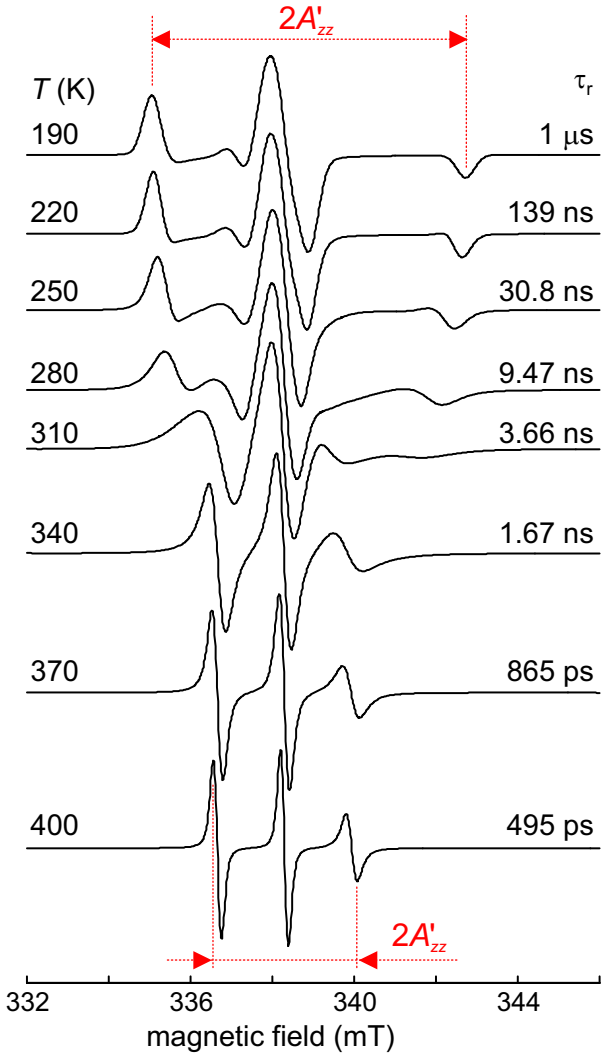

Anisotropic Brownian rotational diffusion

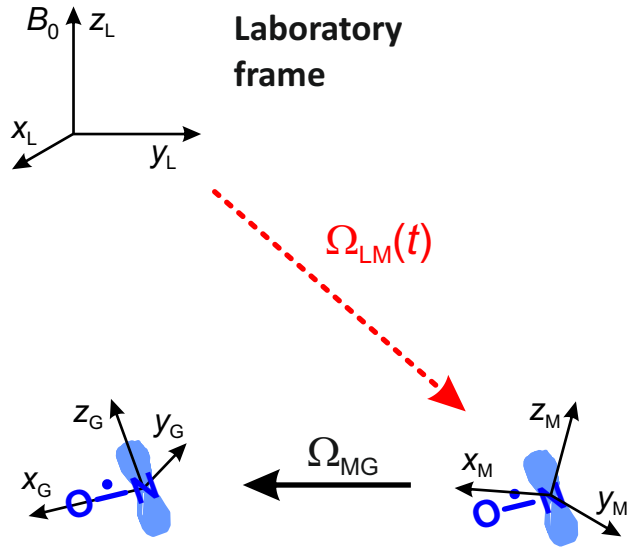

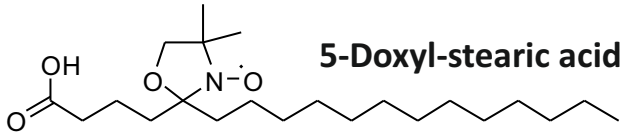

free tumbling in solution

prolate rotor

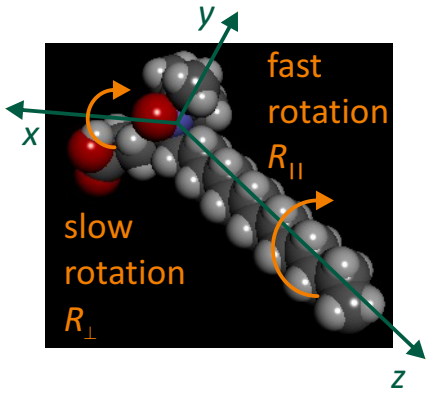

Assumption: $\tau_\perp = 5\ \tau_{||}$

$\tau_r = \sqrt[3]{\tau_\perp^2\,\tau_{||}}$

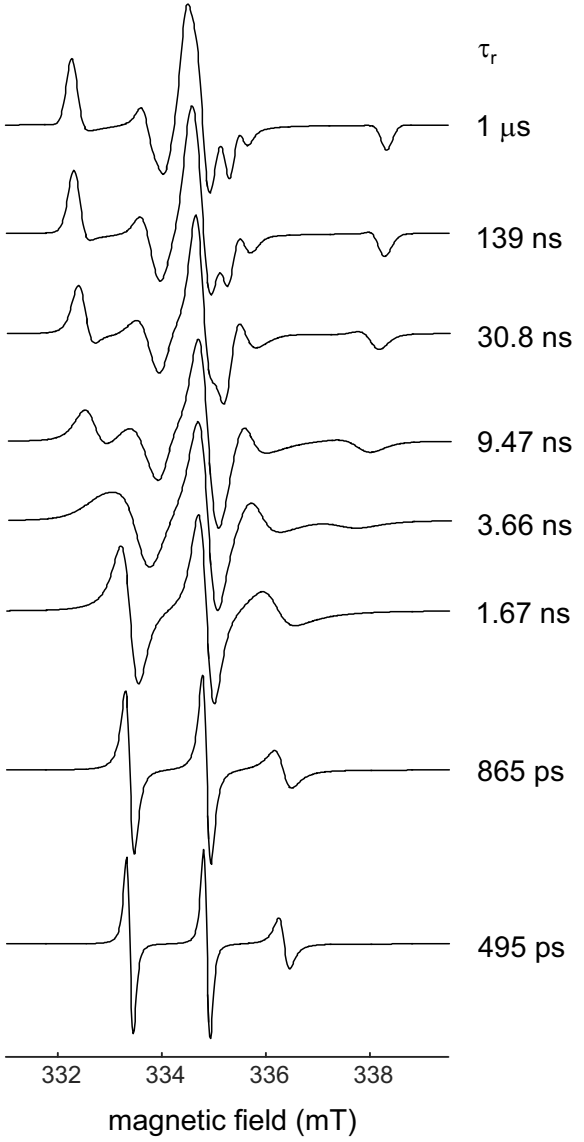

- in general, six parameters for dynamics

  3 diffusion tensor principal values

  3 Euler angles α_{MG}, β_{MG}, γ_{MG}

- often reduced to two parameters

  $R_{||} = 1/6\tau_{||}$, $R_\perp = 1/6\tau_\perp$

  at known α_{MG}, β_{MG}, γ_{MG}

Kivelson theory

In the fast regime, dynamics leads to only transition-dependent line broadening

$$1/T_2(m_I) = a + b\, m_I + c\, m_I^2 \quad \Rightarrow \quad T_2(0)/T_2(m_I) = 1 + B\, mI + C\, m_I^2 \qquad \text{with } B = b/a \text{ and } C = c/a$$

- B and C can be computed for isotropic Brownian diffusion in closed form from spin Hamiltonian parameters and τ_r

$$T_2(0)/T_2(m_I) = I(0)/I(m_I)$$

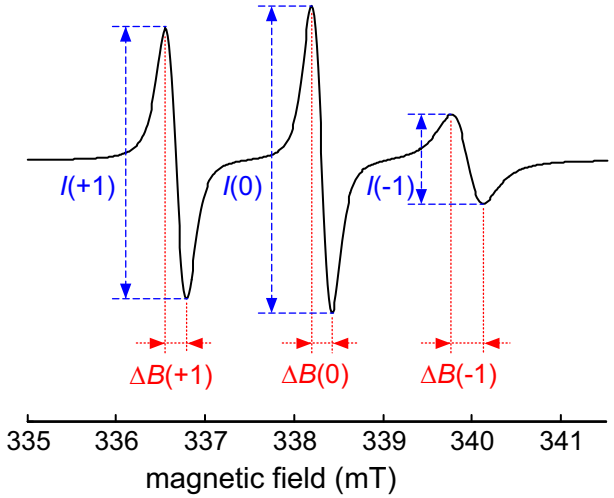

Dependence of the intensity pattern on the preferred rotation axis

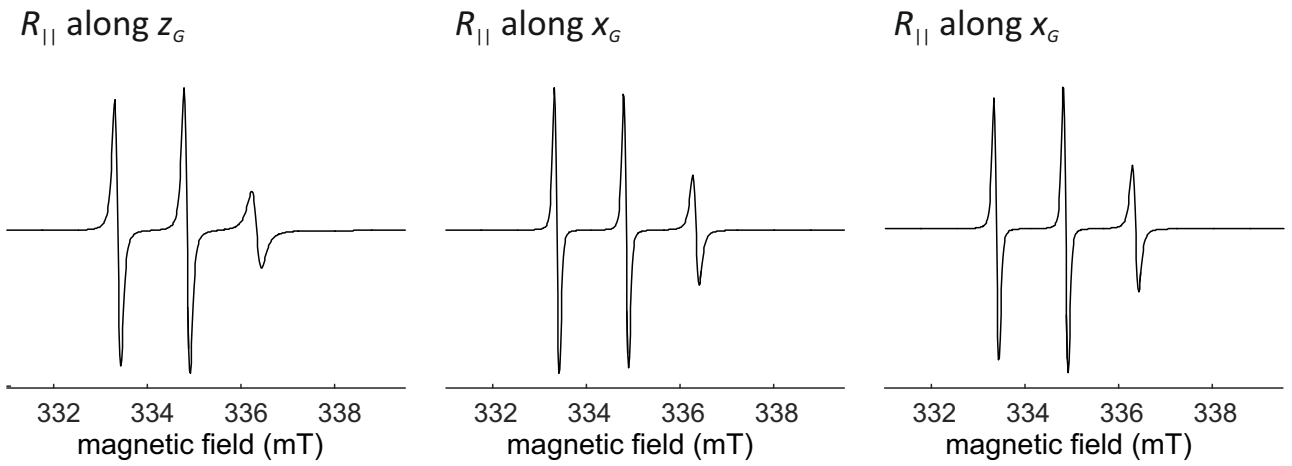

Extrema separation

Example: Thermally activated Brownian diffusion

E_A = 22.9 kJ·mol^{-1}

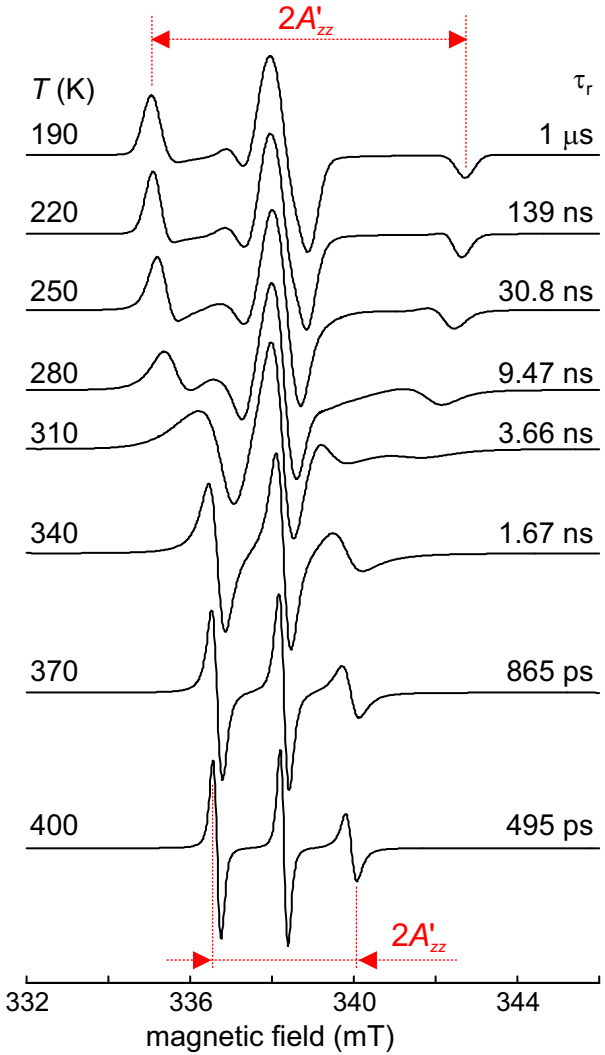

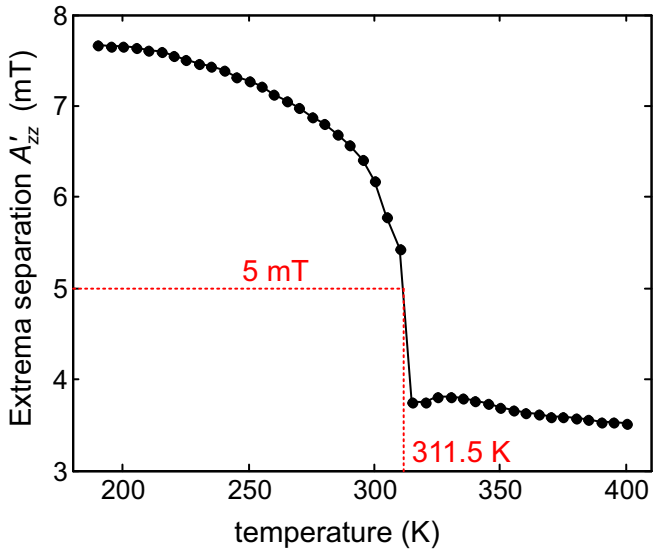

- characteristic parameter T_{5mT} or T_{50G}
- corresponds to "mean" coalescence
- corresponds to $\tau_r \approx 3.5$ ns

Water accessibility by three-pulse ESEEM

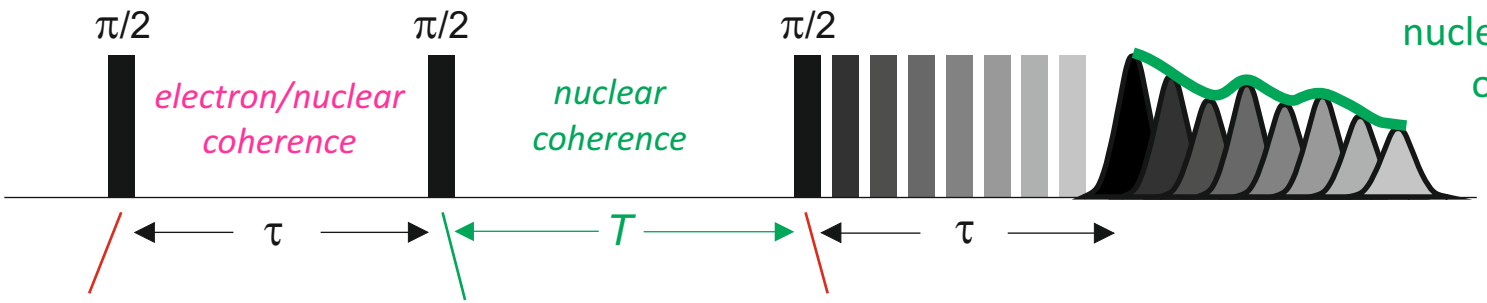

nuclear modulation of electron spin echo decay

forbidden *e/n* transition $\propto r^{-3}$

allowed *e* transition

forbidden *e/n* transition $\propto r^{-3}$

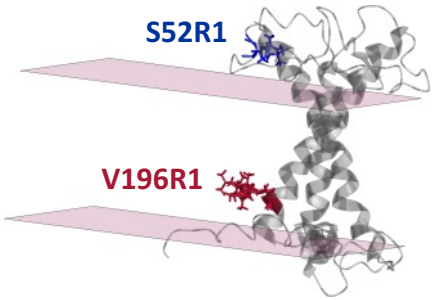

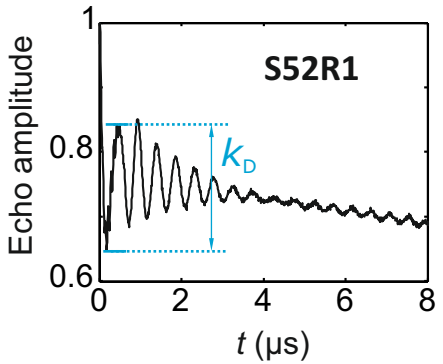

Deuterium modulation from D_2O in spin-labeled LHCIIb

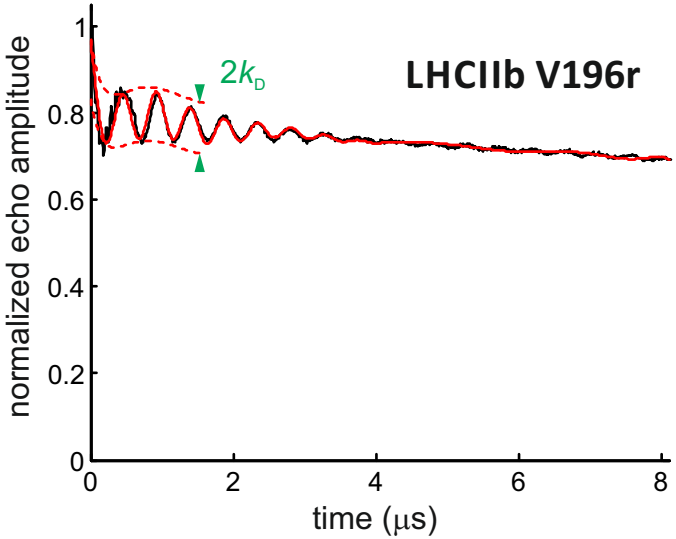

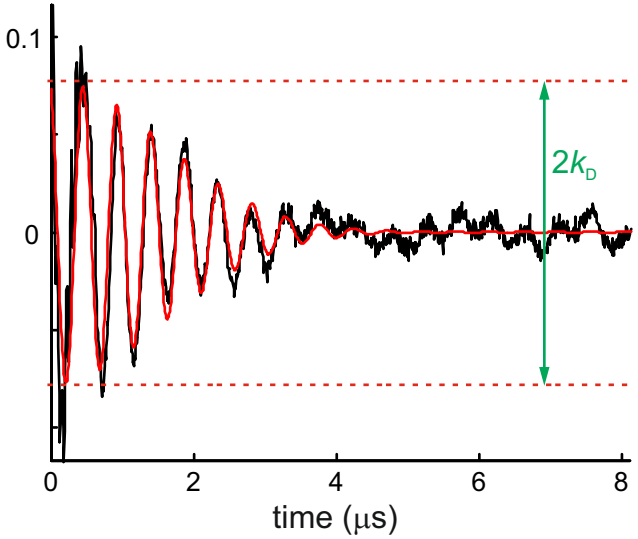

$k = \sin^2 2\eta = (B\,\omega_I / \omega_\alpha\,\omega_\beta)^2$

purely through-space

$\langle k \rangle \propto \langle B^2 \rangle / \omega_I^2 \propto 1/(B_0^2\, r^6)$

- modulation depth $k \propto r^{-6}$ and $k \propto$ number of nuclei

Water accessibility by three-pulse ESEEM (II)

Electron spin echo envelope modulation (ESEEM)

- based on forbidden electron-nuclear transitions
- contrast by *hydrogen/deuterium exchange*
- measurements at cryogenic temperature
- observes modulation (depth) of an echo signal

Spin-label conformations (simulation) in plant light harvesting complex

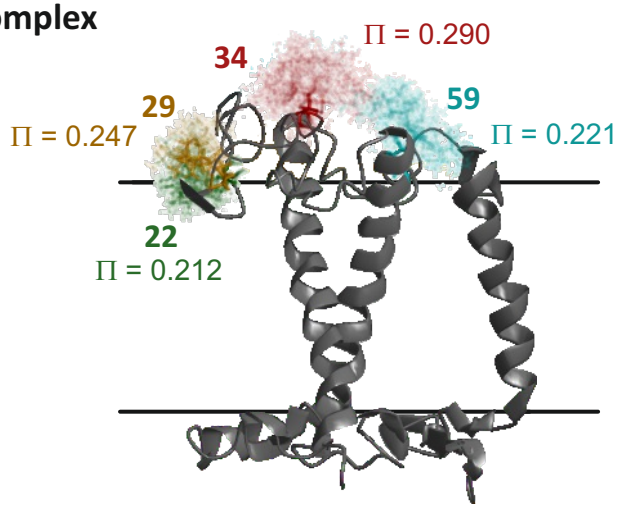

Sensitive range

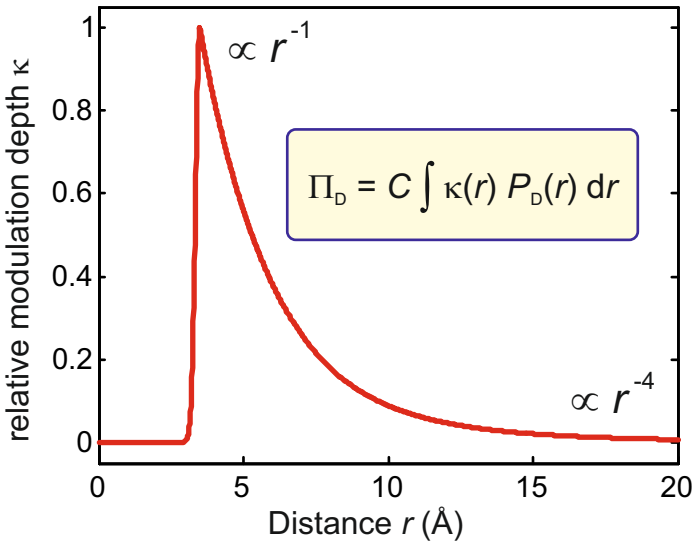

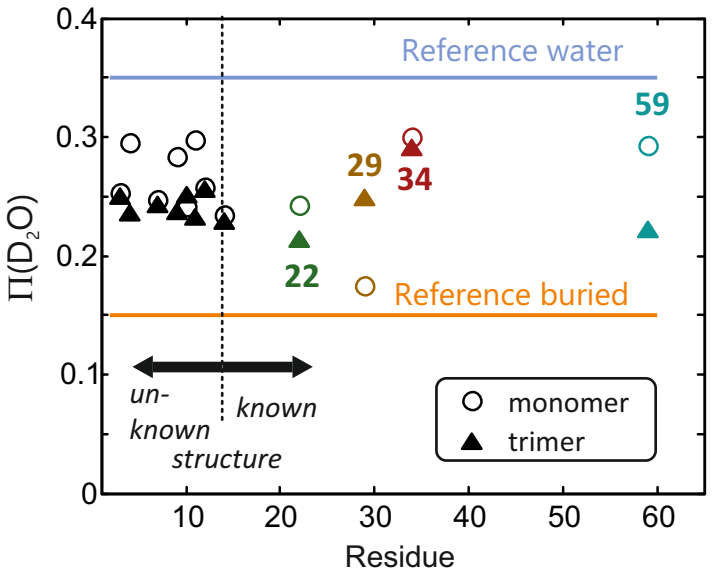

Relaxation via collisional exchange

Diffusing paramagnetic species

before **during** **and after**

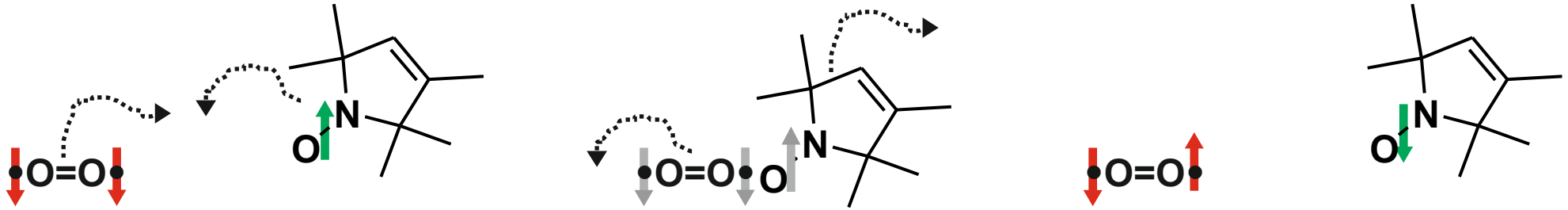

observer spin up ↑

electrons in overlapping orbitals are indistinguishable

observer spin down ↓

collision

$\Rightarrow$ relaxation time T_1 decreases with increasing exchange rate W_{ex}

- most easily detected via saturation curves (CW EPR)

$$\Delta P_{1/2} \propto W_{ex}/T_{2e}$$

ALTENBACH et al., *Proc. Natl. Acad. Sci. USA* **91**, 1667-1671 (1994)

Oxygen accessibility measurement in plant light harvesting complex

Accessibility measurements via relaxation enhancement

Spin-labeled major plant light harvesting complex II (V229C labeled with IA-Proxyl)

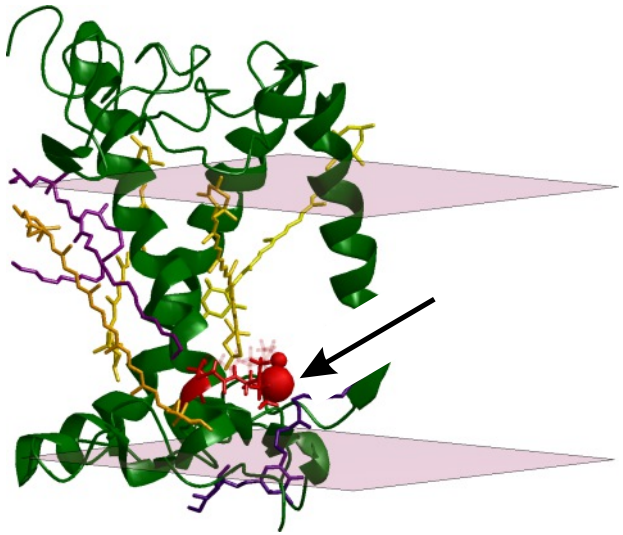

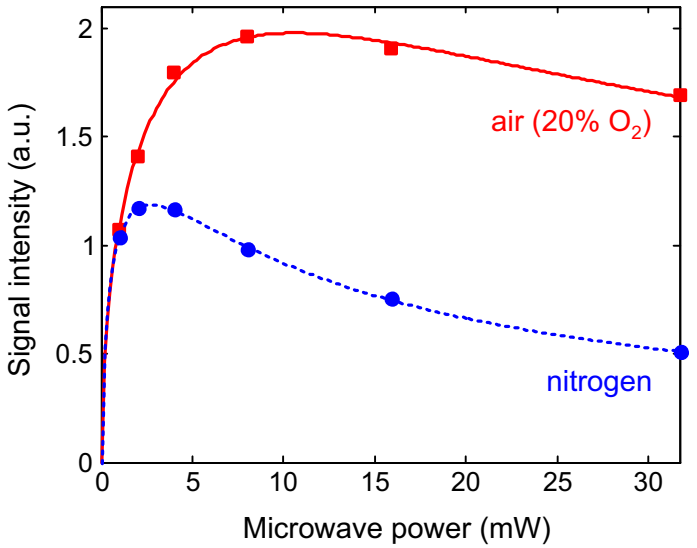

- also used for access by water-soluble paramagnetic quenchers: Cr(III)oxalate (Crox), NiEDDA

Spin trapping- sensitive detection of short-lived radicals

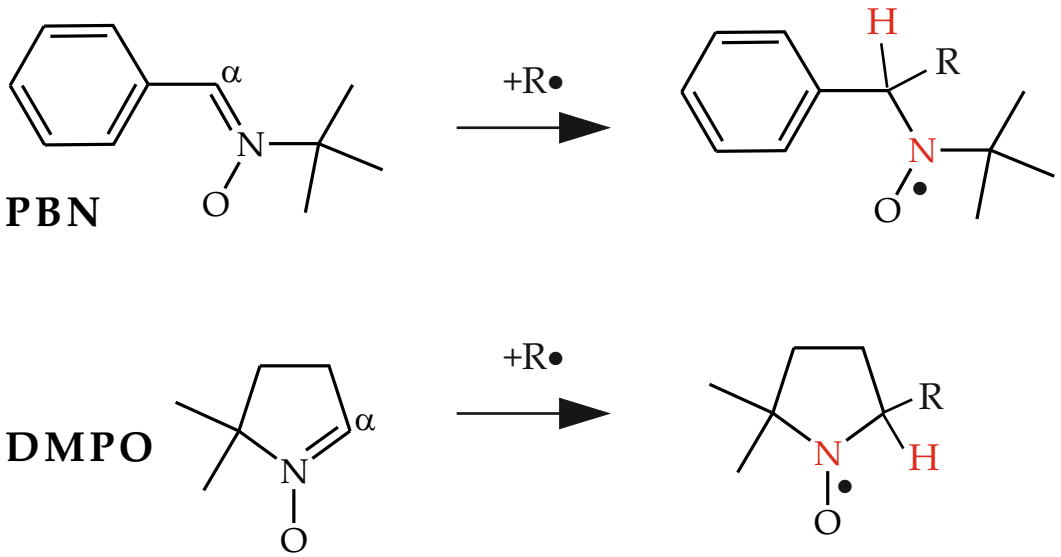

Characteristic parameters:

g value (O- or C-centered)

A^N

A_β^H

Radical identification

If you have a hypothesis on structure:

① search literature for suitable spin trap and observed hyperfine couplings

② if this fails, predict parameters by DFT computation for a few traps

If you don't have a hypothesis on structure:

try a few spin traps and search spin trap database (**https://tools.niehs.nih.gov/stdb/**) by A^N and A_β^H

Spin trapping- example 1

Mechanism of photocatalytic nitration with N-nitrosuccinimide

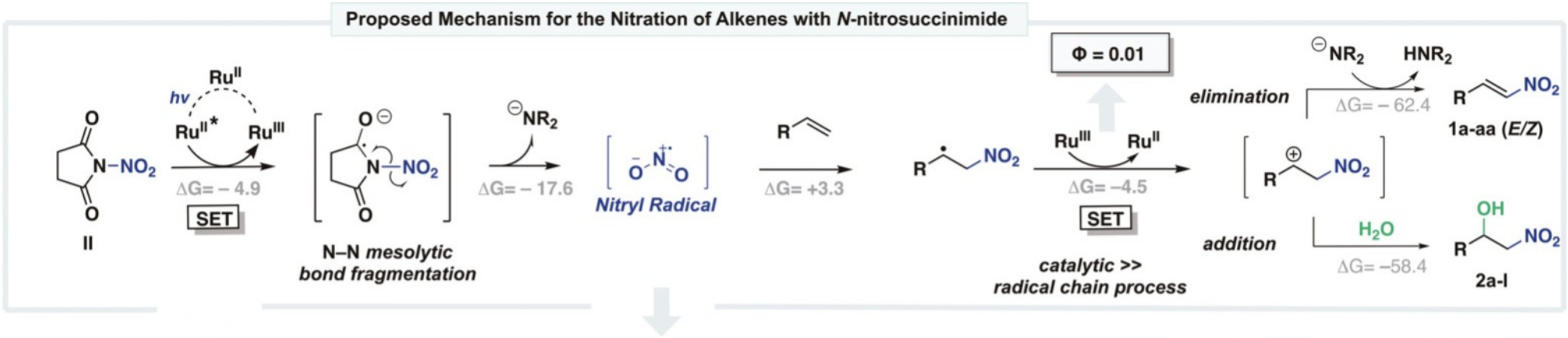

Spin trapping at 243 K in acetonitrile with 1:2 ratio between N-nitrosuccinimide and DEPMPO

A_P = 45.8 G,
A_N = 12.38 G,
A_H = 10.15 G

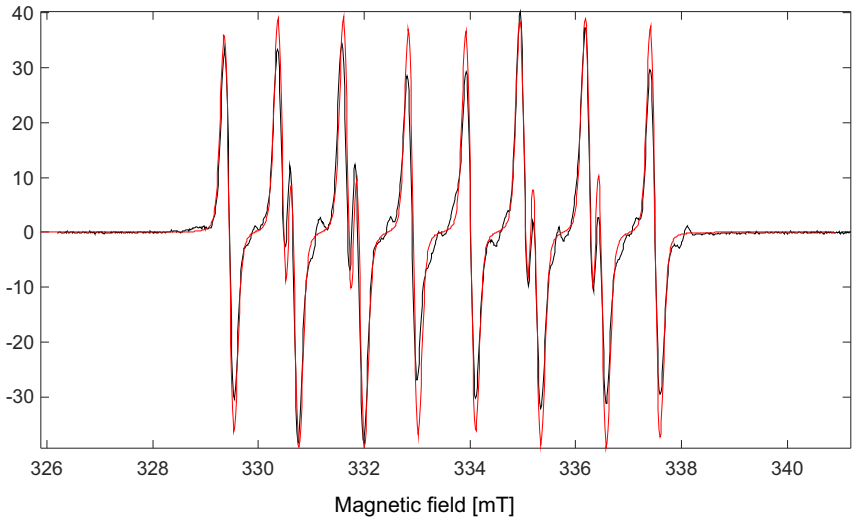

K. ZHANG *et al.*
Chem. Eur. J. **2019**, *25*, 12929–12939

Spin trapping- example 2

Agent for photodynamic therapy

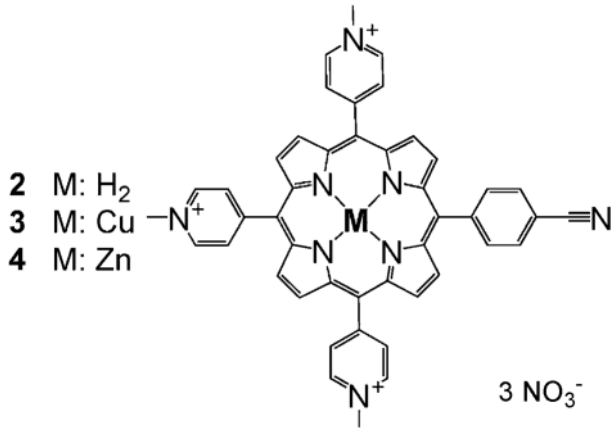

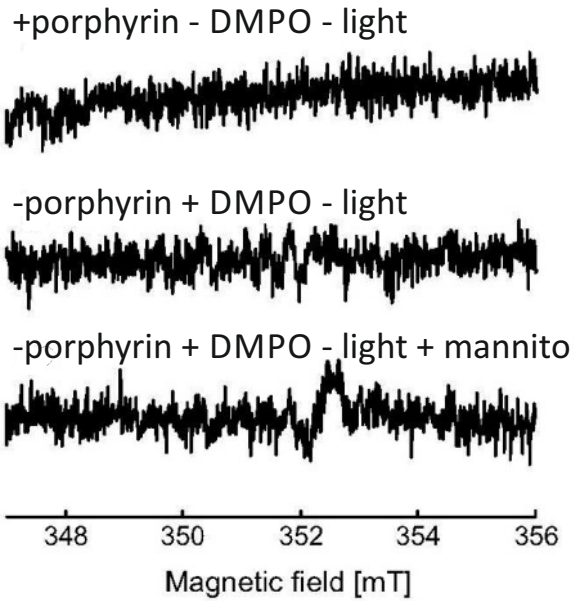

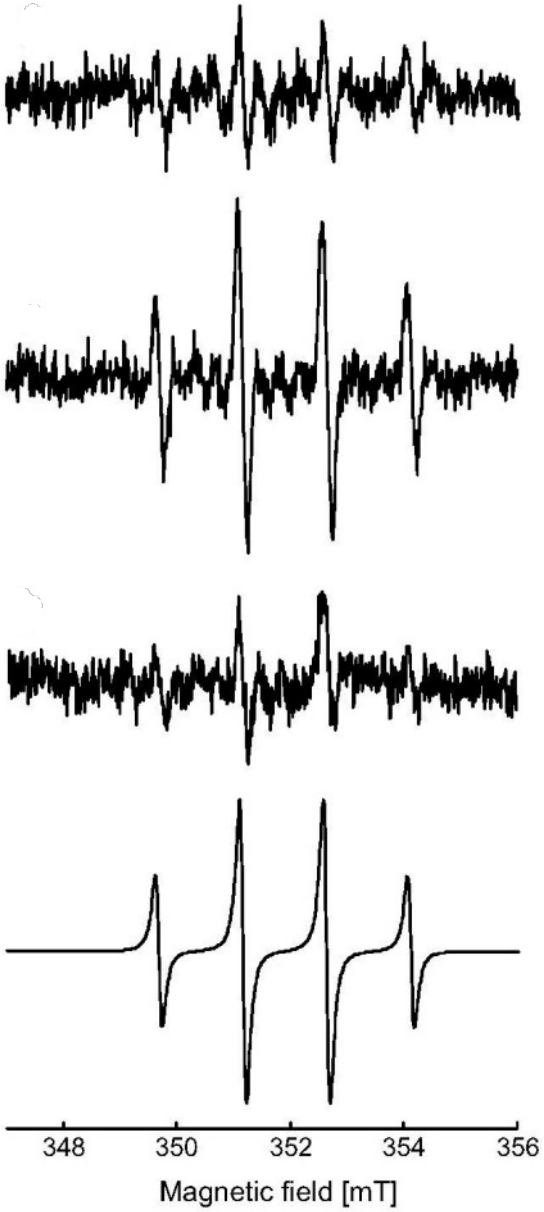

+porphyrin + DMPO - light

+porphyrin + DMPO + light

+porphyrin + DMPO + light + mannitol

simulated spectrum of DMPO-trapped ·OH radicals

P.M. ANTONI *et al.*
Chem. Eur. J. **2015**, *21*, 1179-1183

Prüfungsvorbereitung

- den Fragenkatalog erhalten Sie nach dieser Vorlesungsstunde per E-mail
- die Übungen sind Prüfungsstoff
- die Folien zum EPR-Teil finden Sie unter

  epr.ethz.ch/education/pc-iv-advanced-magnetic-resonance.html

- PC IV/PCV: Sie bekommen entweder einen NMR- oder einen EPR-Prüfer
  ich behalte mir vor, auch NMR zu fragen
- PC IV separat (IN): 30 min, NMR & EPR werden geprüft